A STUDY ON GRAIN REFINEMENT OF AZ91E MAGNESIUM ALLOY WITH Al-5TiB$_2$, Al-Al$_4$C$_3$ AND ZnO ADDITIONS

by

Kenneth Lee

B.Eng, Ryerson University, 2008

A thesis
presented to Ryerson University
in partial fulfillment of the
requirements for the degree of

Master of Applied Science

in the Program of

Mechanical Engineering

Toronto, Ontario, Canada, 2011

© Kenneth Lee 2011

AUTHOR'S DECLARATION

I hereby declare that I am the sole author of this thesis.

I authorize Ryerson University to lend this thesis to other institutions or individuals for the purpose of scholarly research.

_____

Kenneth Lee

I further authorize Ryerson University to reproduce this thesis by photocopying or by other means, in total or in part, at the request of other institutions or individuals for the purpose of scholarly research.

_____

Kenneth Lee

ABSTRACT

A STUDY ON GRAIN REFINEMENT OF AZ91E MAGNESIUM ALLOY WITH Al-5TiB$_2$, Al-Al$_4$C$_3$ AND ZnO ADDITIONS

Master of Applied Science, 2011
Kenneth Lee

Mechanical Engineering
Ryerson University

There is great interest in increasing the use of magnesium (Mg) alloys in transportation applications to reduce weight. The use of these alloys would increase if their strength and castability were improved. Through grain refinement, it is possible to achieve significant improvement in specific mechanical properties such as strength and hardness. For aluminum (Al)-containing Mg alloys, a commonly used grain refiner is hexachloroethane (C$_2$Cl$_6$). Though effective, C$_2$Cl$_6$ use releases harmful chlorinated hydrocarbons. It is therefore desired to find novel grain refiners that are effective and environmentally safe. This thesis focused on the grain refinement of AZ91E alloy with three refiners: Al-5TiB$_2$, Al-Al$_4$C$_3$ and ZnO. The refiners were chosen due to their known grain refinement efficiency in low-Al Mg or Mg-Zn alloys.

Castings with each refiner were made in graphite molds to establish i) the optimum addition levels to achieve the smallest average grain size and ii) the effect of holding time on fading of grain refinement efficiency. These castings were used to collect thermal data and sectioned for microscopy and hardness testing. Castings were also made with the optimum parameters in a permanent mold specifically designed to investigate hot tearing susceptibility.

The results indicated that all three additions enabled grain refinement of the base alloy, and no fading of grain refiner efficiency was observed. These refiners transformed the coarse dendritic microstructure in AZ91E to one that was more equiaxed and globular. At optimal levels, the refinement mechanism was heterogeneous nucleation. Also, hot tearing was significantly decreased with all refiners except for ZnO. The excess Zn from ZnO addition led to an increase in the freezing range, thus increasing the hot tear severity. The hardness of AZ91E did not increase with ZnO addition as it did with the other two refiners.

ACKNOWLEDGEMENTS

TABLE OF CONTENTS

NOMENCLATURE

Abbreviations

ANOVA	Analysis of variance
BCC	Body-centered cubic
cm	Centimeter
EDX	Energy dispersive X-ray
FCC	Face-centered cubic
FR	Freezing range
GRF	Growth restriction factor
HCP	Hexagonal close-packed
HRE	Hardness Rockwell E
HV	Vickers hardness
mm	Millimeter
MPa	Megapascal
SEM	Scanning electron microscope/microscopy
UC	Undercooling
wt. %	Weight percent

Elements

Al	Aluminum
B	Boron
Be	Beryllium
C	Carbon
Ca	Calcium
Ce	Cerium
Cl	Chlorine
Cu	Copper
F	Fluorine
Fe	Iron
Mg	Magnesium

Mn	Manganese
Ni	Nickel
O	Oxygen
Sb	Antimony
Si	Silicon
Sr	Strontium
Ti	Titanium
V	Vanadium
Zn	Zinc
Zr	Zirconium

Greek Symbols

σ_y	Yield strength
σ_o	Material constant
σ_b	Tensile strength
δ	Elongation
μ	Micro

English

Å	Angstrom
℃	Degree Celsius
$C_{o,i}$	Initial composition of the alloy
d	Average grain diameter
k_i	Distribution coefficient
k_y	Material constant – "Locking parameter"
m_i	Slope of the liquidus line
m	Meter
s	Second
T_F	Freezing temperature
T_G	Grain growth temperature
T_N	Undercooling point

LIST OF TABLES

LIST OF FIGURES

LIST OF APPENDICES

CHAPTER 1 – INTRODUCTION

Magnesium (Mg) alloys are among the lightest structural materials, with a density of ~1.80 g/cm³. Mg alloys are ~30% lighter than aluminum (Al) alloys and ~70% lighter than steel. Consequently, there is renewed interest in using Mg alloys for weight reduction in automotive and aerospace applications. Due to environmental concerns related to vehicle emissions, the use of Mg in place of traditional metals will undoubtedly rise. Application of Mg alloys would increase if their strength and castability were improved. Significant material property improvements can be accomplished through grain refinement.

There are generally two classes of magnesium alloys: Al-free and Al-bearing. With Al-free Mg alloys, a commonly used refiner is zirconium (Zr) (Section 2.3). Zr is highly effective, but it is expensive. Regarding Mg-Al alloys, current methods of grain refining (Section 2.4) are often not practical in the industry (e.g. requires rapid cooling, high purity control). Also, many of these methods are harmful to the environment or costly.

Grain refinement has been reported to increase the castability of an alloy. Since the majority of Mg alloy products are manufactured via casting, grain refinement is of paramount importance. For instance, in permanent molds, hot tearing, a common casting defect, may be eliminated through proper grain refinement. The smaller grains are better able to slide relative to each other, hence limiting any potential tears to a localized region. Therefore, an efficient, low cost and environmentally friendly refiner would increase the use of these Mg alloys.

The main goals of this thesis were to:
1. Study the efficiency of three unique grain refiners in the AZ91E alloy through grain size measurements and an understanding of the refinement mechanism.
2. Examine the effects of these additions on the hot tearing susceptibility of the AZ91E alloy through permanent mold castings.
3. Carry out thermal analysis to understand the effects of these additions on alloy solidification.
4. Perform hardness testing to correlate grain refinement with improvements in mechanical property.

A flowchart illustrating the scope of this study is shown in Figure 1.1, while the thesis is divided into the following sections:

- Chapter 1: Introduction and outline of the thesis.
- Chapter 2: A literature review containing background on grain nucleation, crystallographic matching (lattice disregistry and edge-to-edge model), grain refinement methods and hot tearing.
- Chapter 3: Details on the materials and experimental procedures used in this thesis. This includes information on the base alloy and the additions. In addition, graphite and permanent mold experiments are discussed. The chapter ends with procedures regarding thermal and microscopy analyses along with hardness testing.
- Chapter 4: Results are presented, including grain size measurements, optical and scanning electron microscopy (SEM), thermal analysis and hot tearing observations. The chapter ends with hardness testing results. All results are interpreted and discussed.
- Chapter 5: Conclusions are presented in this chapter.
- Chapter 6: Suggestions for future work are presented.

Grain Refiners

→

- Al-5TiB$_2$
- Al-Al$_4$C$_3$
- ZnO

Graphite Mold Castings

→

- Grain size (Optical microscopy)
- General microstructure (Optical microscopy)
- Refinement mechanism (SEM with EDX)
- Undercooling (Thermal analysis)
- Freezing range (Thermal analysis)
- Hardness testing

Permanent Mold Castings

→

- Hot tears (Macroscopic examination)
- Fractography (SEM with EDX)
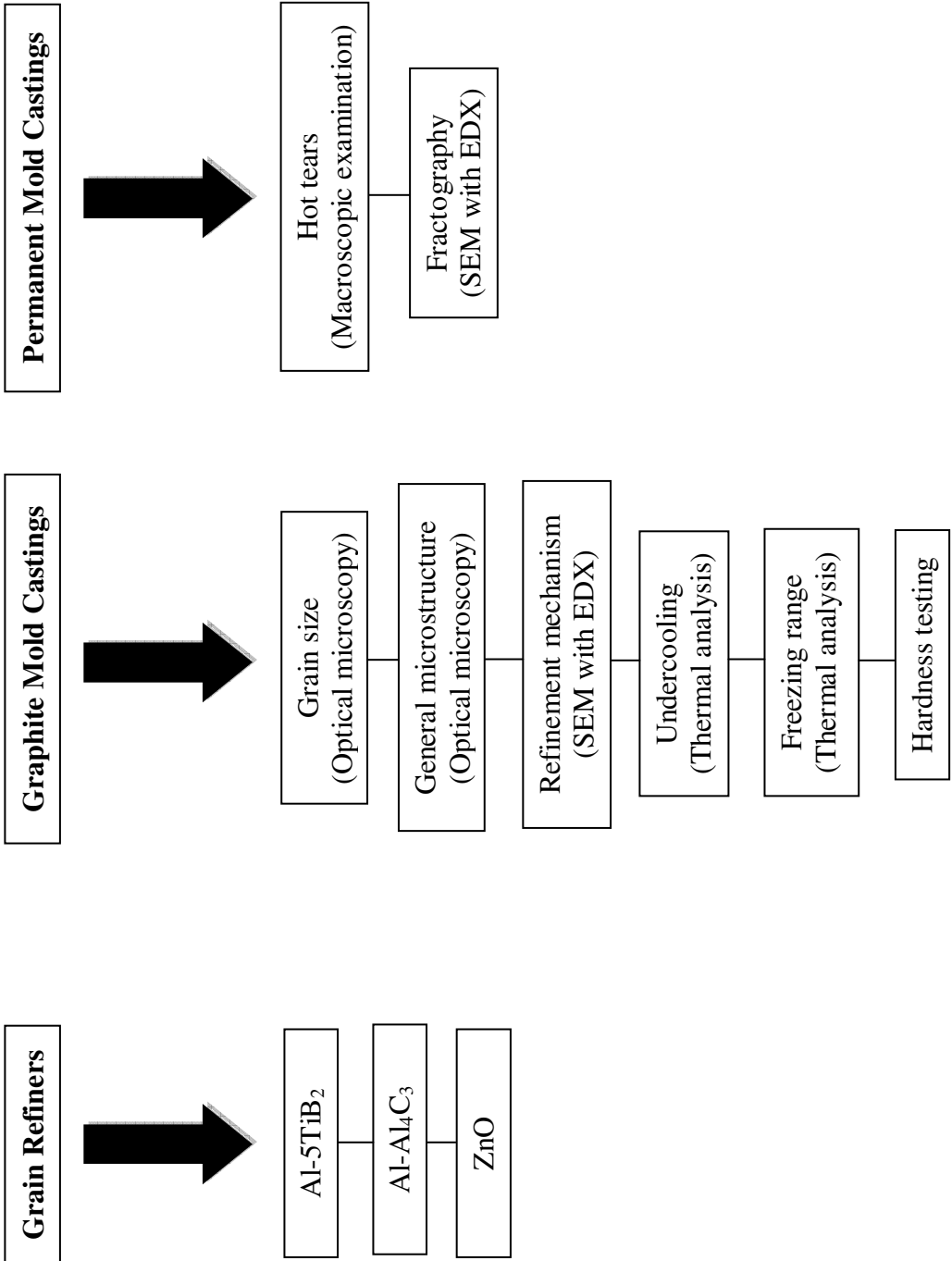
Figure 1.1: Thesis flowchart.

3

CHAPTER 2 – LITERATURE REVIEW

In this section, alloy solidification and grain refinement theory are introduced, followed by a review of grain refinement processes for Al-free and Al-bearing Mg alloys. The section concludes with a review of the effects of grain refinement on hot tearing.

2.1 – Grain Size Control

There are two distinct mechanisms of grain size control: nucleation and growth restriction.

2.2 – Nucleation Theory

It is generally known that metals with smaller grains exhibit enhanced mechanical properties in addition to improved hot tear resistance [1]. The correlation between grain size and yield strength is shown via the Hall-Petch relationship [2, 3]:

$$\sigma_y = \sigma_o + k_y d^{-1/2} \tag{2.1}$$

where: σ_y =   yield strength

σ_o =   "friction stress", representing the overall resistance of the crystal structure to dislocation movement

k_y =   "locking parameter", measuring the relative hardening contribution of grain boundaries (material parameter)

d =   average grain diameter

In order to understand grain refinement, grain nucleation must be discussed. There is a point during solidification where a solid nucleus begins to form and eventually leads to the growth of a grain. Since solidification is a non-equilibrium process, nucleation does not occur at the metal's freezing temperature (T_F). Instead, nucleation occurs at a lower temperature, T_N, via a process called undercooling [4].

As latent heat is released, the temperature of the melt rises to a grain growth temperature, T_G, where most of the solidification occurs. This rise in temperature to T_G is called recalescence. A schematic of a solidification process with undercooling is illustrated in Figure 2.1.
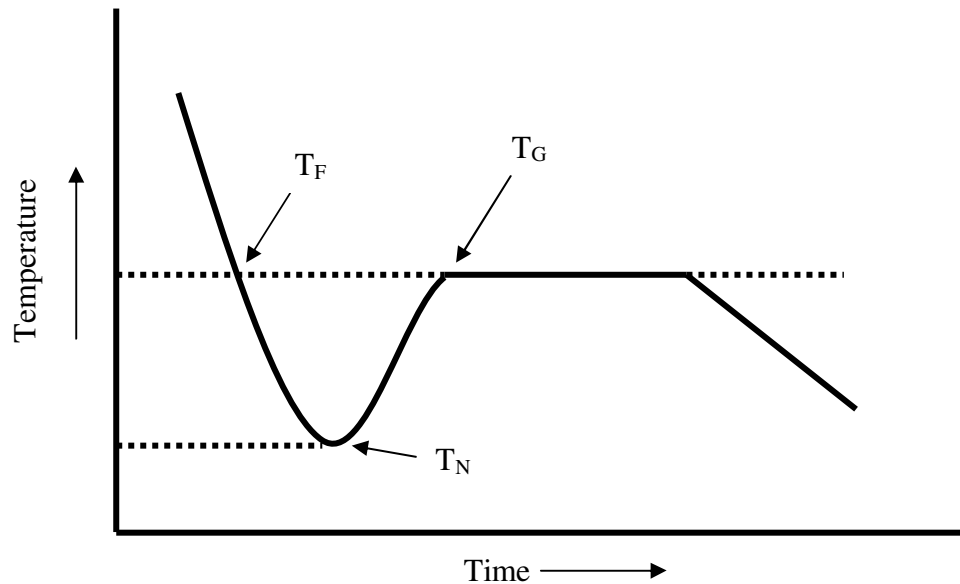
Figure 2.1: Solidification process of liquid metal with undercooling.

2.2.1 – Homogeneous Nucleation

Homogeneous nucleation theory states that the nucleus arises from the bulk of the liquid metal. However, homogeneous nucleation rarely, if ever, occurs in industrial applications due to the presence of melt impurities (metal oxides, carbides) [4]. Thus, homogeneous nucleation may be investigated by studying small droplets of the liquid metal as to minimize the number of undesired foreign particles [4].

As the temperature of the liquid metal decreases, the probability of atoms grouping to form a nucleus increases. In order for a nucleus to form, there is also a critical radius that is needed. This critical radius is the minimum size required for a stable group of atoms, which will not redissolve in the melt [1]. Therefore, the driving force for the creation of a nucleus is the amount of undercooling experienced by the melt [1]. Solidification with a high degree of undercooling is characteristic of homogeneous nucleation.

2.2.2 – Heterogeneous Nucleation

Heterogeneous nucleation theory involves nucleation from a foreign particle in the melt. Heterogeneous nucleation is the most common phenomenon since most melts contain foreign particles such as oxides and grain refiners [4]. Thus, the purpose of most grain refiners is to act as particles in the melt, which will enhance the probability of heterogeneous nucleation [4]. In addition, a grain refiner should work in small amounts, as adding too much would create another alloy in the process [4]. A grain refiner should also be effective even with long melt holding times. In other words, the refiner effectiveness should not fade for the duration of the casting process. Fading occurs when the refiner is rendered ineffective due to settling to the bottom of the crucible, or due to progressive dissolution [5].

Heterogeneous nucleation is promoted when good wetting occurs between the nucleating particle and the melt. In order for this to happen, the atomic structure and lattice parameters of the liquid must be similar to those of the solid particle, resulting in an epitaxial relationship [4]. The most favorable situation for heterogeneous nucleation is when the largest nucleus curvature is created with the least number of atoms. This favorable situation is achieved by good wetting or a very low contact angle between the particle and the liquid [4], as illustrated in Figure 2.2. In order to understand why heterogeneous nucleation occurs more readily than homogeneous nucleation, the two nucleation situations are considered in Figure 2.3. In the case of heterogeneous nucleation, a critical radius of the nucleus is more easily formed on a foreign particle since fewer atoms are required. Clearly, fewer particles are needed compared to forming a nucleus that is completely spherical as in the homogeneous case [4]. The relative number of atoms required to form the nucleus is a few hundred for homogeneous cases and only a few for heterogeneous situations. Thus, the probability of a few atoms forming a nucleus is much greater than a nucleus consisting of a few hundred atoms [4].

Solidification with no undercooling is typical of heterogeneous nucleation, which is shown in Figure 2.4. No recalescence is observed since solidification begins at the freezing temperature. Furthermore, the degree of undercooling is often a measure of homogeneous nucleation. It is thus used to measure the fading of grain refiners.

6
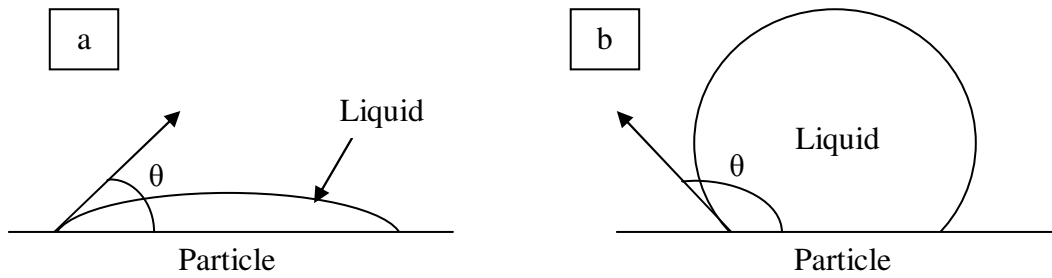
Figure 2.2: a) good wetting, low contact angle (θ), b) poor wetting, high contact angle (θ).
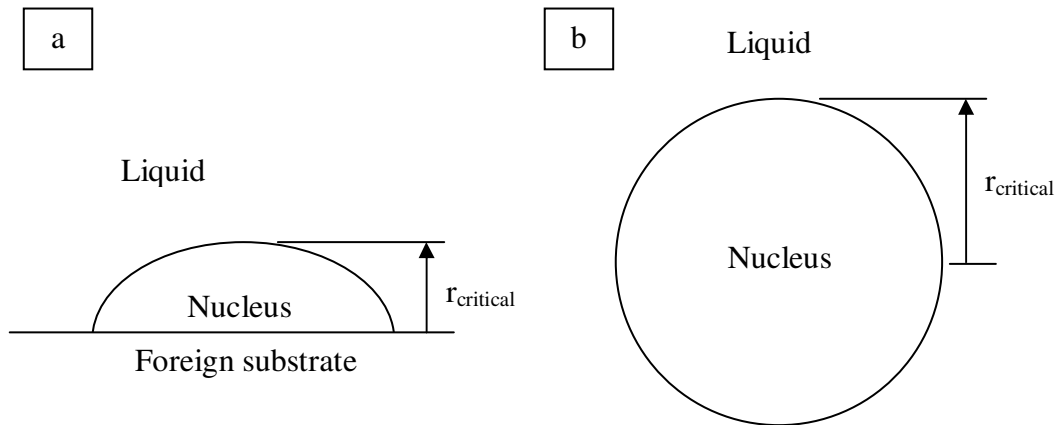
Figure 2.3: Model of a) heterogeneous nucleation, b) homogenous nucleation [4].
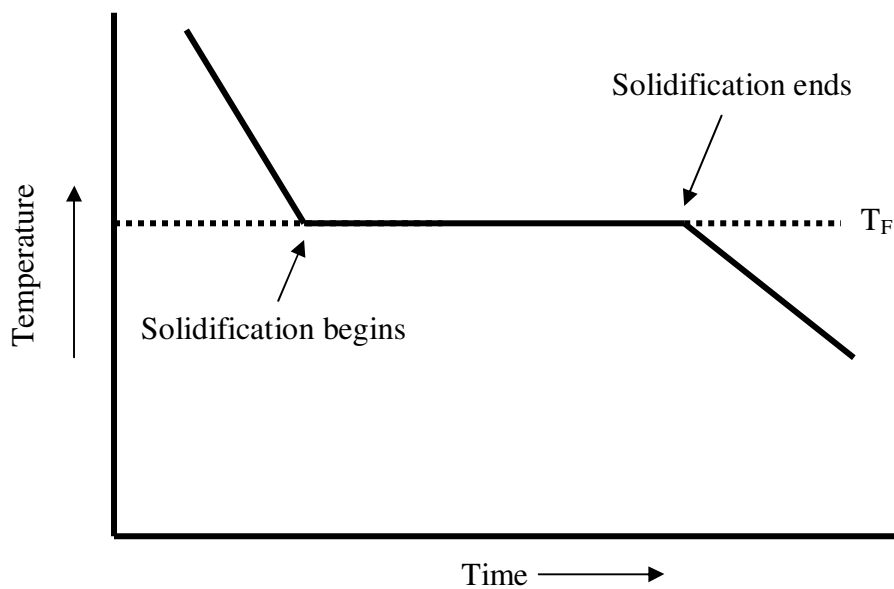
Figure 2.4: Solidification process of liquid metal without undercooling.

2.2.3 – Grain Refiner Crystal Structure

The crystal structure of any melt addition is important, as it determines its efficiency as a heterogeneous nucleation site. For example, an effective grain refiner would likely have a crystal structure similar to the melt. In addition, the lattice disregistry (percentage variation in lattice parameters) between the particle and the melt is also an important factor in gauging nucleation efficiency. The lattice disregistry theory proposed by Bramfitt [6] stated the following necessary condition: the disregistry between the particle and the melt must be less than 15% in order for the particle to be an effective nucleating site.

Another method, called the edge-to-edge matching model can also be used to predict whether a particle would be a good nucleating agent. Zhang and Kelly [7] developed this model, which operates on the basis that a substrate and matrix will always strive to maximize the atom matching at the interface (or edge) of two close-packed or near close-packed planes. A schematic of this edge-to-edge model is shown in Figure 2.5. If atom matching is perfect, then the two matching planes will be parallel to each other. Due to imperfections, the matching will cause the planes to rotate slightly about the matching direction. To qualify as an effective substrate, the inter-atomic mismatch along the matching direction should be less than 10% and the d-value (interplanar spacing between atoms) mismatch should be less than 6% [8].
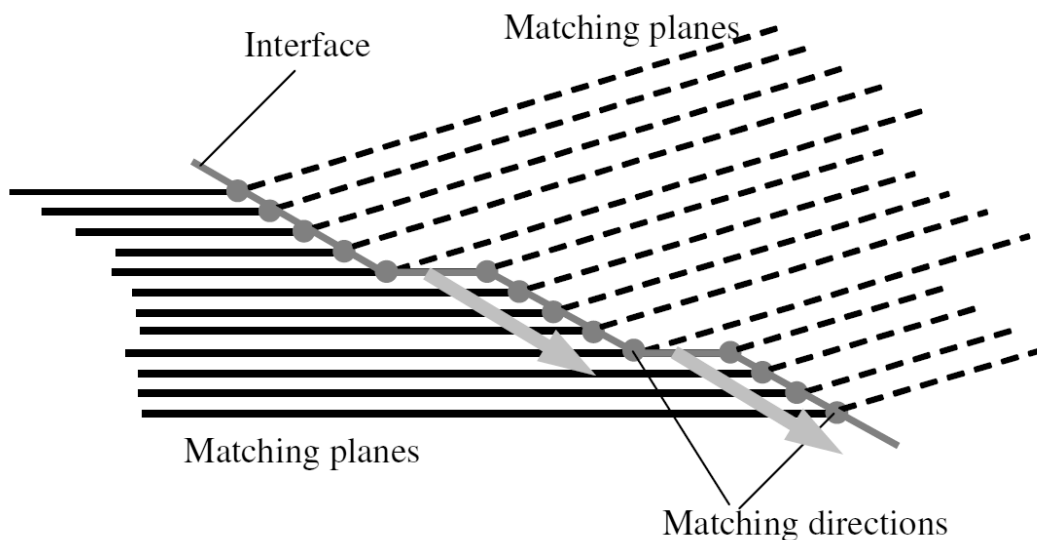
Figure 2.5: Illustration of the edge-to-edge matching model [7].

2.2.4 – Restriction of Grain Growth

There are other grain refiners that work via grain growth restriction. Growth restriction is related to constitutional undercooling, which is the undercooling that occurs when the composition of the alloy changes. The growth restriction factor (GRF) indicates that solute elements (grain refiners) produce a diffusion layer that restricts solute distribution; hence the growth of grains slows [9]. Furthermore, an indicator of growth restricting efficiency is the speed at which a critical undercooling is achieved from a nucleated grain [10]. This means smaller grain sizes are seen when the solute rejected from a nucleating grain occurs after very little grain growth [10]. Thus, the more efficient growth restrictor is accorded a higher GRF value. This GRF is represented mathematically by Equation 2.2 [9]:

$$GRF = \sum_i m_i \, C_{o,i}(k_i - 1) \tag{2.2}$$

where: m_i = slope of the liquidus line

$C_{o,i}$ = initial composition of element i

k_i = distribution coefficient

The GRF values are calculated using binary phase diagrams. The GRF values of various addition elements for Mg are tabulated in Table 2.1. A larger GRF indicates higher grain refinement efficiency when adding that element to Mg.

2.3 – Grain Refinement of Aluminum-free Magnesium Alloys

Magnesium alloys containing very little or no Al, manganese (Mn), silicon (Si) and iron (Fe) have benefited from efficient refinement with the addition of zirconium (Zr). As a refiner, Zr operates via the formation of spherical Zr-rich cores in the middle of Mg grains. The presence of these Zr cores suggested heterogeneous nucleation as the refinement mechanism. In addition, since Zr is high on the GRF list, growth restriction also likely contributed to the grain refinement effect [11].

Table 2.1: GRF values [$m(k - 1)$] of various elements in Mg [11].

Element	m	k	$m(k-1)$
Fe	-55.56	0.054	52.56
Zr	6.90	6.55	38.29
Ca	-12.67	0.06	11.94
Si	-9.25	~0.00	9.25
Ni	-6.13	~0.00	6.13
Zn	-6.04	0.12	5.28
Cu	-5.37	0.02	5.28
Ge	-4.41	~0.00	4.41
Al	-6.87	0.37	4.32
Sr	-3.53	0.006	3.51
Ce	-2.86	0.04	2.74
Sc	4.02	1.65	2.61
Yb	-3.07	0.17	2.53
Y	-3.40	0.50	1.70
Sn	-2.41	0.39	1.47
Pb	-2.75	0.62	1.03
Sb	-0.53	~0.00	0.53
Mn	1.49	1.10	0.15

When impurity elements were present (Al, Mn, Si and Fe), Zr formed stable compounds with the impurities in the Mg alloy, which rendered the Zr ineffective as a refiner [11]. For example, during high melt temperatures (~750 °C), uptake of Fe from the steel crucible occurred, which made Zr ineffective. Despite the effectiveness of Zr refiners, precaution must be taken to minimize melt impurity levels, which may increase processing costs. In addition, the high cost of Zr would also limit its commercial use [11].

2.4 – Current Processes for Grain Refinement of Magnesium-Aluminum Alloys

The following discussion presents a summary of current (published) methods of grain refinement for Mg-Al alloys. Grain refinement may be achieved through: thermal methods (heating and chilling), chemical methods (melt additions) and mechanical methods. All three methods will be discussed below, but the focus of this thesis will be on chemical methods of grain refinement.

<u>2.4.1 – Carbon Addition (Chemical)</u>

The addition of carbon (to form Al_4C_3 nucleating particles) is currently one of the most popular and effective methods of reducing the grain size of Mg-Al alloys. Carbon may be added as a powder, but Motegi [12] found that the most effective carbon addition method was through the use of organic chlorides such as hexachloroethane (C_2Cl_6) and carbon tetrachloride (CCl_4). The use of C_2Cl_6 was advantageous because it offered melt degassing along with grain refinement. However, C_2Cl_6 caused health and environmental concerns as its use released chlorinated hydrocarbons. Also, C_2Cl_6 required relatively high melt temperatures [13], which thereby increased the oxidation of the melt. The high temperatures may also cause intake of iron from the crucible, which was undesirable from a corrosion standpoint. The grain refinement ability of C_2Cl_6 in AZ91E is demonstrated in Figure 2.6 [12]. This figure shows that AZ91E grains were reduced with successive addition levels of C_2Cl_6, up to 0.08 wt. %.

A new development in carbon addition with the use of wax-fluorspar(CaF_2)-C eliminated the environmental problems of C_2Cl_6, while also increasing refinement efficiency [13]. Karlsen et al. [13] studied the separate addition of wax-CaF_2, wax-CaF_2-C, C_2Cl_6, and a combination of 25% C_2Cl_6 and carbon into AZ91D. The results indicated that wax-CaF_2-C was the best refiner over long holding times (four hours) but was not the most effective for short holding times (five minutes). Another problem with carbon addition was that excess carbon may cause corrosion problems in the solidified Mg-Al alloy [11].

Some authors opted to add the Al_4C_3 nucleating particle directly to the melt. Xue et al. [14] directly added the Al_4C_3 refiner into pure magnesium at 0.5 wt. %, and found significant refinement of the grains. They found the refined grains to be generally equiaxed, and addition levels beyond 0.5 wt. % did not cause a further reduction in grain size. In addition, Lu et al. [15] used Al_4C_3 powder to refine Mg-3Al with great effectiveness (grain size reduction of 60%). The aforementioned studies illustrated that the addition of the Al_4C_3 particle directly to the melt may be more effective than formation of the particle by carbon addition.

The main theories regarding the grain refinement mechanism with carbon addition will now be presented. The common theory indicated that carbon interacted with the Al in the melt to form Al_4C_3 nucleating particles [16]. The alternative theory as to the role of carbon in grain refinement was presented by Jin et al. [17]. They proposed that there was no evidence of Al_4C_3 particles that acted as nucleation sites. Instead, carbon was rejected at the solid-liquid interface, which caused constitutional undercooling, and hence, grain refinement. This notion was disproved with the argument that, if segregation of carbon was the cause of grain refinement, then the carbon impurities in commercial Mg would cause refinement in Al-free Mg alloys as well [16].

The majority of authors support the idea of heterogeneous nucleation around Al_4C_3 particles as the method of grain refinement. For example, Han et al. [18, 19] developed an Al-C master alloy to refine AZ31, and proposed duplex nucleation with Al_4C_3 coated Al-Mn particles (refer to Section 2.4.6). Also, Pan et al. [20] refined AZ63B with an Al-1.5C master alloy and found Al_4C_3 nucleating particles. In addition, Lu et al. [15] supported the Al_4C_3 theory via theoretical calculations with Bramfitt's lattice disregistry equation [6].

2.4.2 – Superheating (Thermal)

The superheating refinement process involves heating the molten magnesium alloy melt to approximately 180-300 °C above its liquidus temperature for a short period of time (15 minutes) [12], then rapidly quenching it to the desired pouring temperature [11]. The idea of superheating grain refinement is closely linked to the phenomenon that occurs during carbon inoculation, as it works for Mg-Al alloys only [16].

A few mechanisms were proposed to explain superheating grain refinement. The first explanation was that Al-Fe or Al-Mn-Fe intermetallics precipitated from the melt during the cooling process and acted as heterogeneous nucleation sites [21]. The second theory was that potential existing nucleating particles at normal melt temperatures were too large and too few in number to act as effective nucleation sites. As a result, upon superheating, particles would dissolve in the melt and re-precipitate, upon cooling, as a large number of small and effective nucleation locations. A third major theory was that grain refinement occurred from Al_4C_3

nucleants that formed from the carbon in the steel crucible [11]. The Al_4C_3 nucleant theory was also supported by Motegi [12] who found that numerous Al_4C_3 nucleants formed during the superheating of AZ91E.
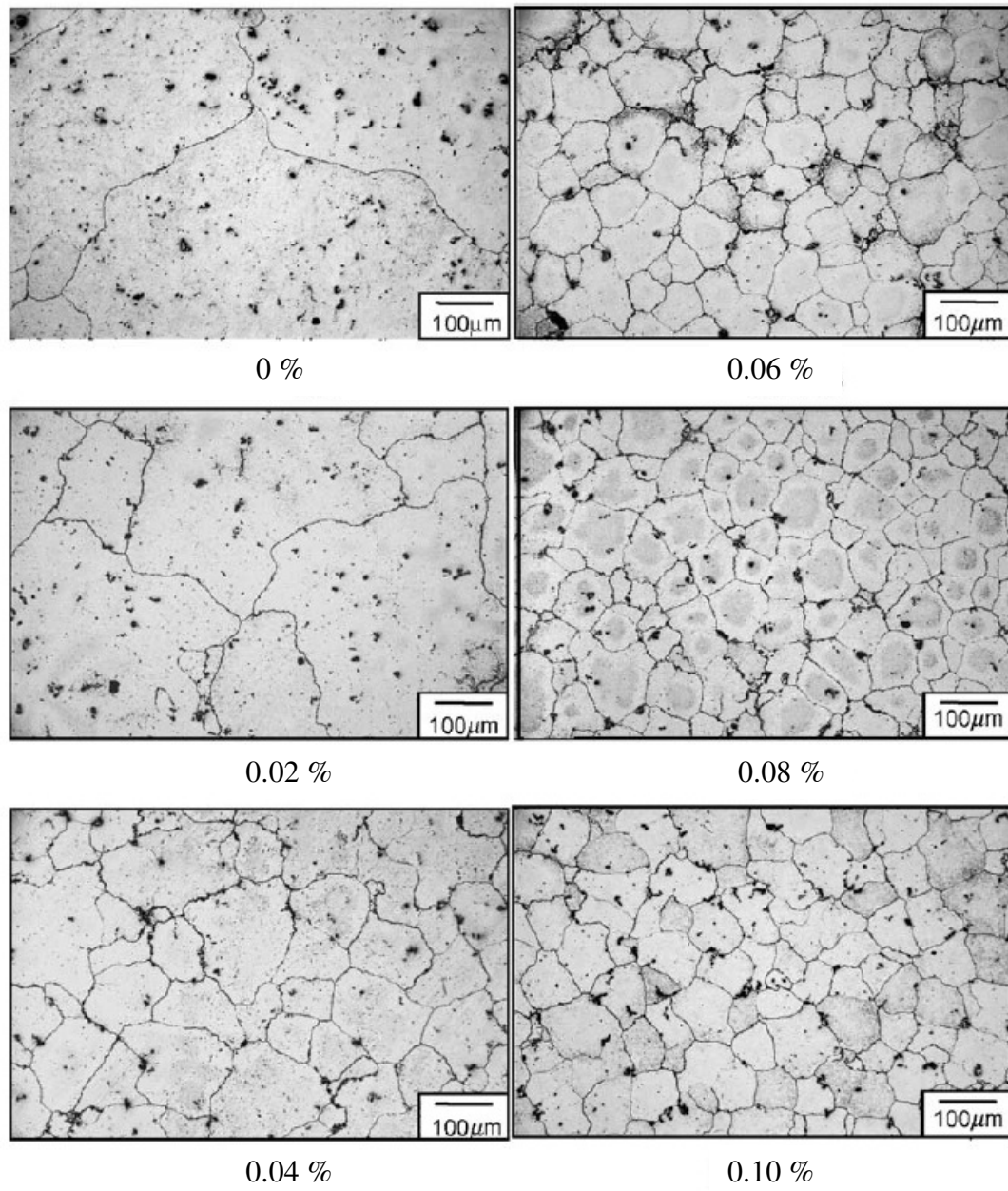
Figure 2.6: Effect of C_2Cl_6 (wt. %) addition on the grain size of AZ91E [12].

Typically, the grain refining effects were greatest with Al content greater than 9% [11]. Similar to superheating, Ning et al. [22] performed experiments on the effectiveness of various pouring superheats on reducing the grain size of AZ91D in a cast iron mold. It appeared that larger superheats caused greater grain growth, as illustrated in Figure 2.7, but the precise mechanism was not established.
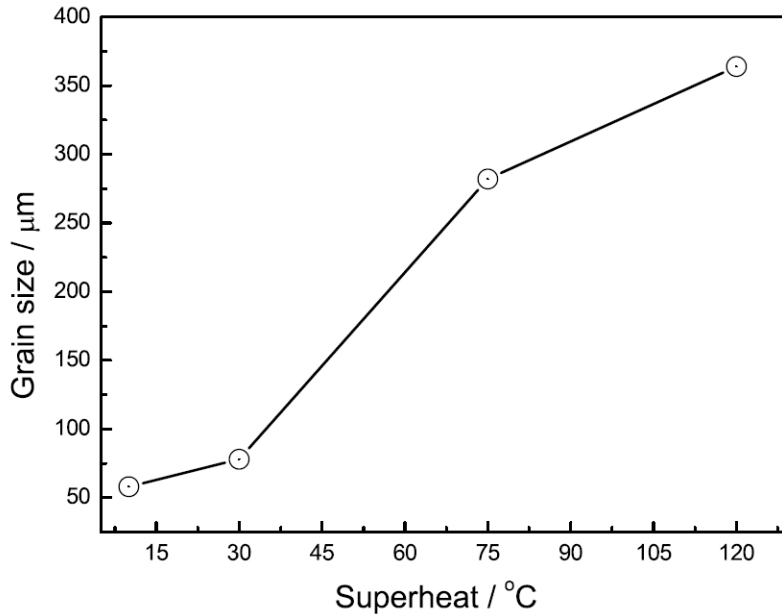
Figure 2.7: Effect of superheat on the grain size of AZ91 [22].

Despite the ability to reduce the grain size without adding a grain refiner, there are also some disadvantages with superheating, which are listed below.

- The grain refinement efficiency by superheating increases with higher manganese and iron content in the Mg alloy. However, increasing the Fe content for grain refinement purposes is detrimental to the corrosion resistance of the Mg product [11].
- Superheating requires rapid cooling from grain refinement superheat to pouring temperature; thus, it is not practical for large batches used in industry [11].
- Superheating requires additional time and power usage, which causes additional thermal stress on equipment and increased cost [11].

14

2.4.3 – Native Grain Refinement (Chemical)

Native grain refinement enables a reduction in the grain size depending on the purity level of the Mg alloy. This grain refinement effect was found to only occur in Mg-Al alloy systems [23]. In high purity Mg-Al alloys (made from 99.98% Mg and 99.99% Al), the underlying theory was that Al_4C_3 particles within the melt (resulting from carbon impurities in the metal) act as very effective heterogeneous nucleation sites, which caused the native grain refinement phenomenon [23].

High purity Mg-Al alloys are required because commercial Mg-Al alloys contain impurities such as Fe and Mn. These impurities form ternary Al–C–Fe or Al–C–Mn particles that lower the effectiveness of Al_4C_3 as a nucleating agent [23]. It was stated that the ternary particles were less potent than the Al_4C_3, hence lowering the nucleation effectiveness of the melt.

Comparisons between the effects of high purity and commercial Mg on the grain size are shown in Figures 2.8 and 2.9. Figure 2.8 illustrates that native grain refinement is extremely effective at low Al levels (0-3 wt. %), but no significant change in grain size occurs at higher Al levels (5-9 wt. %). The greater native grain refinement effect at lower Al levels is illustrated in Figure 2.9 (average grain size of commercial purity Mg-0.5Al was 2500 µm, and decreased to 1500 µm with a high purity alloy). Thus, it can be suggested that native grain refinement entails high cost due to purity of Mg and associated stringent process controls.
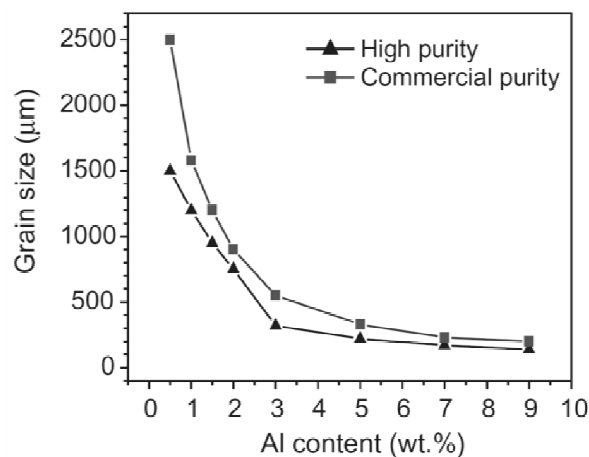
Figure 2.8: Effect of alloy purity on the grain size of Mg-Al alloys [23].

15
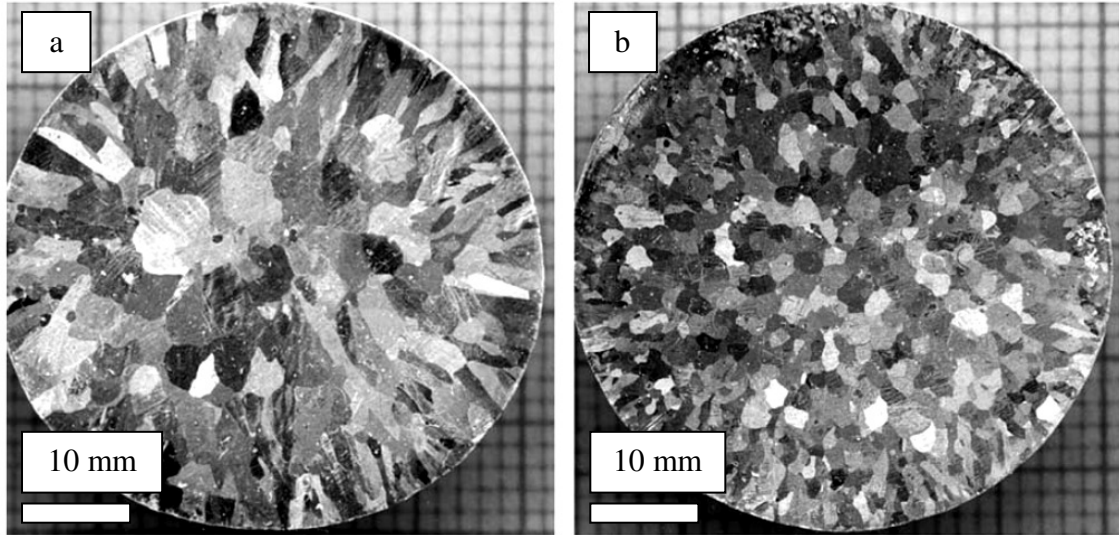
Figure 2.9: As-cast grain structure of Mg–0.5Al from:
a) commercial purity Mg – (average grain size: 2500 µm),
b) high purity Mg – (average grain size: 1500 µm) [23].

2.4.4 – Silicon Carbide Addition (Chemical)

Gunther et al. [24] studied the addition of SiC into AZ31 and found it highly effective in refining the alloy. In this alloy, a significant reduction in grain size was observed with 0.4 wt. % SiC addition. Earlier investigations on grain refinement of Mg-Al alloys (with Al in the range of 1-9%) suggest that SiC was most effective in the alloys with lower Al content.

With the observation of Mg_2Si, it was suggested that SiC enabled the formation of Al_4C_3, an effective nucleant [25, 26]. The SiC particles provide carbon, which would interact with the Al in the melt to form Al_4C_3. In addition to grain refinement, the remaining SiC contributes to increased wear resistance of castings due to the hardness of the SiC particle [27].

It was believed that the presence of Mn decreased the grain refining efficiency (i.e. reduction in grain size) of the SiC addition, as it likely formed less effective Al-Mn carbides [25]. Thus, it appears that SiC is a suitable refiner for Mg-Al alloys. However, compared with AZ31, the higher Al and Mn content in alloys such as AZ91 will decrease the effectiveness of SiC.

16

2.4.5 – Elfinal Process (Chemical)

The Elfinal process involves the addition of ferric chloride ($FeCl_3$) into the Mg alloy melt. This process causes the formation of Al-Fe or Al-Mn-Fe intermetallics in the melt that act as nucleation sites for primary Mg [9, 20, 28]. StJohn et al. [11] also observed that grains nucleated from Al- and Fe-rich intermetallics but found that the presence of Zr and Be would hinder the process as they were iron removal agents.

However, the major concerns for adding $FeCl_3$ are its toxicity and the potentially harmful release of chlorine and hydrochloric acid [11]. Furthermore, the addition of Fe into Mg decreases the corrosion resistance of an already corrosion-prone metal.

2.4.6 – Manganese Addition (Chemical)

Cao et al. [29] studied the efficiency of Mn grain refinement using various Al levels. Using 0.1-1% of an Al-60Mn master alloy, they found that grain refinement efficiency with Mn improved with increasing Al content, as shown in Figure 2.10. Further, Elsayed et al. [30] found that 0.5 wt. % Mn addition using a Mn-25Al master alloy decreased the average grain size of AZ91D from 215 µm to 174 µm.

The mechanism behind Mn grain refinement could be related to the Elfinal process, where Al-Mn-Fe-rich compounds act as potent nuclei. Another theory regarding the nucleation of grains with Mn addition was proposed by Du et al. [31]. They indicated the formation of an Al_4C_3 coating film around Al-Mn intermetallic compounds, which acted as nuclei for Mg grains. It was possible that the existing carbon impurities and the Al in the melt formed the Al_4C_3 coating film. A schematic illustrating this coating film theory is presented in Figure 2.11. From this figure, a layer of Al_4C_3 coating film initially forms on Al-Mn intermetallic compounds. This layer of Al_4C_3 eventually thickens and the entire coated particle becomes the nuclei for Mg grains. Du et al. [31] concluded that this coating theory explained the refining efficiency observed with Mn addition.
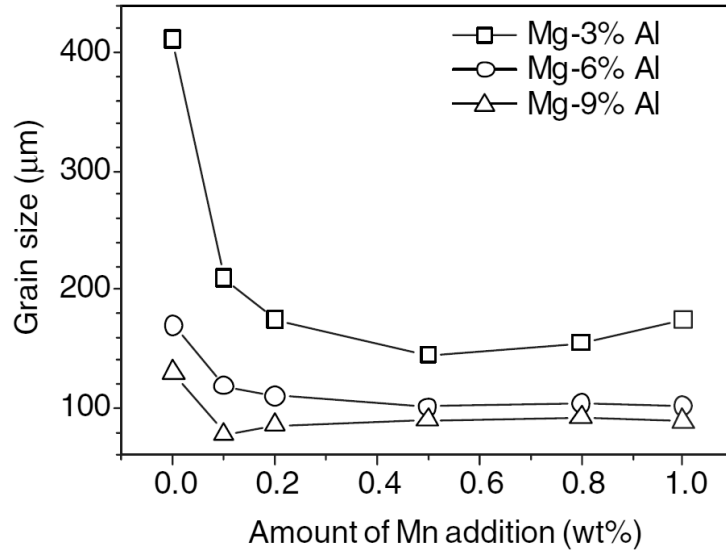
Figure 2.10: Effect of Mn content on the grain size of Mg-Al alloys [29].
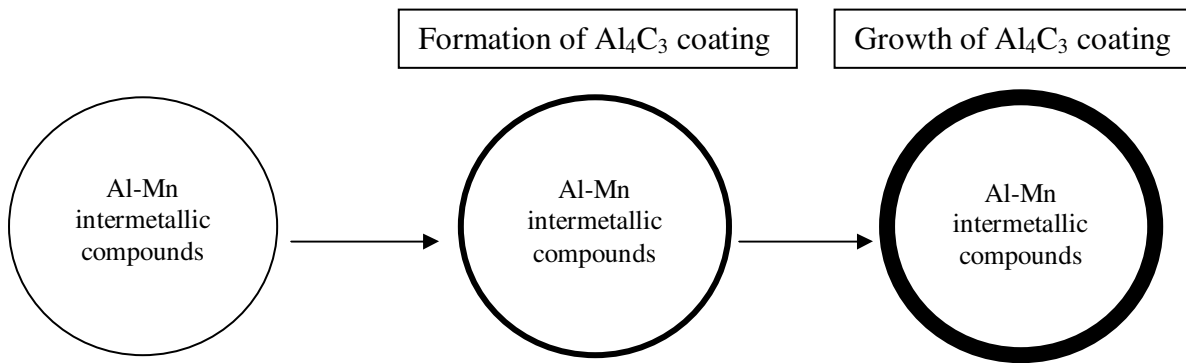
Figure 2.11: The Al_4C_3 coating film theory [31].

2.4.7 – Titanium Addition (Chemical)

The use of titanium (Ti)-boron (B)-based refiners, such as the commercially available Al-5Ti-1B (Tibor), is very popular in Al alloys but not so much in Mg alloys. Grain refinement occurs with Ti-B-based refiners due to the formation of the TiB_2 particle. Several theories were proposed to explain the grain refinement effect of titanium.

Recently, there has been research on the viability of adding master alloys that form TiB_2 particles within Mg melts. These popular master alloys are often Al-Ti-B based [32]. For instance, Wang et al. [32] used an Al-4Ti-5B master alloy at 0.3 wt. % to successfully refine the grains in

18

the AZ31B alloy. The reduction in grain size was significant, with a decrease of approximately 90% (Figure 2.12). Through theoretical calculations, the lattice disregistry between nucleant and primary Mg should be less than 15% (Section 2.2.3). With TiB_2, the lattice disregistry is 5.6%. Furthermore, energy dispersive X-ray (EDX) analysis had shown that the TiB_2 particles acted as heterogeneous nuclei.

There is also published research showing that TiB_2 particles caused grain refinement by growth restriction. For instance, Wang et al. [33], using an Al-TiB_2 master alloy, formed an AZ91/TiB_2 metal-matrix composite with the addition of 7.5 wt. % TiB_2 particles. After solidification, they noticed that the TiB_2 particles were moved to the last solidified region with the eutectic $Mg_{17}Al_{12}$. Furthermore, very few TiB_2 were observed at the center of Mg grains. As a result, Wang et al. concluded that TiB_2 refined AZ91 primarily through growth restriction. Therefore, the refinement mechanism of TiB_2 does not seem to be solely heterogeneous nucleation or growth restriction, but a combination of both. Consequently, it would be worthwhile to further study the nucleation mechanism of TiB_2 in an alloy such as AZ91, via the direct addition of the TiB_2 particle. The refinement efficiency of this TiB_2 particle in AZ91 should be studied at lower addition levels as a grain refiner, and not as a metal-matrix composite (e.g. ≤ 1 wt. % compared with 7.5 wt. %).
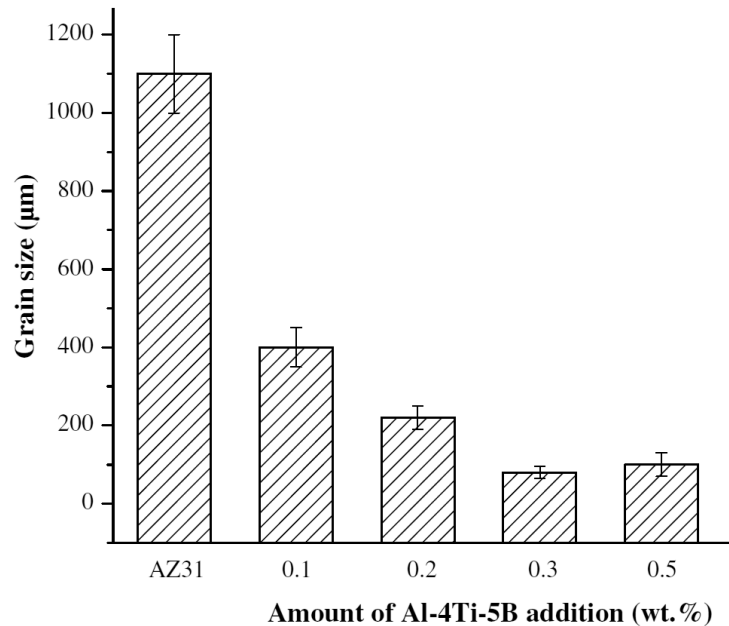
Figure 2.12: Effect of Al-4Ti-5B master alloy level on the grain size of AZ31 [32].

19

<u>2.4.8 – Calcium Addition (Chemical)</u>

Calcium (Ca) has been explored as a grain refiner by various researchers due to its relatively high GRF value, but results are contradicting. According to Table 2.1, Ca has a high GRF that is only second to Zr. The work of Lee et al. [9] showed Ca to be an excellent grain refiner for pure Mg. The grain refinement effect of a cast sample of pure Mg with Ca addition is shown in Figure 2.13. Lee et al. [9] found that Ca content beyond 0.4 wt. % did not produce significant grain refinement. Furthermore, Ca was also found to be a viable refiner for Mg-Al alloys such as AZ91D as shown by Li et al. [34, 35].

Contrary to the observed grain refinement with Ca addition, some researchers found a reduction in mechanical properties of Mg alloys containing Ca. This may have occurred due to an increase in grain size and the formation of an Al_2Ca intermetallic phase along the grain boundaries [36, 37]. The decrease in mechanical properties with Ca addition is illustrated in Figure 2.14.
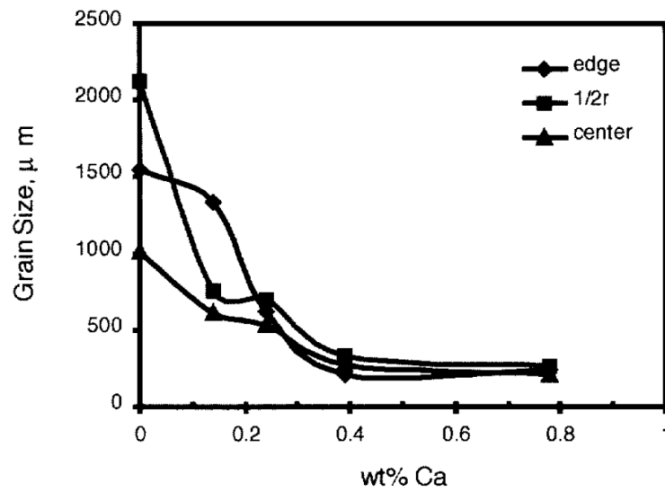
Figure 2.13: Effect of Ca on the grain size of pure Mg. The top-right legend indicates the sample position at which grain size was measured. A cylindrical mold was used, thus grain size was measured at the edge, between the edge and center (1/2r) and at the center [9].
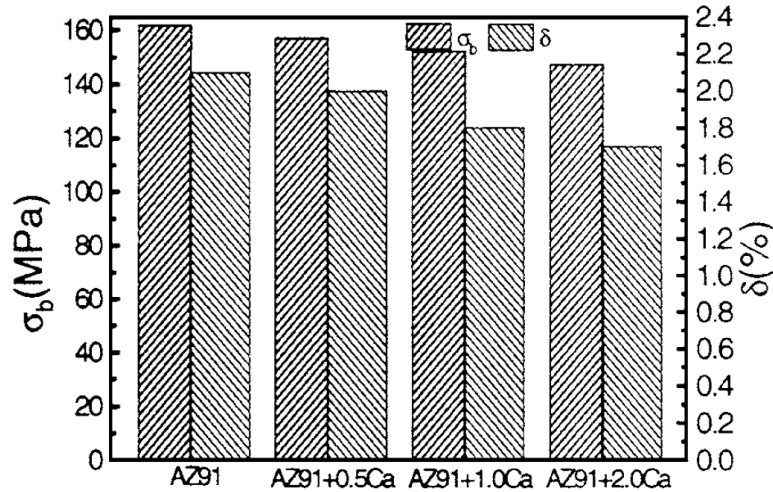
Figure 2.14: Effect of Ca addition on the tensile strength (σ_b) and elongation (δ) of AZ91 [36].

Similarly, the work of Elsayed et al. [30] with AZ91D indicated a decrease in hardness with Ca addition. They found that a soft Al_2Ca phase precipitated in the same region as the hard β-$Mg_{17}Al_{12}$ intermetallic phase. Microhardness tests confirmed the presence of the softer phase. The hardness of the β-intermetallic in unmodified AZ91D was 68 HV, which decreased to 52 HV with 1.5 wt. % Ca addition. Furthermore, an increase in grain size with Ca levels up to 1 wt. % was also observed. The etched surfaces from an AZ91D casting with 0.5 and 1.0 wt. % Ca respectively are shown in Figure 2.15. With a change in the concentration of Ca from 0.5 to 1.0 wt. %, the grain size increased from 284 µm to 846 µm [30]. It appears that Ca is not a reliable grain refiner for Mg-Al alloys despite its high GRF value.
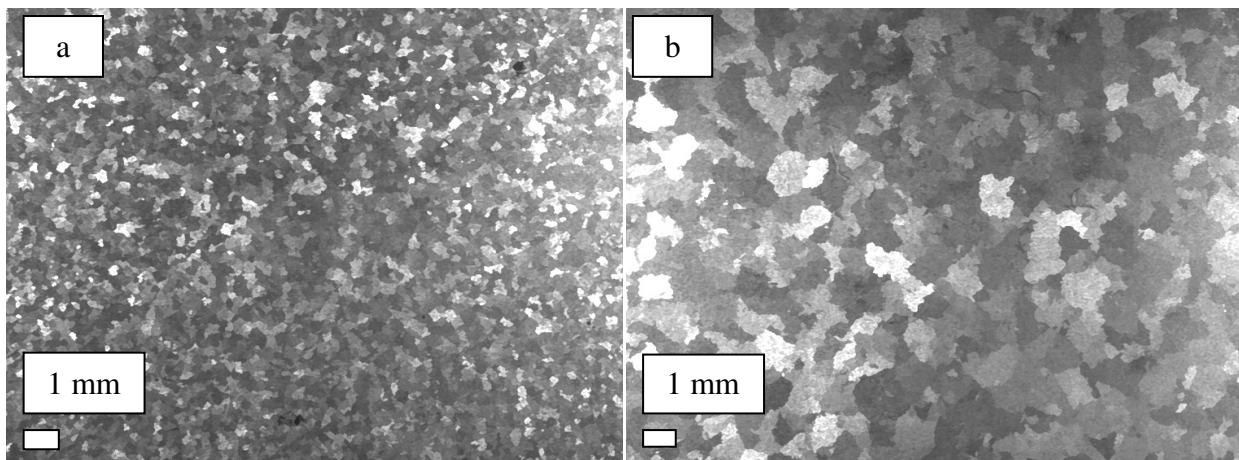
Figure 2.15: As-cast grain structure of AZ91D with calcium addition:
a) AZ91D + 0.5 wt. % Ca, b) AZ91D + 1.0 wt. % Ca [30].

21

2.4.9 – Strontium Addition (Chemical)

The use of strontium (Sr) as a grain refiner has been studied, and two theories have been proposed. The first theory, as stated by Yang et al. [38], concluded that Sr caused grain refinement because of the low solubility (0.11%) of Sr in Mg. This low solubility allowed for Sr to enrich the liquid ahead of the solid interface, causing constitutional undercooling (or grain growth restriction).

With respect to the second theory, Pan et al. [39] believed that no experimental evidence had shown that Sr grain refines via only grain growth restriction. They found a high concentration of Sr particles around the grain boundaries, which suggested solute rejection. In addition, they found the particles in the center of grains to be rich in Al, Fe, Mn, Mg, and Sr. Al-Fe-Mn intermetallic compounds were found to act as nucleation sites from superheating grain refinement. Thus, they proposed that Al-Fe-Mn and Mg-Sr compounds precipitated from the melt, then combined to form heterogeneous nucleation particles [39]. Sr seems able to refine Mg alloys, but its lower GRF value may deem it not as effective as other addition elements.

2.4.10 – Antimony and Cerium Addition (Chemical)

The addition of 0.5 wt. % Sb to AZ64 by Ma et al. [40] led to refinement of the Mg grains and the secondary phases {$Mg_{12}(Al, Zn)_{17}$ and $Mg_{21}(Zn, Al)_{17}$} of the alloy, which resided along the grain boundaries. Since the solid solubility of antimony (Sb) in Mg is very low, the added Sb would contribute to constitutional undercooling as the solute is rejected at the solid-liquid interface during solidification [40].

Li et al. [41] observed that a combination of cerium (Ce) and Sb formed a CeSb phase within the AZ91D melt, which led to refinement of the Mg grains. According to the lattice disregistry theory [6], if a misfit between crystal faces is less than 15%, then the new compound may act as a nucleation site. The misfit of the crystal face of the CeSb phase is 0.09% with the α-Mg phase, and therefore acts as a nucleant for the primary Mg grains [41]. Furthermore, the high melting point of the CeSb phase will cause it to precipitate first during solidification. Thus, some of the

CeSb phase will be rejected to the solid-liquid interface, causing grain growth restriction [41]. Although Sb and Ce may be effective grain refiners, their high cost would deter commercial use.

2.4.11 – Mechanical Processes

The mechanical methods of grain refinement generally involve the agitation of the melt to break apart developing dendrites. These broken dendrites would spread in the melt to act as additional heterogeneous nucleation sites. Lee et al. [9] determined the process was most effective at high temperatures, around the levels used for superheating grain refinement. These higher temperatures increased the rate of formation of the nucleant phase (likely Al_4C_3) throughout the melt, promoting grain refinement [9]. Mechanical agitation at superheating temperatures appeared to enable a combination of broken dendrites and Al_4C_3 particles to act as nucleation sites. Similarly, Liu et al. [42] proposed that vibration caused cavities to form in the melt, which attracted impurity particles and enabled them to become nucleation sites.

Some researchers found coarse dendritic Mg grains in untreated melts, but after melt agitation, these coarse grains were modified to a spherical shape [42, 43]. The differences in grain shape with and without mechanical vibration with AZ91D are shown in Figure 2.16. While mechanical agitation appeared to work well in refining Mg grains, it requires additional equipment and processing, thus increasing the cost of the final product.
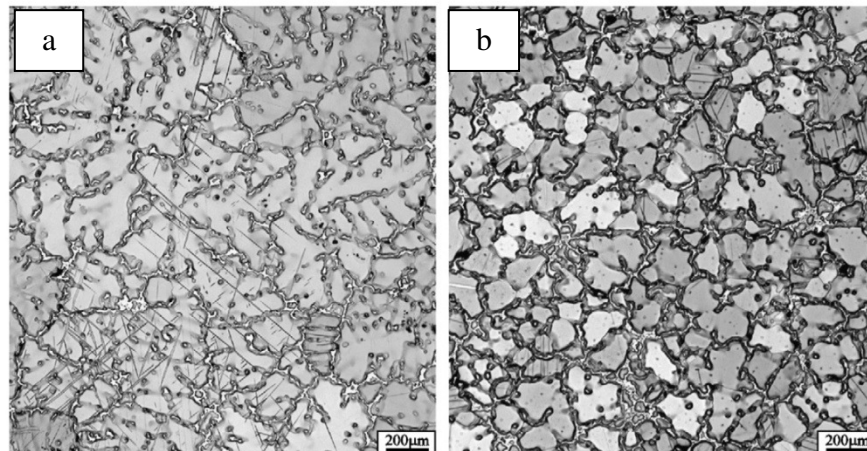
Figure 2.16: As-cast microstructure of AZ91D magnesium alloy:
a) without vibration, b) with vibration [42].

2.5 – Potential Grain Refiners for Mg-Al Alloys

Various grain refinement methods have been used with success in pure Mg and Mg-Zn alloys. However, the methods have not been studied in Mg-Al alloys. Part of this research is, in effect, an attempt to study their viability for Mg-Al alloys.

2.5.1 – Vanadium Addition (Chemical)

Buha [44] observed a reduction in the grain size of Mg-Zn alloys with the addition of vanadium (V). The interesting aspect about this addition was that V has a body-centered cubic (BCC) crystal structure, while Mg has a hexagonal close-packed (HCP) structure. It was stated that, even though the crystal structures were dissimilar, heterogeneous nucleation occurred because V particles were the best nucleation sites available during solidification [44]. Figure 2.17 shows the difference in grain size with the addition of 0.3 wt. % V for a Mg-Zn alloy, in which the microstructure appears noticeably finer. The addition of V has not been studied in Mg-Al alloys. Thus, further study is warranted, but V is a relatively expensive element that may discourage its commercial use.
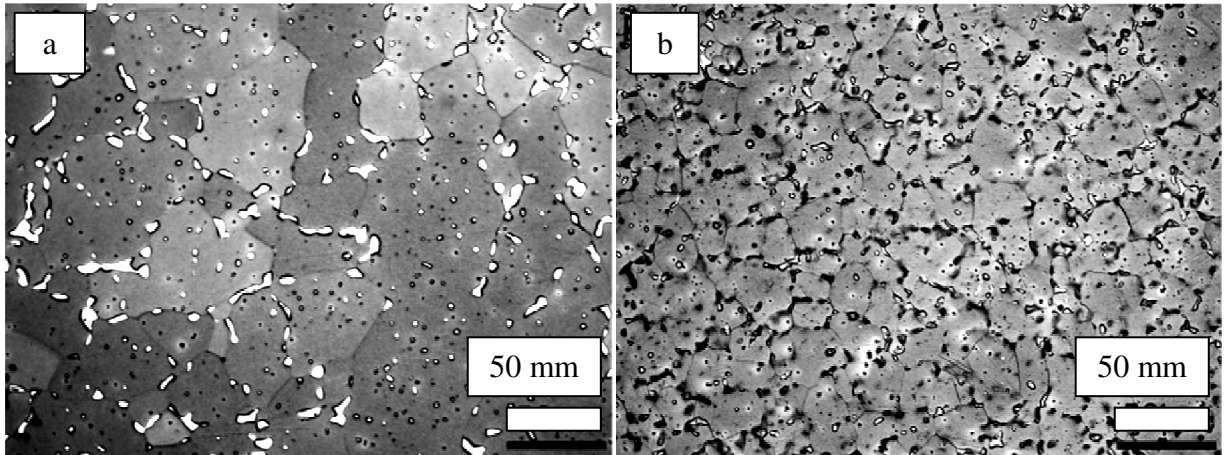
Figure 2.17: Grain structure of: a) Mg–Zn, b) Mg–Zn–0.3V [44].

24

2.5.2 – Zinc Oxide Addition (Chemical)

Fu et al. [45] identified ZnO as a potential grain refiner from the edge-to-edge crystallographic model. ZnO has a HCP crystal structure with lattice parameters similar to those of Mg, as shown in Table 2.2. When ZnO is added to molten Mg, part of ZnO is reduced to Zn as shown in Equation 2.3. Fu et al. [45] believed that the Zn contributed to grain growth restriction, while the remaining ZnO provided suitable heterogeneous nucleation sites.

The addition of 3 wt. % ZnO effectively reduced the grain size of pure Mg by 63%, as shown in Figure 2.18. Also, the addition of 1 wt. % ZnO to Mg-3Zn moderately reduced the grain size by 26% [45]. A disadvantage with ZnO addition is the formation of MgO. If not removed (through filters or skimming), the entrapped MgO may reduce castability and mechanical properties of the casting. ZnO may be suitable for reducing the grain size in Mg-Al alloys such as AZ91 based on its grain refinement efficiency in pure Mg and Mg-3Zn.

$$Mg + ZnO \rightarrow Zn + MgO \tag{2.3}$$

Table 2.2: Lattice parameters of Mg and ZnO [46].

	Lattice Parameters	
	a (Å)	c (Å)
Mg	3.209	5.211
ZnO	3.265	5.219
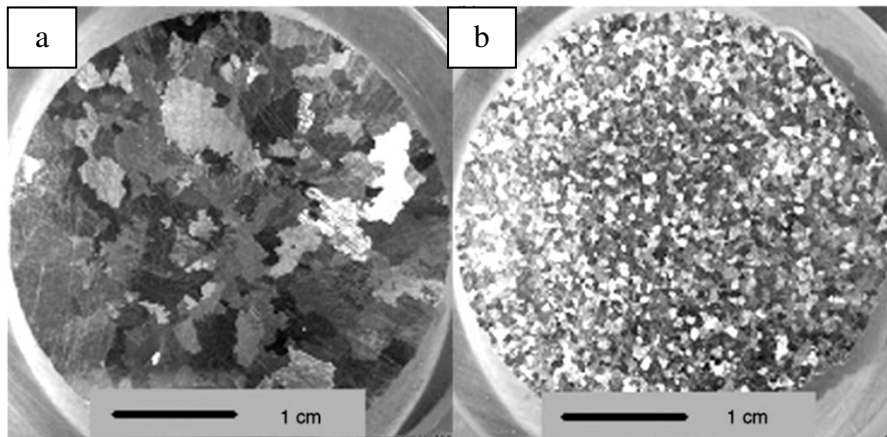
Figure 2.18: Grain structure of: a) pure Mg, b) pure Mg + 3 wt. % ZnO powder [45].

2.6 – Effect of Grain Refinement on Hot Tearing

A hot tear is an irreversible crack forming in the solidifying semi-solid metal. Hot tears formed mainly as a result of thermo-mechanical stresses (thermal-volumetric contraction, geometric constraints and sharp corners) [47]. Various studies have examined hot tearing in Mg alloys and some solutions have been proposed to minimize hot tear formation, including mold heating and grain refinement.

Bichler et al. [47] studied the effect of permanent mold heating on hot tearing severity with AZ91D. They found that raising the permanent mold temperature from 140 °C to 380 °C virtually eliminated any macro cracks. This appears to be a very simple solution, but it would not be viable when a specific cooling rate is required or mold heating is impractical. The solution in these cases would be to reduce or eliminate hot tears through grain refinement.

Metz et al. [48] studied hot tearing in Al alloys and proposed that refined grains reduced hot tearing tendencies through the alloy's increased ability to resist strain. A grain refined alloy would be free of long dendrite arms and the resultant small grains would move relative to each other to accommodate the strain. In essence, small grains limit the influence of one grain onto another, with alloy deformation focused near the local region of the shear stress. When a hot tear forms, it is the result of dendrite separation to accommodate solidification strain [48].

Easton et al. [49] also supported the fact that fine grains decreased the hot tearing susceptibility. They stated that grain refinement delayed the onset of interdendritic feeding, which could decrease hot tearing. It was also mentioned that hot tearing susceptibility may be increased if the size of refined globular grains was further decreased. If globular grains became too small, then semi-solid metal permeability lowers and hot tearing susceptibility increases. Easton et al. did not explain the correlation between permeability and hot tearing susceptibility.

Impact of Literature Review – Scope of the Thesis

The foregoing literature review suggested that the direct addition of Al_4C_3, TiB_2 and ZnO should be studied for the following reasons. Firstly, the direct addition of Al_4C_3 particles into AZ91E had not yet been studied. Secondly, TiB_2 had been used in AZ91 at a high addition level (7.5 wt. % to make a metal-matrix composite) but not as a refiner at lower addition levels (e.g. 0.1-1 wt. %). Thirdly, ZnO additions effectively refined grains in pure Mg and Mg-3Zn and appeared to be promising for Mg-Al alloys. All three additions were chosen due to their low cost, previous grain refinement effectiveness and lack of harmful emissions. Based on these considerations, it was envisaged that the proposed research should focus on the grain refinement of AZ91E using these compounds. The crystal structures and lattice parameters for the melt additions are presented in Appendix 1. Also, a summary of results based on the refining techniques discussed in the literature review is presented in Appendix 2.

CHAPTER 3 – EXPERIMENTAL PROCEDURE

This section describes the procedures used to perform the two types of casting processes: graphite mold and permanent mold castings. In addition, the methods for hot tear testing, thermal analysis, microscopy, fractography and hardness testing are discussed.

3.1 – Materials

3.1.1 – AZ91E

In this thesis, the AZ91E alloy was used as the base material. The AZ91 alloy is popular due to its low cost and strength (die-cast yield strength: 160 MPa, ultimate tensile strength: 250 MPa) [50]. There are letter designations associated with AZ91 alloys ranging from A-E, which indicate composition and maximum allowable impurity levels [50]. This alloy is used in a variety of products, such as electronic device casings. A phase diagram for the Mg-Al system is presented in Appendix 3.

The AZ91E base alloy was received as ingots and the composition (actual batch analysis from the supplier) of the alloy is given in Table 3.1.

Table 3.1: Composition of AZ91E Alloy (wt. %).

Mg	Al	Zn	Mn	Si	Cu	Fe	Ni	Other
90.18	8.7	0.53	0.23	0.05	0.006	0.003	0.0008	< 0.3

3.1.2 – Grain Refiners

The Al-5TiB$_2$ and Al-Al$_4$C$_3$ grain refiners were received as rods. The method for the production of each master alloy is described in Appendix 3. The ZnO grain refiner was received as a powder at 99% purity, with a median size of 0.52 ± 0.38 µm. A representative particle size distribution (accurate to two decimal places) and trace analysis for the ZnO powder are also shown in Appendix 3.

3.2 – Graphite Mold Casting

Castings produced with graphite molds were used to establish the effectiveness of the three refiners used in this study. Graphite molds were used because of their low thermal conductivity, as slow cooling rates (~1.5 °C/s) were required to reduce the effect of large undercooling on grain refinement. The AZ91E alloy was melted in a steel crucible with a carbon dioxide (CO_2) cover gas at a flow rate of 0.28 m³/hour. The CO_2 cover gas was used to prevent the oxidation of the molten AZ91E alloy.

The master alloys were cut to the desired weight and pre-heated to remove moisture before they were added to the melt. The ZnO powder was added to the melt in a plastic bag to prevent loose powders from scattering in the air before reaching the molten metal. All refiners were added to the melt at 730 °C and stirred for 30 seconds using a steel propeller coated with boron-nitride. The melt was held at 730 °C for 5, 10, and 20 minutes [15, 33] to study any fading effects. The pour was made with a ladle coated with boron-nitride, and any oxide layers that formed on the top layer of the melt were skimmed before pouring. The pour was made at a temperature of 720 °C.

The melt was poured into an open graphite mold pre-heated to 750 °C. A photograph and a schematic of the casting are shown in Figure 3.1. The inner diameter of the graphite mold was 40 mm, with a wall thickness of 15 mm and a depth of 50 mm. A steel plate with a thermocouple hole covered the top of the mold after pouring. A K-type thermocouple was then inserted into the mold cavity 20 mm from the top. The graphite mold casting parameters are summarized in Table 3.2. For Al-5TiB$_2$ and Al-Al$_4$C$_3$ refiners, small addition levels up to 1 wt. % were used to test their effectiveness. With ZnO, the addition levels were based on those used by Fu et al. [45]. All castings were performed twice to ensure repeatability. The graphite mold castings were used to determine the optimal addition level and holding time (to yield the smallest average grain size) for each refiner.
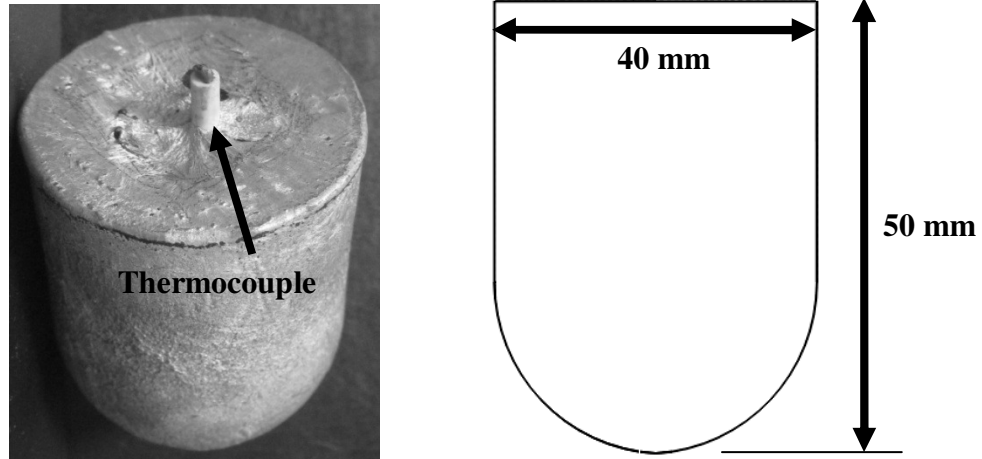
Figure 3.1: Photograph and schematic of the graphite mold casting.

Table 3.2: Summary of graphite mold casting parameters.

Pouring Temperature (°C)	Graphite Mold Temperature (°C)	Holding Time (min)	Al-Al$_4$C$_3$ / Al-5TiB$_2$ Addition (wt. %)	ZnO Addition (wt. %)
720	750	5, 10, 20	0.1	1
			0.2	2
			0.5	3
			1	4

3.3 – Permanent Mold Casting and Hot Tear Testing

Permanent mold casting is a process where molten metal is poured into a non-expendable mold, such as one made from steel. The mold is usually coated with a graphite or ceramic slurry to assist with thermal insulation and ease of casting ejection. This permanent mold process usually produces stronger castings as compared to lost foam or sand castings because of higher cooling rates. The castings are also of higher dimensional accuracy. This is attributed to the molds, which are accurately machined and are strong, compared with coarser and more flexible sand molds [51].

30

Despite the advantages of the permanent mold, some alloys are prone to a serious problem with this casting process called hot tearing. Hot tears are irreversible cracks that form during solidification when the alloy is in a semi-solid state. Geometric restrictions such as corners prevent the casting from freely contracting and provide localized stress concentrations, which promote tears.

The permanent mold used in this thesis, depicted in Figure 3.2, was designed to induce hot tears at the indicated 90° corner. In this mold, there was also an end restraint that prevented contraction of the molten metal. This end restraint further helped induce hot tears along with the 90° corner. The mold was made from H13 tool steel and coated with Foseco Dycote 36 for ease of casting ejection and thermal insulation.

The effectiveness of the grain refiners in mitigating the hot tearing susceptibility of AZ91E alloy during permanent mold casting was investigated. The castings were produced using the optimal addition level for each grain refiner. These optimal addition levels, shown in Table 3.3, were determined from the graphite mold castings. All grain refiner additions were added to the melt at 740 °C and stirred using a steel propeller coated with boron-nitride for 30 seconds. The pouring temperature used for the permanent mold castings was 720 °C. Since the results from graphite mold castings indicated that holding time had no effect, the shortest holding time of five minutes was used. The degree of hot tearing (hairline or wide and long cracks) was also observed for each casting.

Table 3.3: Permanent mold casting parameters.

	Grain Refiners		
	$Al\text{-}Al_4C_3$	$Al\text{-}5TiB_2$	ZnO
Pouring Temperature (°C)	720	720	720
Mold Temperature (°C)	180	180	180
Optimal Addition Level (wt. %)	0.1	0.2	2
Holding Time (min)	5	5	5
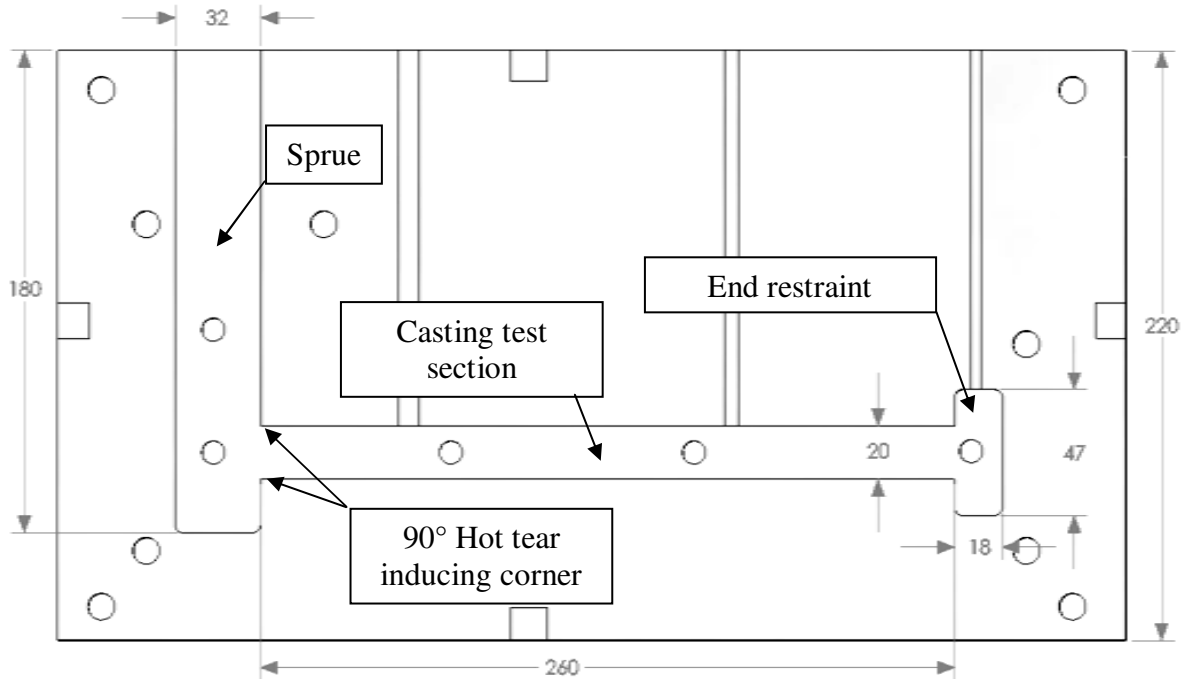
Figure 3.2: Drawing of the permanent mold, all dimensions in mm.

3.4 – Thermal Analysis

K-type thermocouples used in these casting trials were connected to a Daytronic System 10 data acquisition unit. The data were collected at 7 readings per second. Cooling curves were generated for each casting condition to determine undercooling (UC) and freezing range (FR). These parameters are indicated using a cooling curve of AZ91E (Figure 3.3).

3.5 – Optical Microscopy (OM)

Samples for microscopy (OM and SEM) were taken near the bottom part of the casting as shown in Figure 3.4. The samples were first polished using successively finer silicon carbide discs (600, 800 and 1200 grit), and finally with a diamond suspension compound of 3 µm. An etchant consisting of 15 vol. % acetic acid, 10 vol. % distilled water and 75 vol. % ethyl alcohol was used to reveal the grain boundaries. The samples were slightly agitated in the etching solution for two minutes, then quickly rinsed with ethyl alcohol and dried using compressed air.
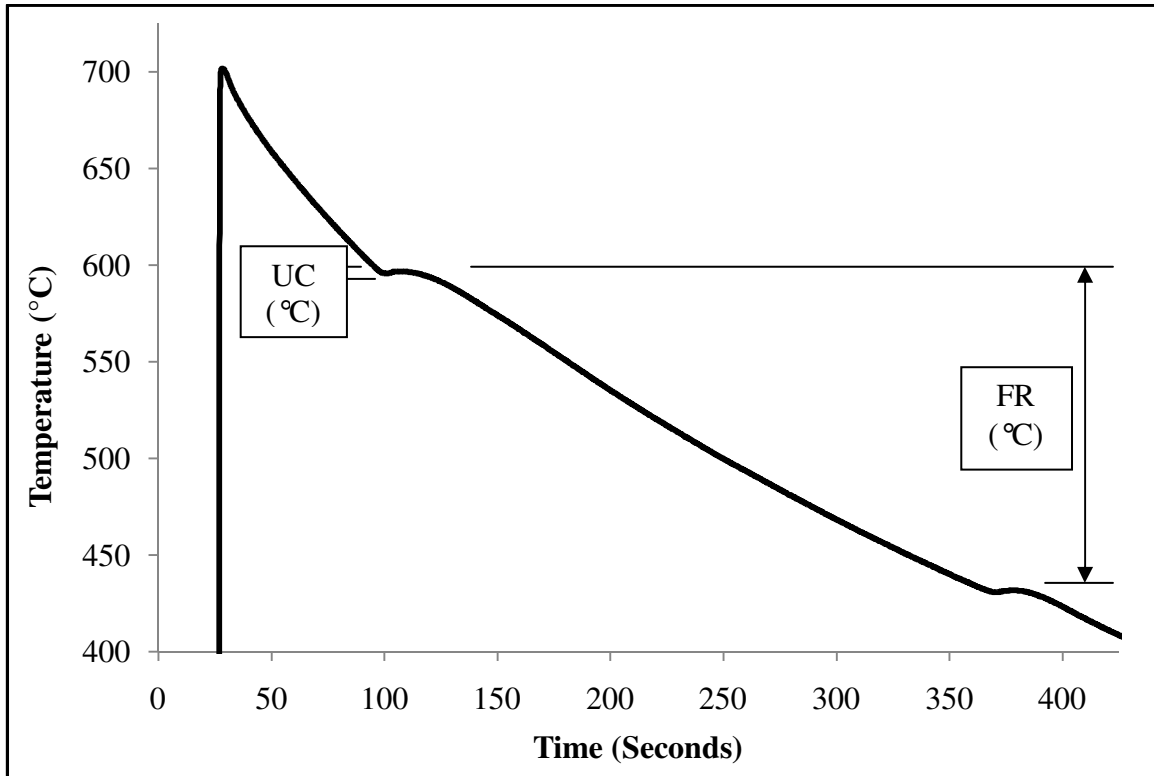
Figure 3.3: Cooling curve of AZ91E in a graphite mold.

The etched samples were observed using an optical microscope. Grain size was measured using the linear intercept method. A minimum of 100 measurements were taken for each sample, with an accuracy of one decimal place. The grain sizes were rounded to the nearest whole number for clarity.

3.6 – Scanning Electron Microscopy (SEM)

Subsequent to optical microscopy, the samples (Figure 3.4) were examined at the same locations using an SEM. The JEOL SEM enabled back-scattered electron imaging at a working distance of 11 mm and a potential of 20 kilovolts. Also, SEM fractography analysis was performed on hot tear samples to examine the crack propagation and phases present along the crack boundaries.

3.7 – Hardness Testing

A total of six Rockwell E readings were taken for each hardness sample, with measurements taken on the face of a rectangular slice of the casting (Figure 3.4). Vickers microhardness results were also obtained using the same samples.

Hardness measurements

Microscopy surface
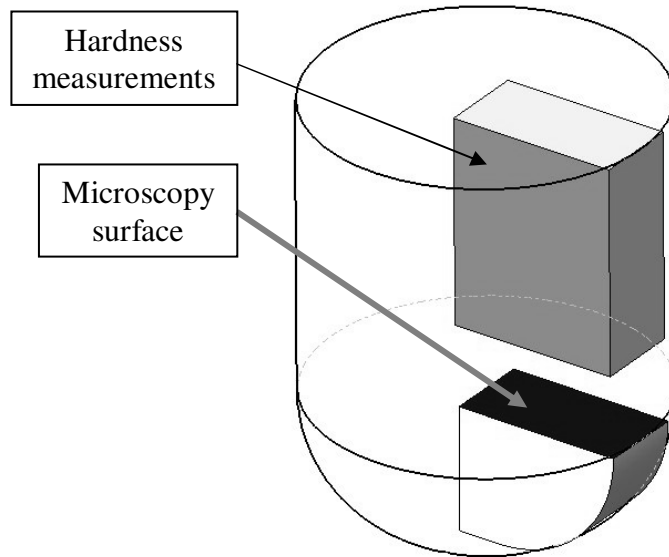
Figure 3.4: A schematic of the graphite mold casting.

CHAPTER 4 – RESULTS AND DISCUSSION

The following section presents and analyzes the results of the casting trials performed with the three refiners: Al-5TiB$_2$, Al-Al$_4$C$_3$ and ZnO. All analyses were performed on graphite mold castings unless stated otherwise. Also, all error bars presented in graphs represent the standard deviation of the measurements. The major components of the microstructure in the base AZ91E are shown in Figure 4.1. These parts consist of the primary α-Mg and β-Mg$_{17}$Al$_{12}$ phases.
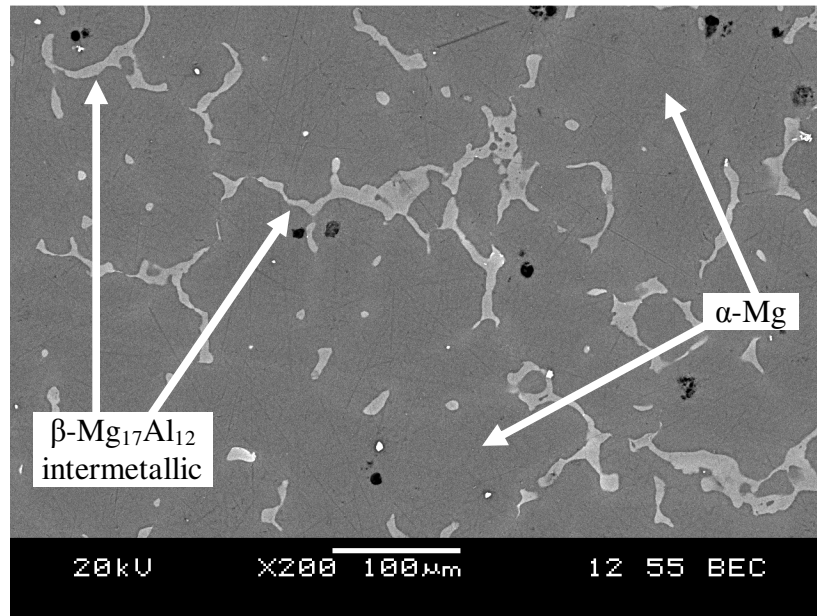
Figure 4.1: Microstructure of the base AZ91E.

4.1 – Microscopy

4.1.1 – Grain Size Measurement

The grain size of graphite mold cast AZ91E alloy (without the addition of a grain refiner) was 782 µm. This was used as the reference mark for graphite mold castings with grain refiner additions. The optimal level for each refiner corresponds to the addition level resulting in the smallest average grain size. Figures 4.2-4.4 show the etched as-cast grain structure for the base alloy and the grain refined castings for all addition levels and holding times. A listing of all measured grain sizes are presented in Tables 4.1 and 4.2.

4.1.1.1 – Al-5TiB$_2$ Addition

The variations of average grain size with holding times for various levels of Al-5TiB$_2$ are shown in Figure 4.5. It was observed that the addition of Al-5TiB$_2$ resulted in a significant reduction in grain size. The grain sizes were relatively smaller at lower levels (0.1 and 0.2 wt. %) compared with higher levels (0.5 and 1 wt. %). The best addition level for Al-5TiB$_2$ was 0.2 wt. %, which resulted in an average grain size of 318 µm (reduction of 59%). For all Al-5TiB$_2$ levels, it was observed that the holding time did not influence the grain size of AZ91E. The absence of fading indicated that the master alloy was effective up to 20 minutes holding time.

An analysis of variance (ANOVA) indicated the significant reduction of grain size at all addition levels (P$_{\alpha max}$ > 99.9%, reject the null hypothesis that the treatments had no effect if P$_{\alpha max}$ > 90%), while holding time had no effect (P$_{\alpha max}$ < 75%, accept null hypothesis if P$_{\alpha max}$ < 85%). Furthermore, 0.2 wt. % of Al-5TiB$_2$ was chosen instead of 0.1 wt. %, as the former had a significantly lower average grain size (P$_{\alpha max}$ = 95.2%). Ideally, a lower addition level is desirable for reduced cost. Details of the ANOVA are shown in Appendix 4. Moreover, compared to research by Wang et al. [33], the reduction in grain size was 71% for their metal-matrix composite with 7.5 wt. % TiB$_2$. The grain size reduction (59%) achieved with TiB$_2$ in the current research is significant since a very small amount of refiner was added.

4.1.1.2 – Al-Al$_4$C$_3$ Addition

A significant decrease in grain size occurred for all levels of Al-Al$_4$C$_3$ (Figure 4.6). An analysis of variance (ANOVA, Appendix 4) indicated the significant reduction of grain size at all addition levels (P$_{\alpha max}$ > 99.9%), while holding time had no effect (P$_{\alpha max}$ = 83.7%). The lack of fading indicated that Al-Al$_4$C$_3$ addition was also effective up to 20 minutes. The addition of 0.1 wt. % Al-Al$_4$C$_3$ produced the smallest average grain size of 282 µm (reduction of 64%).

In comparison, the addition of 0.5 wt. % Al$_4$C$_3$ to pure Mg resulted in a grain size reduction of 87% [20]. It appears that Al$_4$C$_3$ addition is a viable alternative to C$_2$Cl$_6$ (refer to Section 2.4.1) as it achieved grain refinement in AZ91E without the release of chlorinated hydrocarbons.

4.1.1.3 – ZnO Addition

The grain size of AZ91E significantly decreased for all addition levels and holding times with ZnO addition. Figure 4.7 shows a graph of average grain size versus holding time for all ZnO concentrations. Comparing holding times at each addition level, there was no significant change in grain size. The absence of fading indicated that ZnO was also effective up to 20 minutes. The addition of 2 wt. % ZnO produced the smallest average grain size of 192 µm, which denoted a reduction of 75%. This level with ZnO represented the smallest percentage reduction in grain size achieved out of the three refiners used in graphite mold castings.

Analysis of variance (ANOVA), which is discussed in Appendix 4, showed a significant reduction in grain size at all addition levels ($P_{\alpha max} > 99.9\%$), while fading was not observed ($P_{\alpha max} < 75\%$). Furthermore, 2 wt. % was chosen as the best addition level for ZnO addition as it had a significantly lower average grain size ($P_{\alpha max} = 95.1\%$) compared with 1 wt. % ZnO. In addition, the reduction in grain size with 2 wt. % ZnO in AZ91E was much greater than the 26% reduction observed with 1 wt. % ZnO in Mg-3Zn [45]. The effectiveness of ZnO addition in AZ91E may lead to greater application of this grain refiner (refer to Chapter 6).

4.1.2 – Grain Shape

The grain structure of the base AZ91E was highly coarse and dendritic in morphology (Figure 4.8a). In contrast, AZ91E with 0.2 wt. % Al-5TiB$_2$ did not have a dendritic structure in the alloy and appeared to be more equiaxed, as shown in Figure 4.8b. Similarly, the addition of 0.1 wt. % Al-Al$_4$C$_3$ also changed the dendritic base AZ91E morphology into one that was equiaxed and also more globular in shape, as shown in Figure 4.8c. Further, the alloy with 2 wt. % ZnO had a highly equiaxed and globular morphology, which is shown in Figure 4.8d. This refiner level achieved the greatest percentage reduction in grain size relative to the base AZ91E alloy. Therefore, the refined grains can enable more isotropic properties (e.g. strength) and improve castability by reducing the tendency for hot tearing [48].

1 mm

Addition level and holding time are indicated below each micrograph.

Base AZ91E

0.1 wt. %, 5 minutes

0.1 wt. %, 10 minutes

0.1 wt. %, 20 minutes

0.2 wt. %, 5 minutes

0.2 wt. %, 10 minutes

0.2 wt. %, 20 minutes

0.5 wt. %, 5 minutes

0.5 wt. %, 10 minutes

0.5 wt. %, 20 minutes

1 wt. %, 5 minutes

1 wt. %, 10 minutes

1 wt. %, 20 minutes
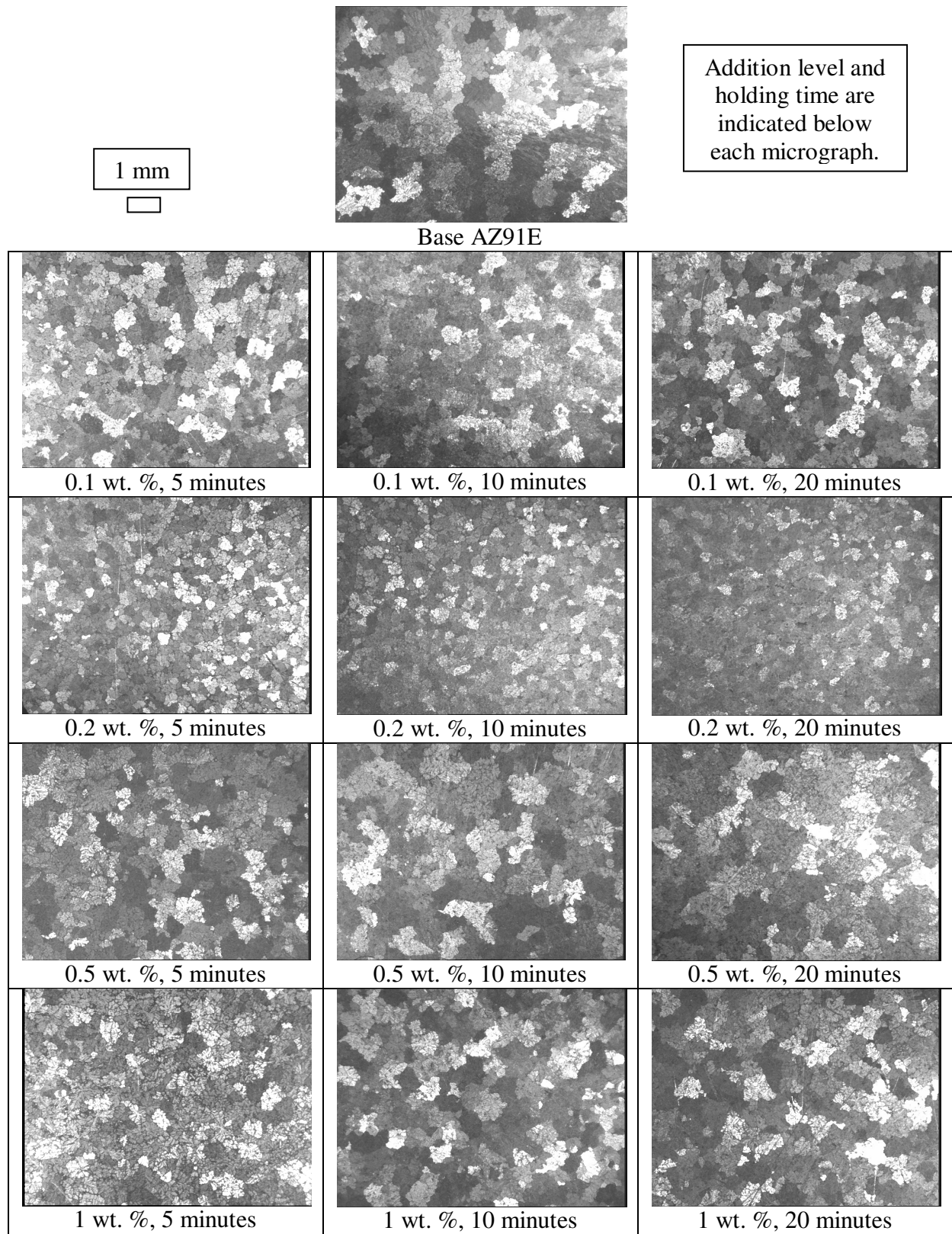
Figure 4.2: Etched as-cast grain structure for Al-5TiB$_2$ addition, with base reference.

1 mm

Addition level and holding time are indicated below each micrograph.

Base AZ91E

0.1 wt. %, 5 minutes	0.1 wt. %, 10 minutes	0.1 wt. %, 20 minutes
0.2 wt. %, 5 minutes	0.2 wt. %, 10 minutes	0.2 wt. %, 20 minutes
0.5 wt. %, 5 minutes	0.5 wt. %, 10 minutes	0.5 wt. %, 20 minutes
1 wt. %, 5 minutes	1 wt. %, 10 minutes	1 wt. %, 20 minutes
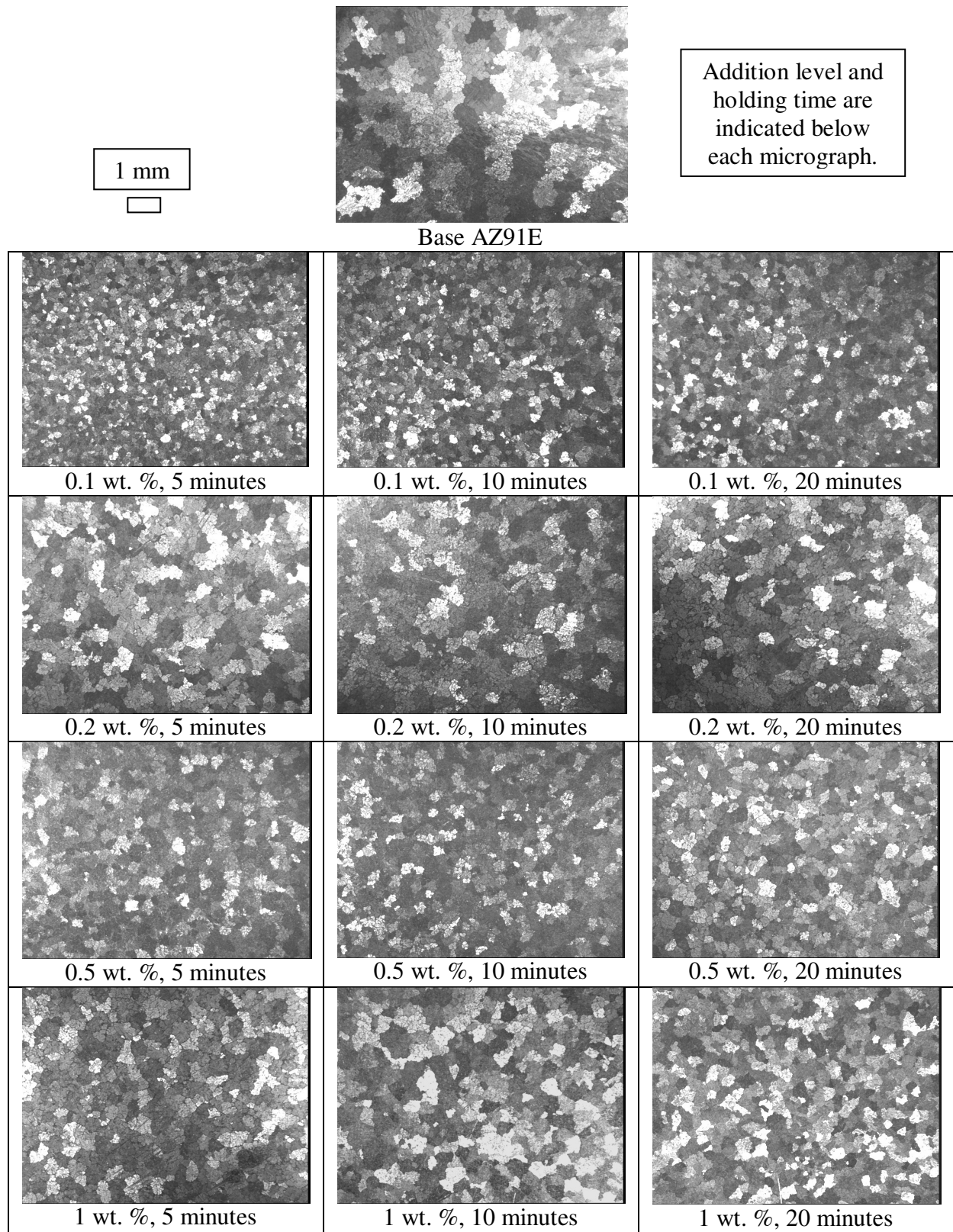
Figure 4.3: Etched as-cast grain structure for Al-Al$_4$C$_3$ addition, with base reference.

Base AZ91E

1 mm

Addition level and holding time are indicated below each micrograph.

1 wt. %, 5 minutes	1 wt. %, 10 minutes	1 wt. %, 20 minutes
2 wt. %, 5 minutes	2 wt. %, 10 minutes	2 wt. %, 20 minutes
3 wt. %, 5 minutes	3 wt. %, 10 minutes	3 wt. %, 20 minutes
4 wt. %, 5 minutes	4 wt. %, 10 minutes	4 wt. %, 20 minutes
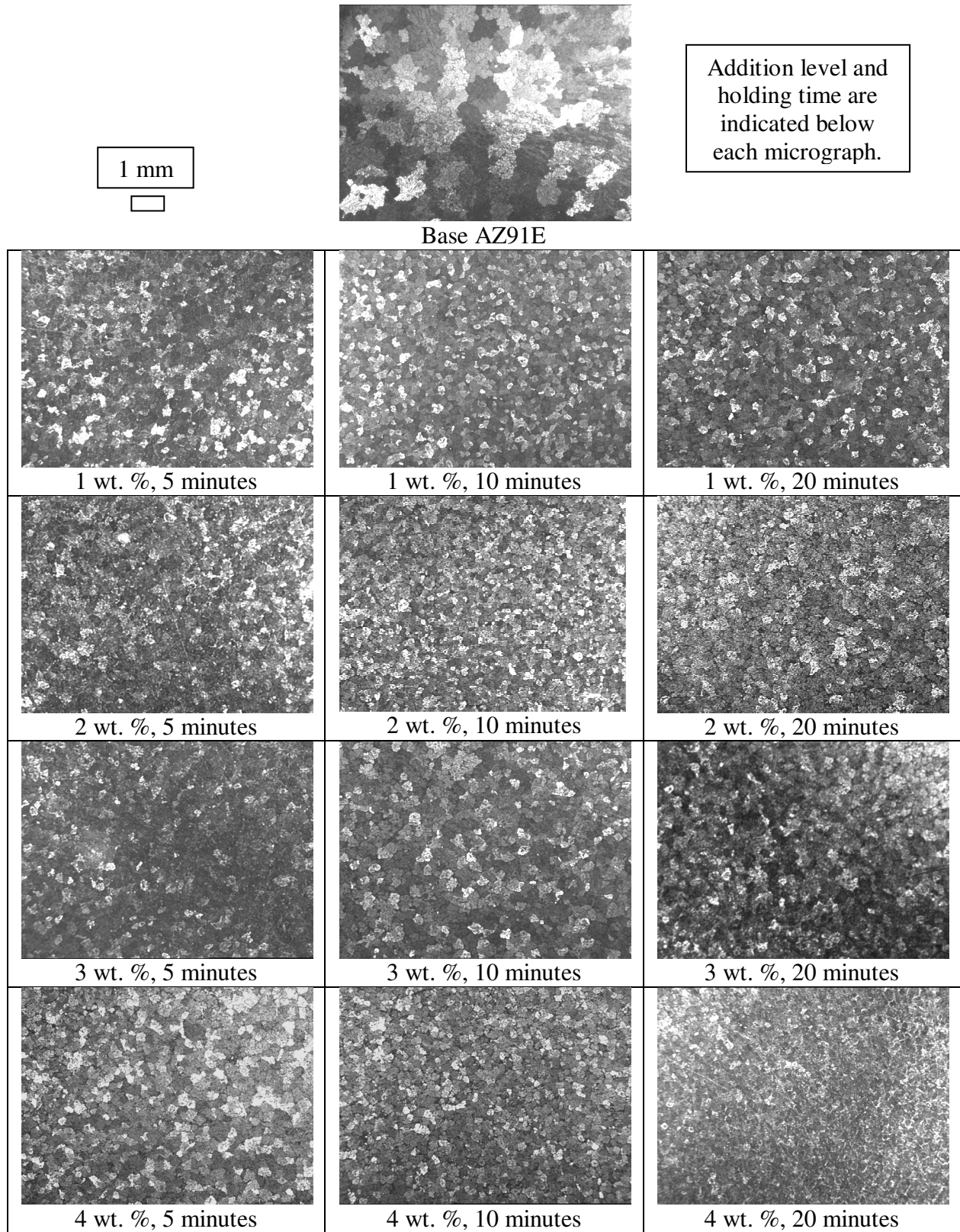
Figure 4.4: Etched as-cast grain structure for ZnO addition, with base reference.

40

Table 4.1: Listing of measured grain sizes (µm) for Al-5TiB$_2$ and Al-Al$_4$C$_3$ additions.

Grain size measurement of base AZ91E is 782 ± 131 µm.

Addition Level (wt. %)	Holding Time (min)	Grain Size (Al-5TiB$_2$) (µm)	Percentage Reduction (Al-5TiB$_2$)	Grain Size (Al-Al$_4$C$_3$) (µm)	Percentage Reduction (Al-Al$_4$C$_3$)
0.1	5	370 ± 67	53	282 ± 47	64
	10	372 ± 63	52	302 ± 35	61
	20	386 ± 51	51	317 ± 79	59
0.2	5	332 ± 49	58	374 ± 52	52
	10	318 ± 53	59	386 ± 98	51
	20	339 ± 58	57	386 ± 56	51
0.5	5	519 ± 69	34	372 ± 81	52
	10	553 ± 76	29	390 ± 90	50
	20	576 ± 54	26	357 ± 63	54
1	5	512 ± 63	35	329 ± 54	58
	10	579 ± 54	26	382 ± 82	51
	20	561 ± 63	28	327 ± 52	58

Table 4.2: Listing of measured grain sizes (µm) for ZnO additions.

Grain size measurement of base AZ91E is 782 ± 131 µm.

Addition Level (wt. %)	Holding Time (min)	Grain Size (µm)	Percentage Reduction
1	5	244 ± 54	69
	10	238 ± 37	70
	20	254 ± 69	68
2	5	278 ± 52	64
	10	192 ± 38	75
	20	266 ± 46	66
3	5	258 ± 49	67
	10	270 ± 46	65
	20	215 ± 23	73
4	5	248 ± 36	68
	10	212 ± 25	73
	20	250 ± 59	68
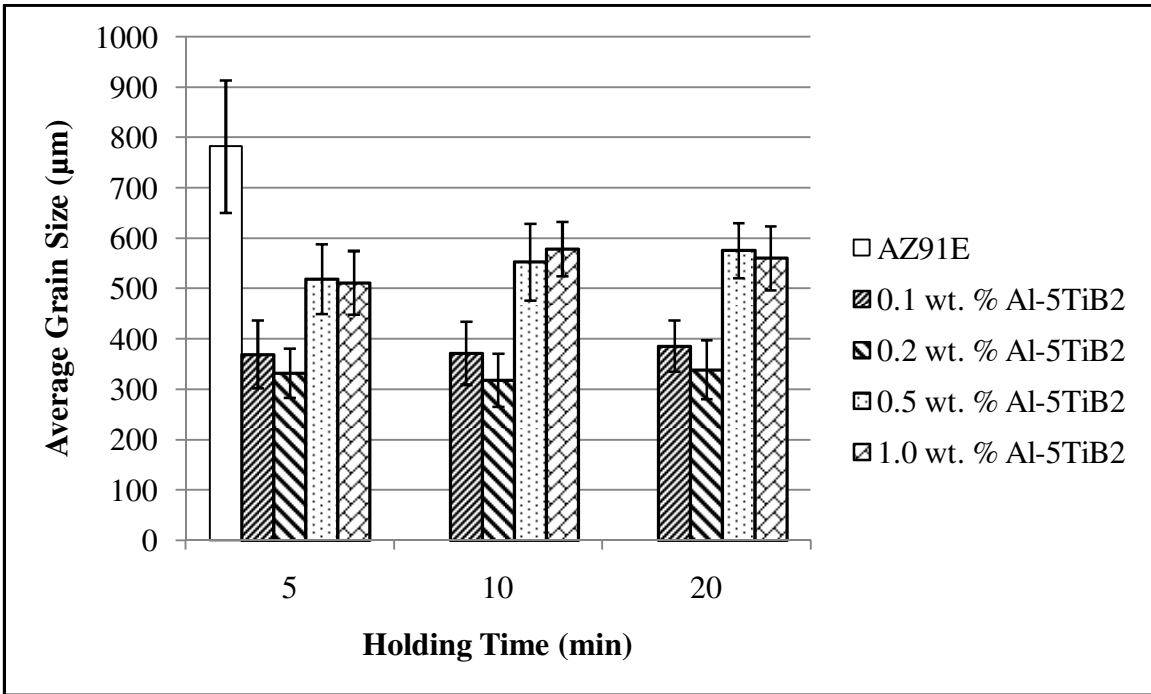
Figure 4.5: Influence of Al-5TiB$_2$ level and holding time on the grain size of AZ91E.
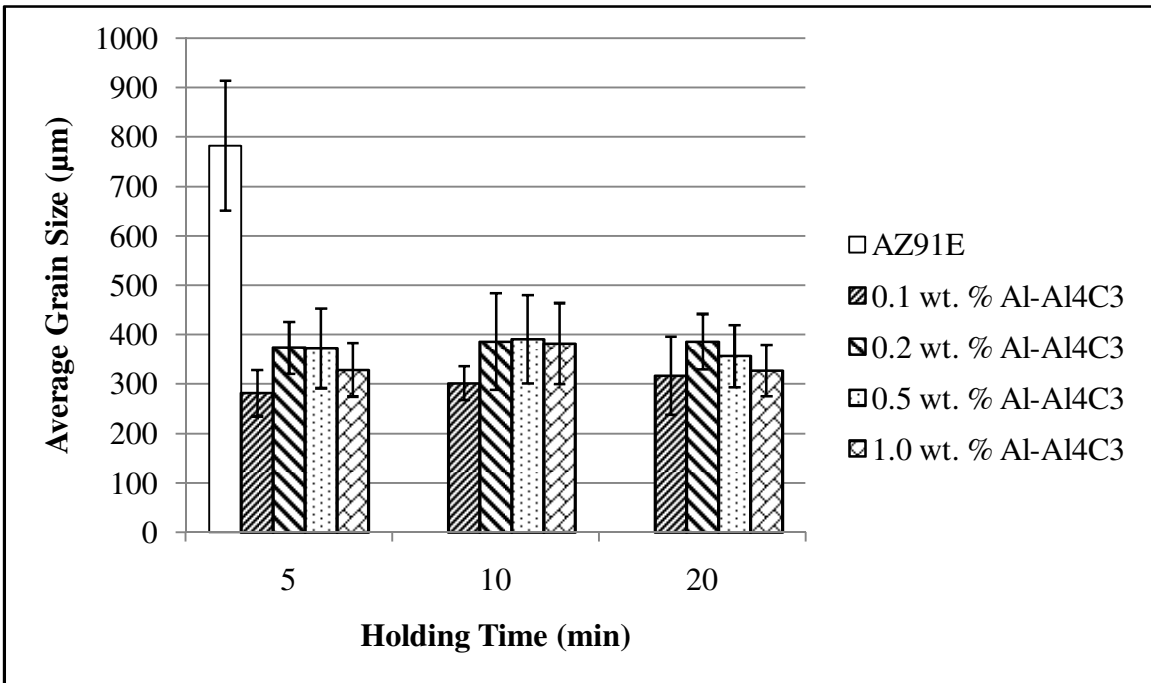
Figure 4.6: Influence of Al-Al$_4$C$_3$ level and holding time on the grain size of AZ91E.
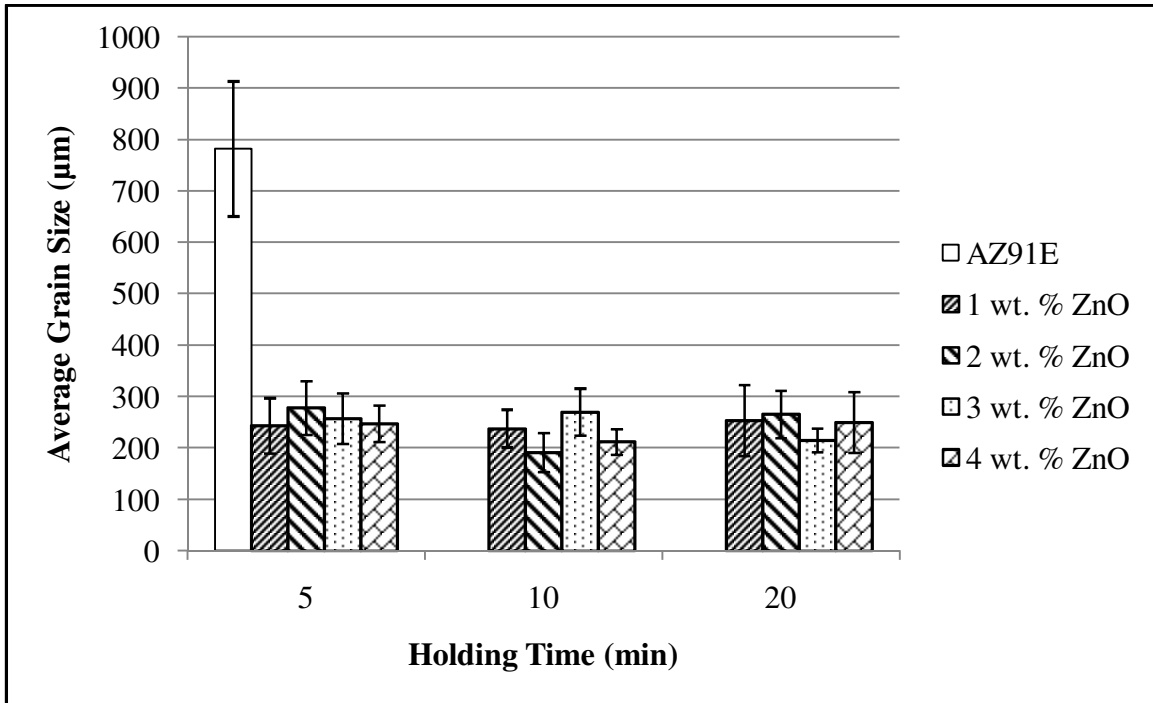
Figure 4.7: Influence of ZnO level and holding time on the grain size of AZ91E.
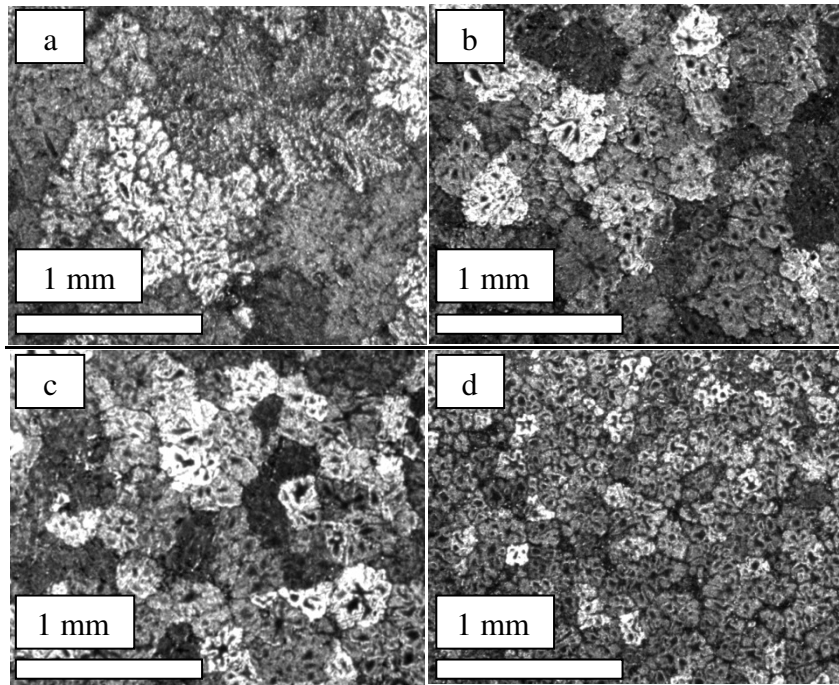
Figure 4.8: Microstructure of graphite mold specimens: a) AZ91E,

b) AZ91E + 0.2 wt. % Al-5TiB$_2$,

c) AZ91E + 0.1 wt. % Al-Al$_4$C$_3$,

d) AZ91E + 2 wt. % ZnO.

4.1.3 – Refinement Mechanism

4.1.3.1 – Al-5TiB$_2$ Addition

The location of the TiB$_2$ particles at different master alloy concentrations was determined using SEM. It was likely that the TiB$_2$ particles behaved as nucleation sites at lower concentrations (confirmed by the undercooling results in Section 4.2.1.1). At the highest concentration of 1 wt. %, the TiB$_2$ particles appeared to agglomerate near the β-Mg$_{17}$Al$_{12}$ phase, as shown in Figure 4.9. Higher concentrations of TiB$_2$ likely caused these particles to group together, causing grain refinement via growth restriction.
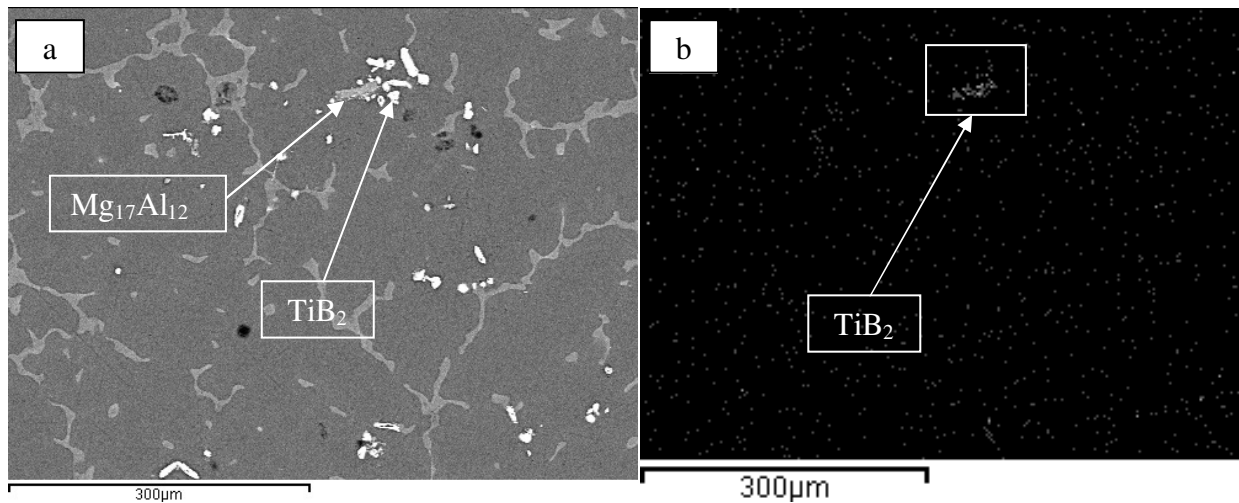
Figure 4.9: SEM image and EDX map of AZ91E with 1 wt. % Al-5TiB$_2$:

a) Reference area, b) Titanium mapping

4.1.3.2 – Al-Al$_4$C$_3$ Addition

The location of the Al$_4$C$_3$ particles was indirectly determined through SEM microscopy. Al$_4$C$_3$ should be located near the center of Mg grains due to its heterogeneous nature. Figure 4.10 shows an image of a pore in the middle of a Mg grain. The corresponding EDX point analysis indicated the presence of carbon and Al on the pore rim (black arrow), which confirmed the Al$_4$C$_3$ particle location. During the polishing process, Al$_4$C$_3$ reacted with water, and created

pores on the sample surface [15], hence indirectly indicating the particle location. As a result, Al_4C_3 provided effective nucleation sites for Mg grains, as shown in Figures 4.3 and 4.6.
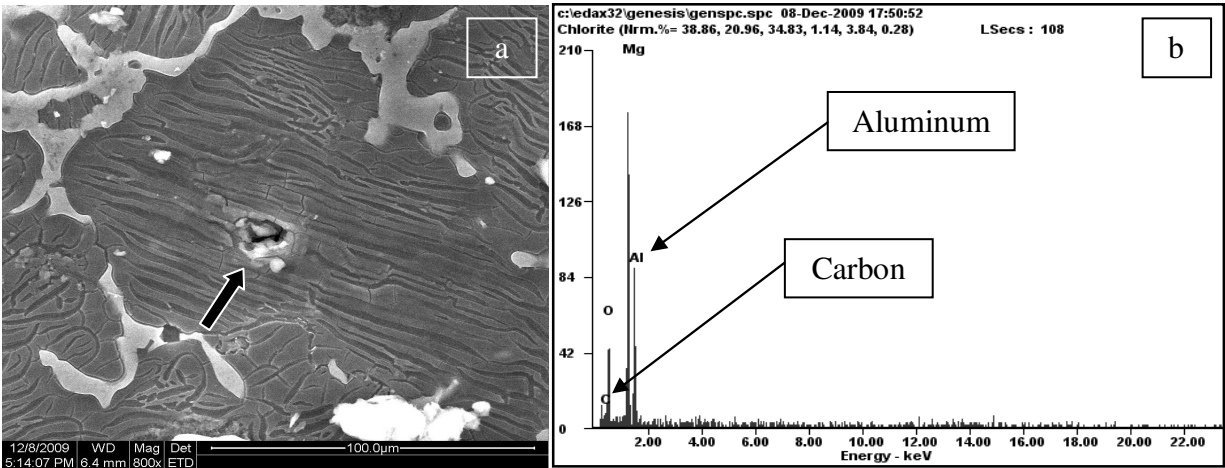
Figure 4.10: SEM image and EDX of AZ91E with 0.1 wt. % Al-Al_4C_3:
a) SEM micrograph of pore, b) EDX point analysis of pore rim.

4.1.3.3 – ZnO Addition

A spectrum analysis of AZ91E with 2 wt. % ZnO is shown in Figure 4.11. The analysis indicated that the Zn from the AZ91E alloy and ZnO additions segregated along the grain boundaries. Since Zn has a relatively high growth restriction factor [11], the extra Zn from ZnO may have assisted with grain refinement. The additional Zn may only have a small influence on grain size reduction, however, as heterogeneous nucleation is more effective than growth restriction.

Spectrum analysis of a ZnO core in AZ91E with 4 wt. % ZnO is shown in Figure 4.12, which confirmed the presence of Zn and O. In addition, the dimensions of some ZnO cores (agglomerated areas of ZnO) were measured (Figure 4.13). Given that the ZnO powder had a particle range of 0.20-4.00 µm (Figure A3.1) and formed cores of various dimensions, it appeared that Mg grains nucleated from a variety of core sizes. The ZnO core sizes did not appear to influence the grain size of AZ91E. The grain size was relatively uniform for each addition level and holding time (Figures 4.4 and 4.7). It was not possible to relate the ZnO core size to grain size.
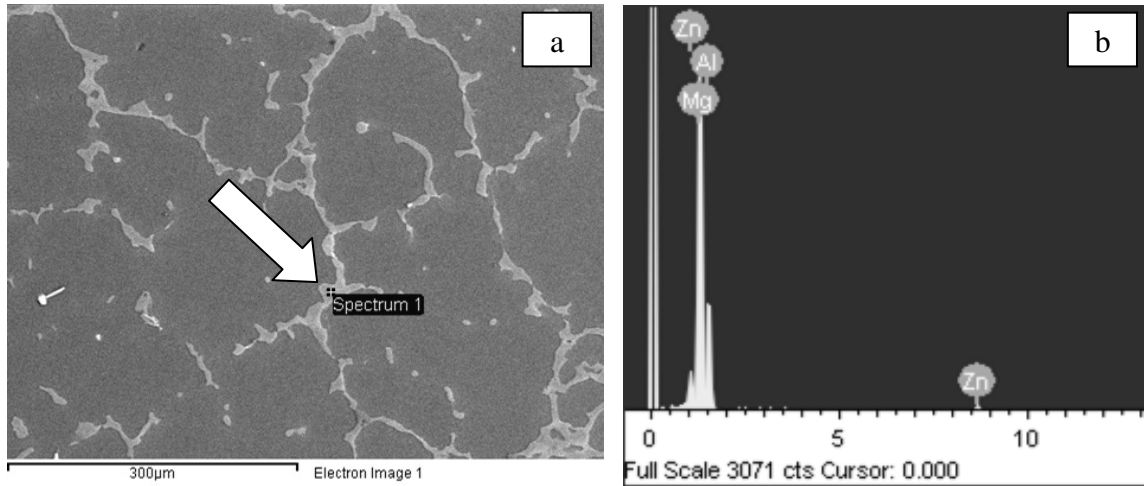
Figure 4.11: AZ91E + 2 wt. % ZnO: a) Spectrum location, b) Spectrum analysis.
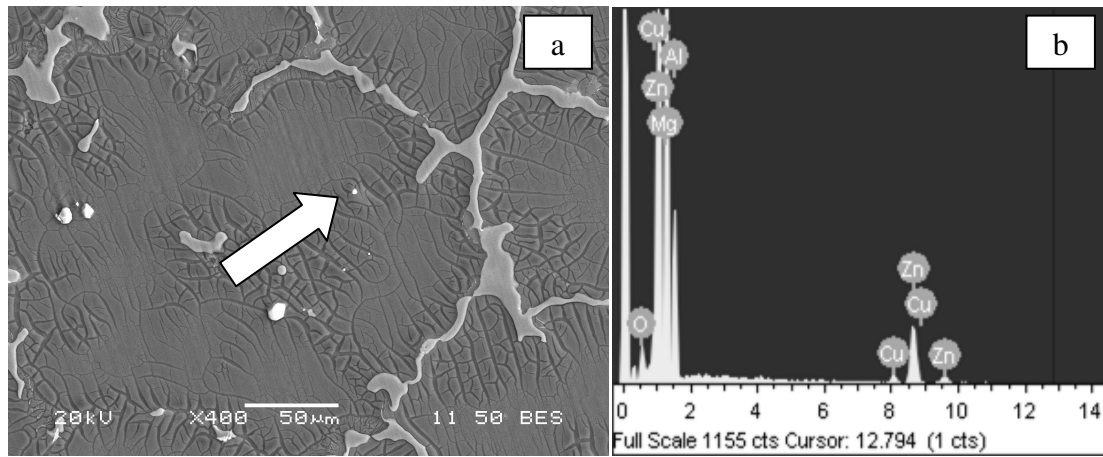
Figure 4.12: SEM of AZ91E + 4 wt. % ZnO: a) ZnO core (indicated by arrow),

b) Spectrum analysis of the core location.
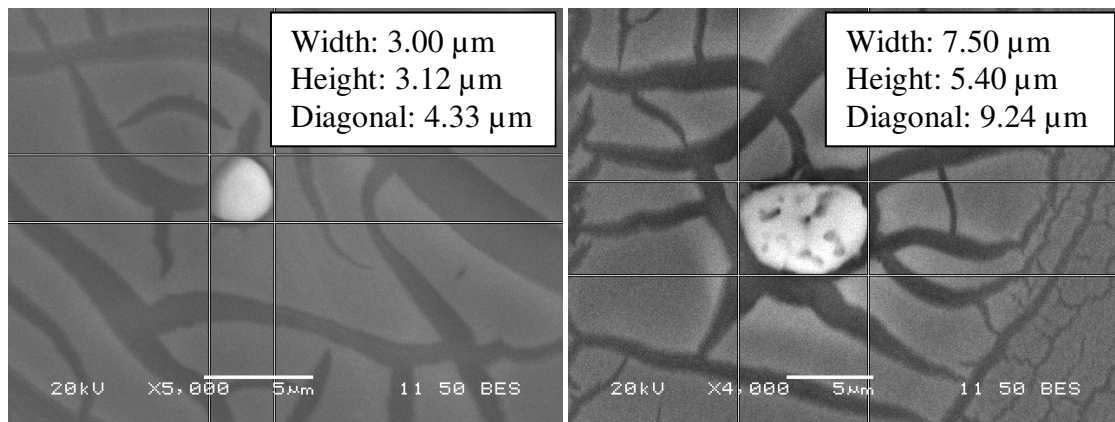
Figure 4.13: Sample ZnO core size measurements from AZ91E + 4 wt. % ZnO.

46

4.2 – Thermal Analysis

4.2.1 – Undercooling (UC)

The undercooling of the AZ91E castings at each refiner level and holding time was measured to confirm the grain refinement mechanism.

4.2.1.1 – Al-5TiB$_2$ Addition

Lower addition levels of Al-5TiB$_2$ generally resulted in a reduction in the UC as compared with the base AZ91E (Figure 4.14). Addition levels of 0.1 and 0.2 wt. % Al-5TiB$_2$ produced the lowest UC, with a maximum value of 0.4 °C and a minimum value of 0.2 °C.

At higher addition levels of 0.5 and 1 wt. % Al-5TiB$_2$, the UC was generally more pronounced, with a maximum value of 1.2 °C. It may be suggested that at lower addition levels, the TiB$_2$ particles were able to act as nucleation sites. At higher levels, the excess particles were pushed towards the grain boundaries, which increased the presence of growth restriction. Growth restriction is not as efficient as heterogeneous nucleation for grain refinement; hence, the lower addition levels (0.1 and 0.2 wt. %) generally resulted in a smaller grain size compared with higher addition levels (0.5 and 1 wt. %).

4.2.1.2 – Al-Al$_4$C$_3$ Addition

All levels of Al-Al$_4$C$_3$ additions resulted in a large reduction in the UC as compared with the reference AZ91E (Figure 4.15). The largest UC was 0.6 °C with a minimum at zero UC. The minimal UC experienced with Al-Al$_4$C$_3$ addition indicated that the grains were likely refined via efficient heterogeneous nucleation [15, 14], for all combinations of addition level and holding time.
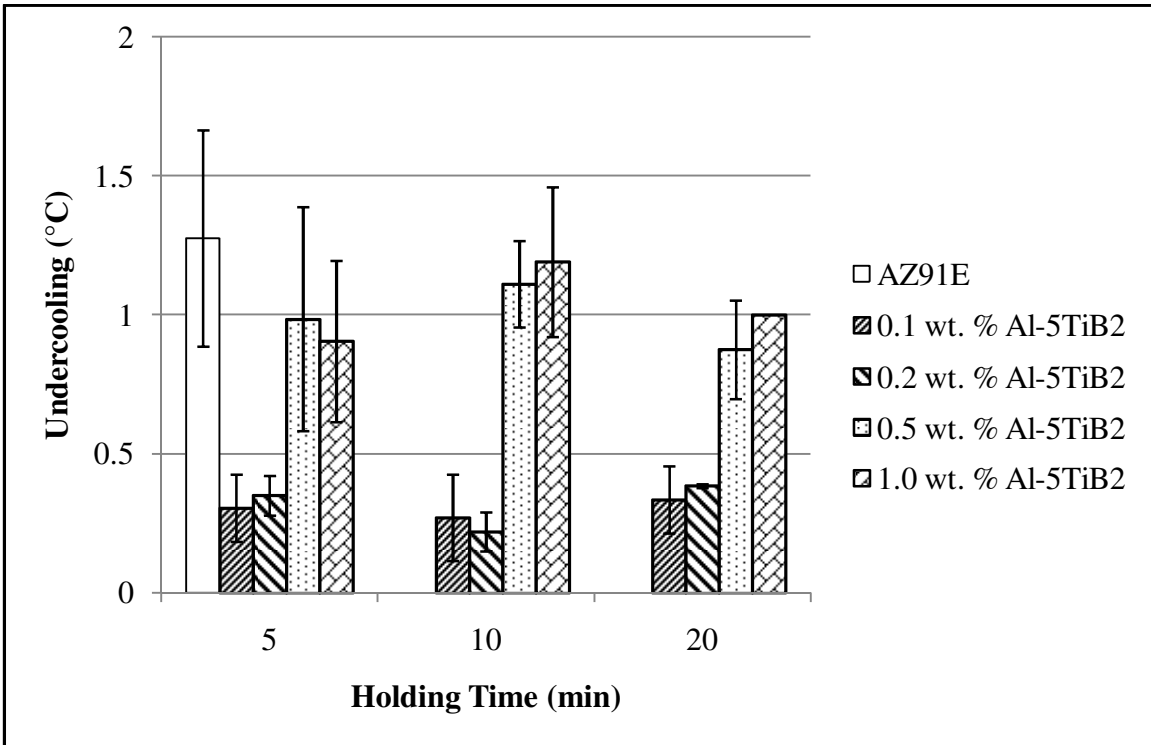
Figure 4.14: Influence of Al-5TiB$_2$ level and holding time on the undercooling of AZ91E.
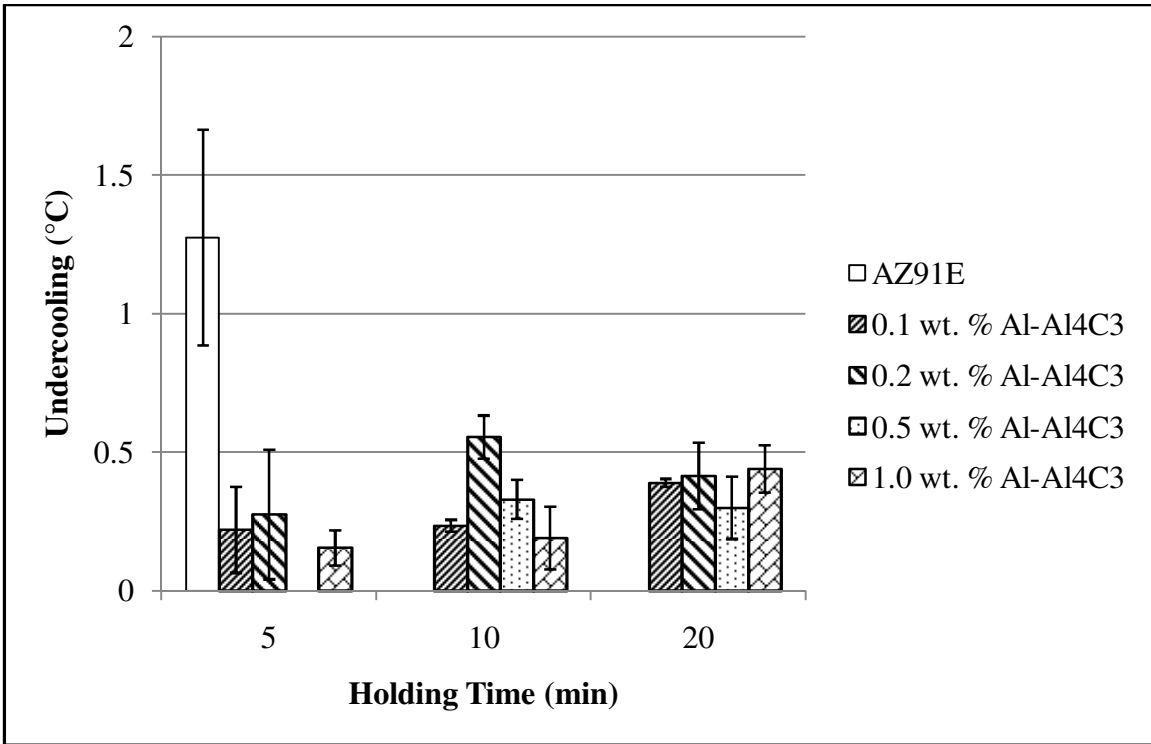
Figure 4.15: Influence of Al-Al$_4$C$_3$ level and holding time on the undercooling of AZ91E.

4.2.1.3 – ZnO Addition

The ZnO additions resulted in a large reduction in the UC at all addition levels, as compared with the reference AZ91E (Figure 4.16). The largest UC was 0.2 °C with a minimum at zero UC. The UC measurements for ZnO additions were the lowest among the three refiners. These results suggested that the refinement mechanism for ZnO addition was primarily heterogeneous nucleation, with minimal growth restriction.
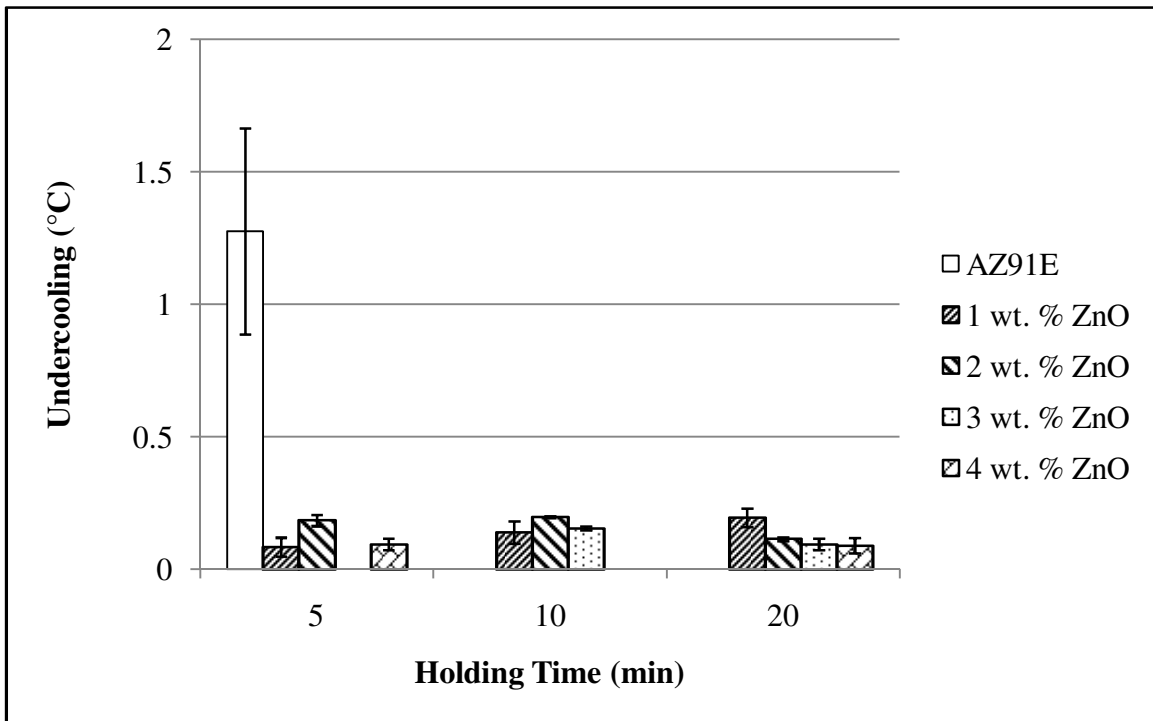
Figure 4.16: Influence of ZnO level and holding time on the undercooling of AZ91E.

4.2.2 – Freezing Range (FR)

The alloy FRs for the best refiner levels are shown in Figures 4.17. The FR was measured as the temperature difference between the liquidus and solidus points, shown in Table 4.3. There was not a significant change to the FR when Al-5TiB$_2$ or Al-Al$_4$C$_3$ refiners were added. The FR for the base AZ91E was 164 °C, while Al-5TiB$_2$ and Al-Al$_4$C$_3$ additions yielded FRs of 165 °C and 166 °C respectively. In contrast, the FR significantly increased with 2 wt. % ZnO addition to 172 °C. This increase in FR with ZnO addition will likely affect the castability of AZ91E (such

as increasing hot tearing susceptibility). For instance, an alloy with an increased freezing range would enable a semi-solid crack to propagate further, which would increase the severity of hot tears [52].
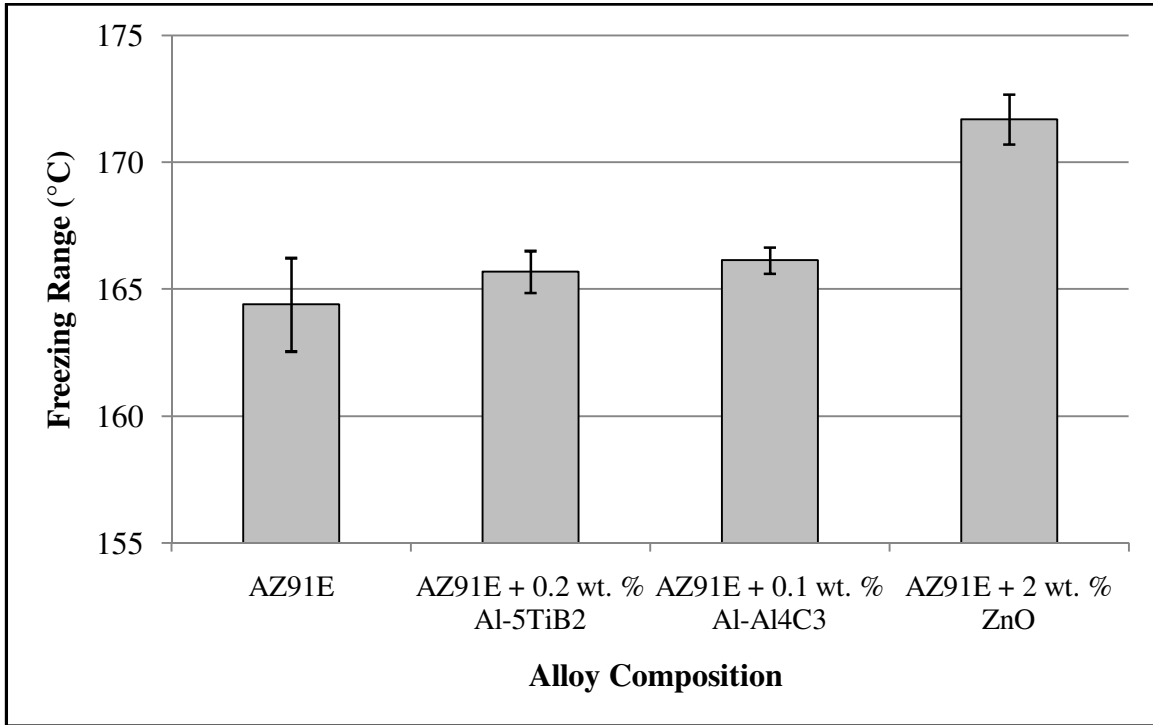
Figure 4.17: Influence of grain refiner addition on the freezing range of AZ91E.

Since the FR with 2 wt. % ZnO was significantly larger than the base AZ91E, lower addition levels (0.1, 0.2 and 0.5 wt. %) of ZnO were studied for comparison. The FRs for these graphite mold castings are presented in Figure 4.18. It was suggested that a small addition level of ZnO would increase the FR of AZ91E.

The solidus point also decreased significantly with 2 wt. % ZnO when compared with the base AZ91E. This shift in solidus temperature may be attributed to the increased solute content in the AZ91E alloy [53, 54]. The average grain size and undercooling at the lower ZnO levels, and the increase in Zn detected at each ZnO addition level are presented in Appendix 5.
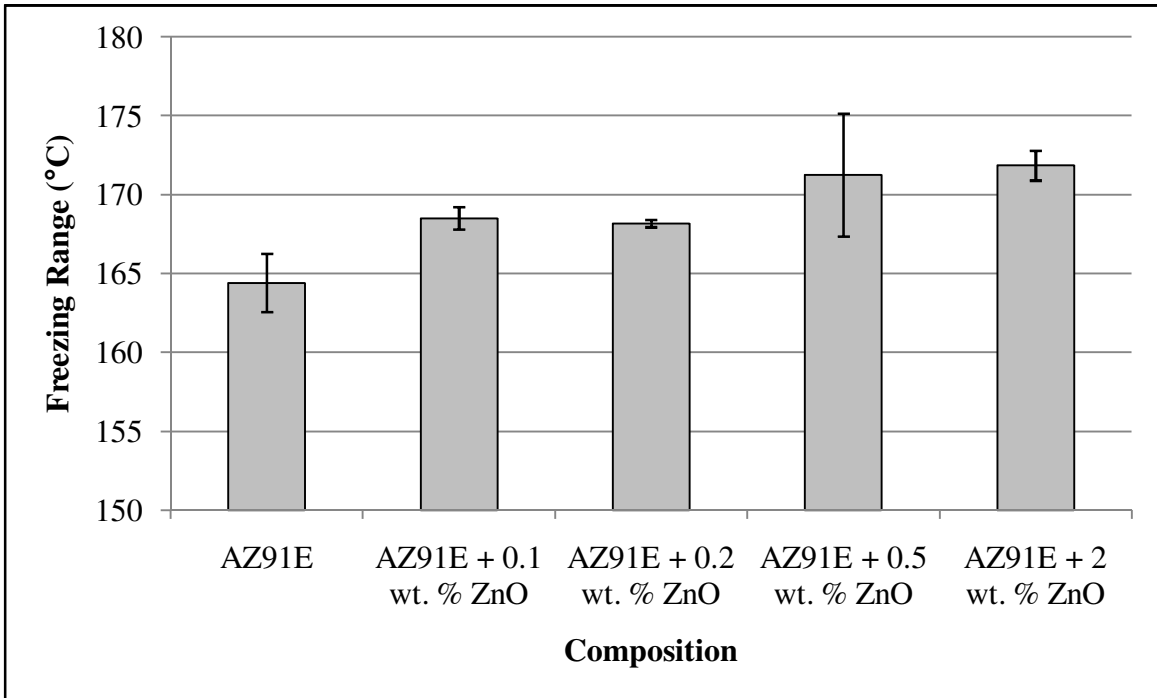
Figure 4.18: Influence of ZnO level on the freezing range of AZ91E.

Table 4.3: Average liquidus and solidus temperatures with various additions.

	Liquidus (℃)	Solidus (℃)
AZ91E	595.5 ± 1.4	430.8 ± 0.0
AZ91E + 0.2 wt. % Al-5TiB$_2$	595.6 ± 0.8	429.8 ± 0.1
AZ91E + 0.1 wt. % Al-Al$_4$C$_3$	597.3 ± 0.8	431.1 ± 0.3
AZ91E + 0.1 wt. % ZnO	596.5 ± 0.3	429.5 ± 0.7
AZ91E + 0.2 wt. % ZnO	597.0 ± 0.0	430.1 ± 0.2
AZ91E + 0.5 wt. % ZnO	596.3 ± 0.9	423.4 ± 3.8
AZ91E + 2 wt. % ZnO	592.8 ± 0.9	420.9 ± 0.1

4.3 – Permanent Mold Castings

Permanent mold castings were performed using the refiner levels from graphite molds that yielded the smallest average grain sizes.

4.3.1 – Grain Size Measurement

In permanent mold casting, the addition of the three refiners led to a significant decrease in grain sizes, which is shown in Figure 4.19. The percentage decrease in grain sizes was comparable to those observed in graphite mold castings, with a maximum difference of 7%. These grain size reduction measurements showed that all three refiners appeared to be very effective in permanent molds. In addition, ZnO again yielded the smallest percentage reduction in grain size in this casting process. The combination of an effective grain refiner and a high cooling rate in the permanent mold enabled the formation of the smallest grain sizes measured in this thesis. Table 4.4 compares the percentage decrease in grain size for the two casting methods.
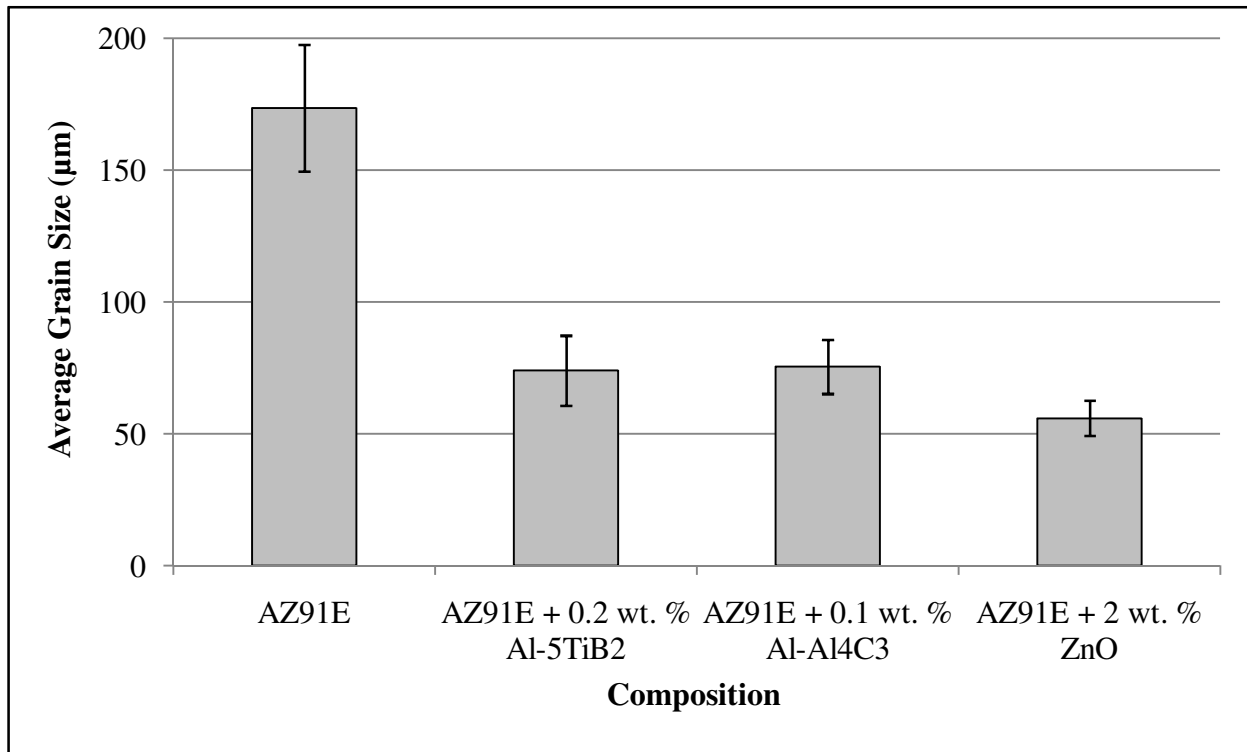
Figure 4.19: Influence of grain refiners on average grain size of AZ91E in permanent molds.

Table 4.4: Percentage reduction in grain size of AZ91E for various casting processes.

	0.2 wt. % Al-5TiB$_2$	0.1 wt. % Al-Al$_4$C$_3$	2 wt. % ZnO
Graphite Mold Casting	59%	64%	75%
Permanent Mold Casting	57%	57%	68%

4.3.2 – Hot Tearing

The hot tearing susceptibility of AZ91E with the three refiners was also studied in this permanent mold. The castings with short ($\leq$ 5 mm) hairline fractures were considered to be hot tear resistant, while the ones with long or wide (> 5 mm) fractures were considered hot tear susceptible. All hot tear samples are shown in Figure 4.20.

4.3.2.1 – Al-5TiB$_2$ Addition

The refiner level at 0.2 wt. % Al-5TiB$_2$ resulted in the smallest grain size relative to the base AZ91E, as shown in Figure 4.5. Consequently, the hot tear was dramatically reduced (Figure 4.20b) compared with the base AZ91E (Figure 4.20a). A hot tear was still visible as indicated by the white arrow, but it was only a hairline fracture instead of a large crack spanning the entire height of the casting section. The refined and equiaxed grains (Figure 4.8) seen with this refiner level appeared to be a reason for the decrease in hot tearing severity. A refined alloy would be free of long dendrite arms and the resultant smaller grains would be able to accommodate local strains, to prevent hot tears [48].

4.3.2.2 – Al-Al$_4$C$_3$ Addition

Compared with the base AZ91E, the addition of 0.1 wt. % Al-Al$_4$C$_3$ resulted in the smallest grain size (Figure 4.6). The hot tear was significantly reduced compared with the base AZ91E (Figure 4.20c). Some small hot tears were still visible as indicated by the white arrows, but they were small fractures as compared to the large crack present in the unrefined AZ91E. The refined

and globular grains (Figure 4.8) seen with this refiner level dramatically reduced the severity of hot tears in AZ91E.

4.3.2.3 – ZnO Addition

The refined permanent mold casting with 2 wt. % ZnO had a hot tear condition more severe than the base AZ91E, as shown in Figure 4.20e. While the base alloy had a tear, the casting was still intact. In contrast, the casting with 2 wt. % ZnO completely separated. The casting with ZnO addition at 2 wt. % had the smallest measured grain size relative to the base AZ91E (Figure 4.7). The highly refined grains were supposed to resist the greatest local strains. Thus, this level of ZnO addition should have correlated to an even greater reduction in hot tearing, but the opposite was observed.

The reason for the severe tear was likely the increased FR that appeared with ZnO addition. It was stated by Campbell [1] that Zn-containing Mg alloys would have a larger FR, which would consequently increase hot tearing tendencies. From Fu et al. [45], the addition of ZnO into Mg formed MgO and Zn. This excess Zn increased the FR of the alloy and consequently, the hot tearing susceptibility. In addition, a hot tear test was performed using 0.1 wt. % ZnO. As shown in Figure 4.20d, a complete casting separation was also observed with this addition level. The hot tearing severity of the AZ91E alloy appeared to be very sensitive to increases in FR.
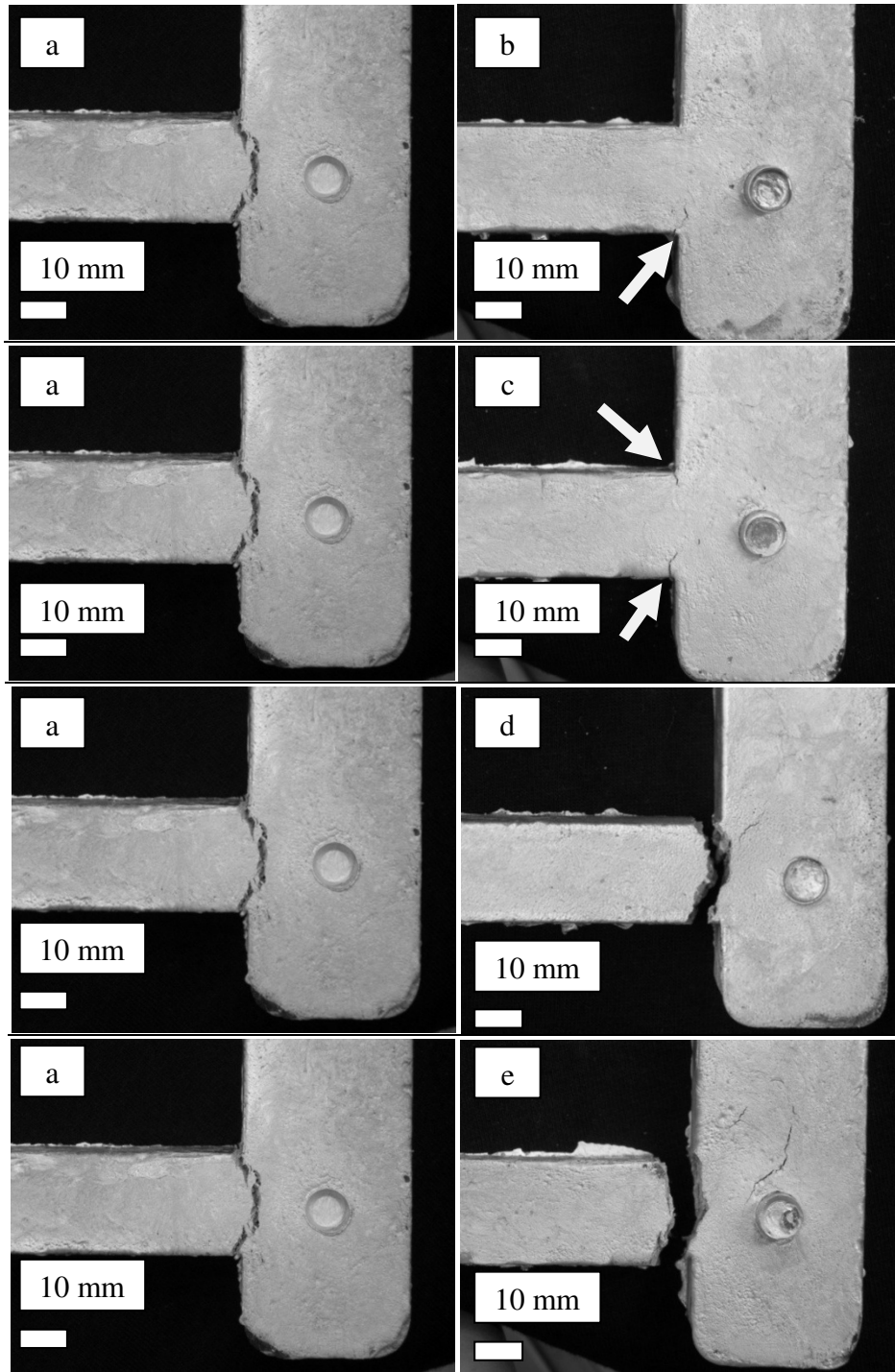
Figure 4.20: Permanent mold hot tearing samples: a) AZ91E reference,

b) AZ91E + 0.2 wt. % Al-5TiB$_2$,

c) AZ91E + 0.1 wt. % Al-Al$_4$C$_3$,

d) AZ91E + 0.1 wt. % ZnO,

e) AZ91E + 2 wt. % ZnO.

The hot tear fractures from Sections 4.3.2.1-4.3.2.3 were further examined using the SEM. In the case of a complete fracture of the casting, the fracture surface was examined instead. All hot tears had intergranular fractures, as shown by the rough crack profiles (Figures 4.21a, 4.22a and 4.23a). This type of fracture was confirmed with a spectrum analysis along the grain boundaries. The analysis indicated the presence of Mg, Al and Zn, which represented the $Mg_{17}Al_{12}$ intermetallic and elemental Zn along the grain boundaries (Figures 4.21c, 4.22c and 4.23c). The $Mg_{17}Al_{12}$ intermetallic appears as a bright region with the SEM.

This presence of $Mg_{17}Al_{12}$ along the crack region suggests that hot tears likely developed before the complete formation of the intermetallic phase. This occurs during the interdendritic separation stage of solidification, where the permeability of the solid network is severely reduced, which impedes liquid metal flow [52]. Characteristics of this type of hot tear formation are jagged fracture surfaces and sometimes solid bridges that would connect both sides of a crack (Figure 4.21a) [52]. Furthermore, the presence of porosity (black spots) near the crack boundaries may have contributed to the formation of the hot tears.

The complete separation of the hot tear sample of AZ91E + 2 wt. % ZnO allowed for the analysis of the fracture surface (Figure 4.24a). On this surface, cleavage planes were observed, which are indicated by the white arrows. This indicated that the fracture mode was brittle, which was expected for Mg alloys. The HCP structure of Mg has up to six slip systems, which is comparatively lower than the 12 slip systems associated with a more ductile material, such as FCC Al [2]. Similarly, spectrum analysis (Figure 4.24c) on the fracture surface showed the presence of Mg, Al and Zn, which indicated the hot tear occurred at the grain boundary regions.
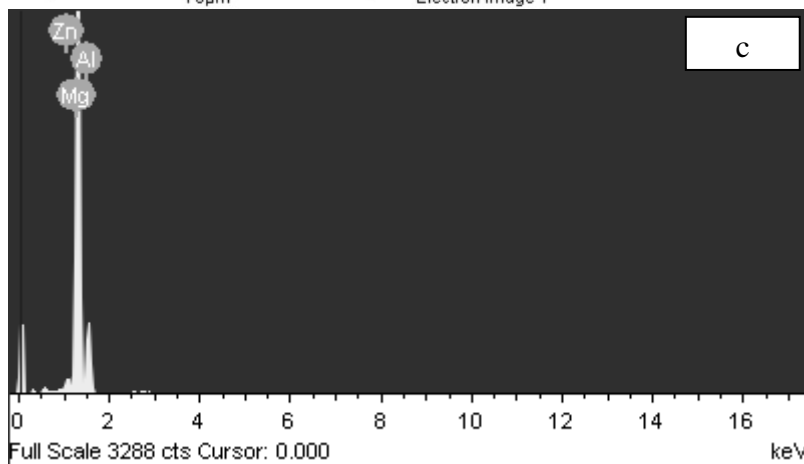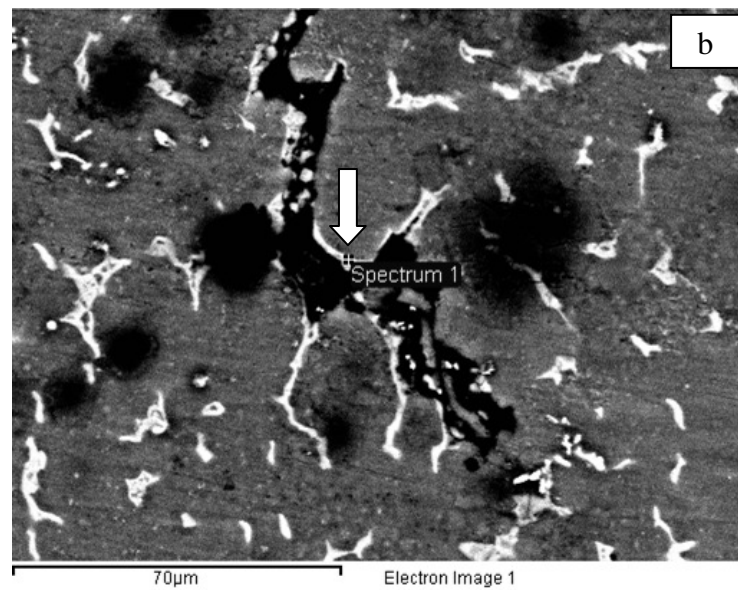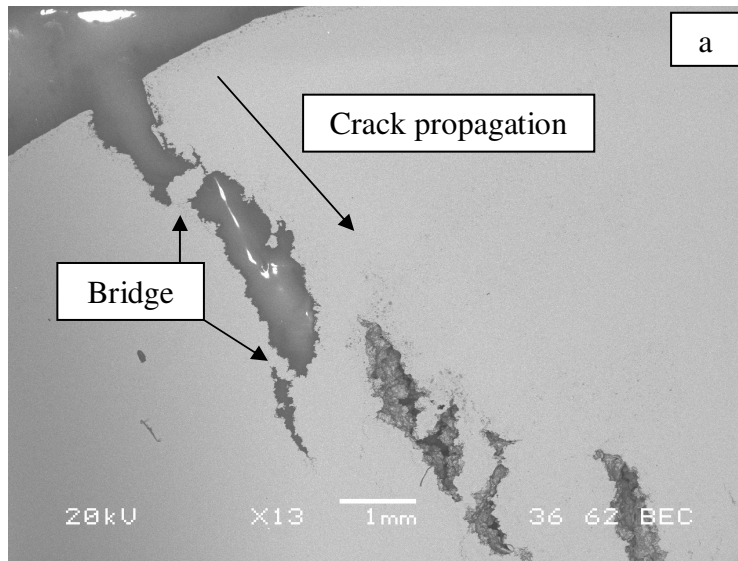
Figure 4.21: Hot tear SEM of AZ91E: a) Crack and propagation direction,
b) Location of spectrum analysis (white arrow), c) EDX spectrum.
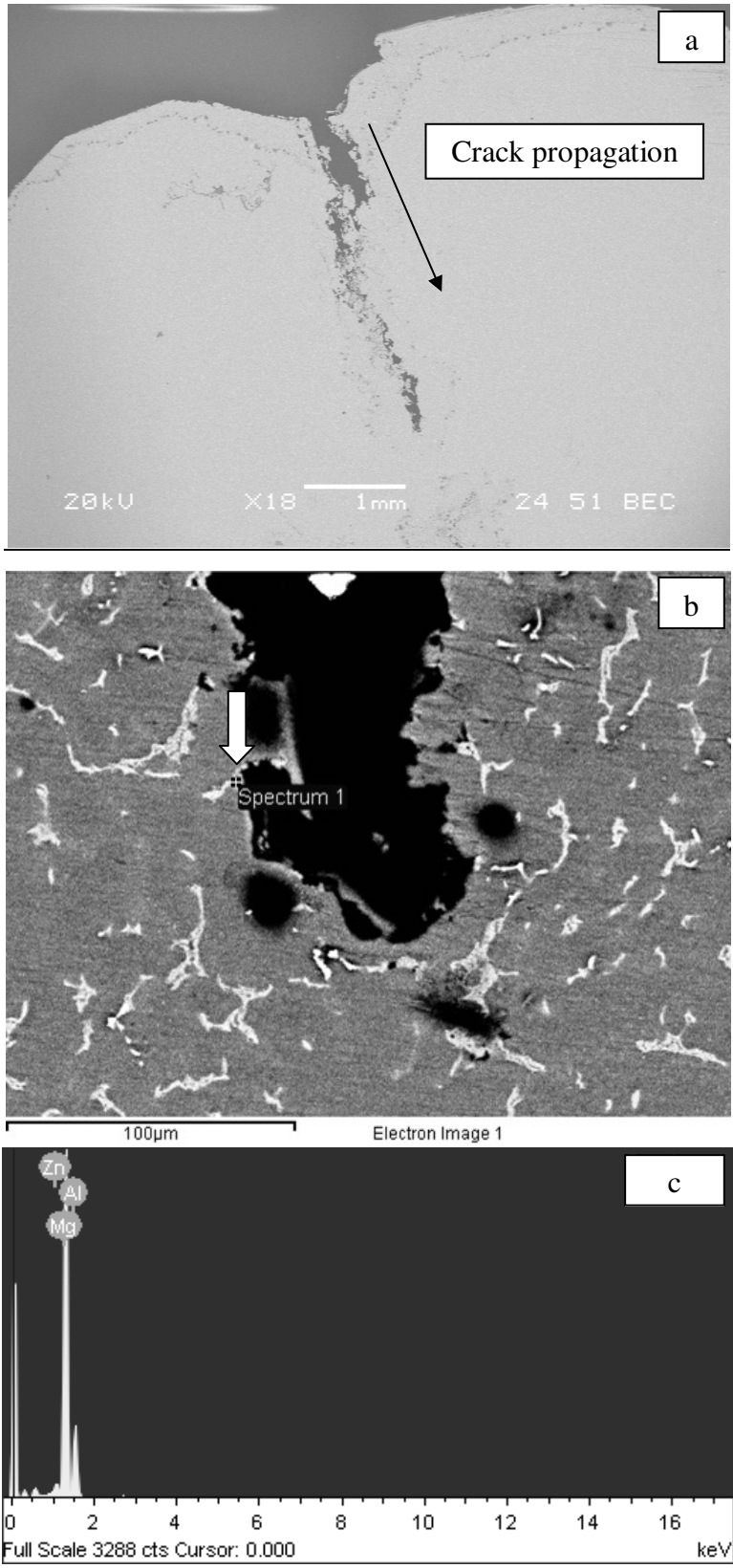
Figure 4.22: Hot tear SEM of AZ91E + 0.2 wt. % Al-5TiB$_2$: a) Crack and propagation direction,
b) Location of spectrum analysis (white arrow), c) EDX spectrum.
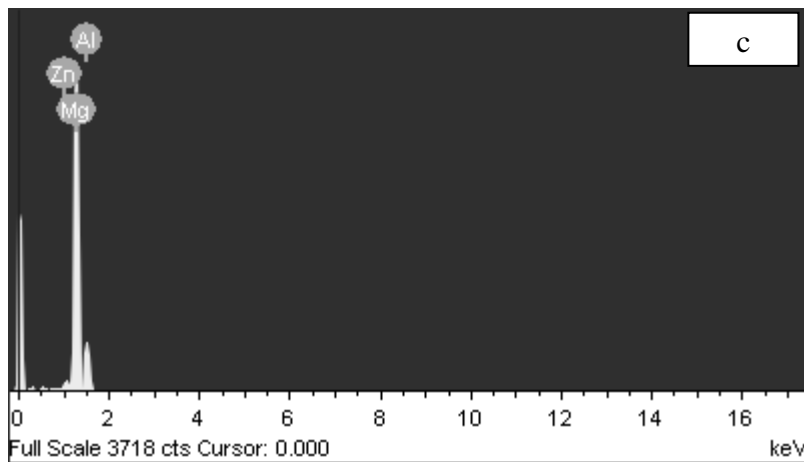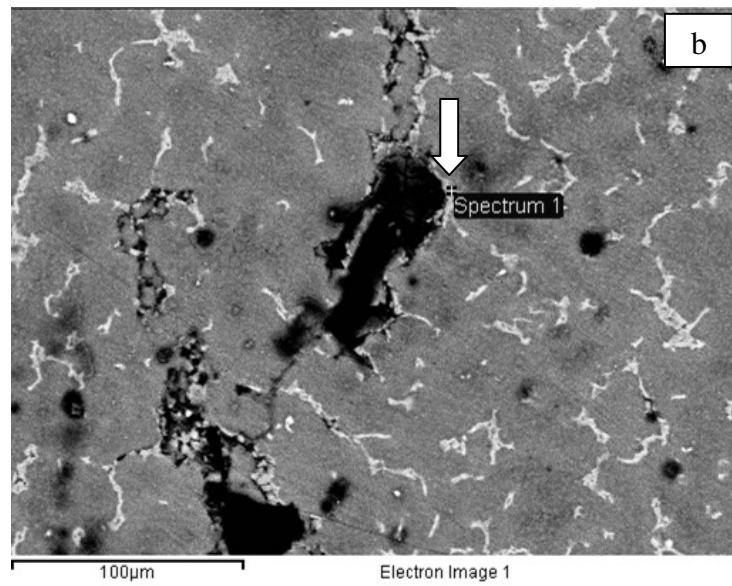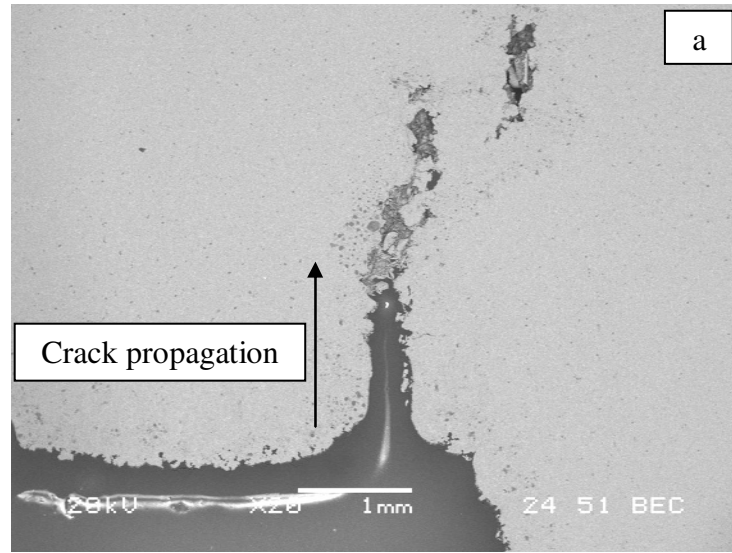
Figure 4.23: Hot tear SEM of AZ91E + 0.1 wt. % Al-Al$_4$C$_3$: a) Crack and propagation direction, b) Location of spectrum analysis (white arrow), c) EDX spectrum.
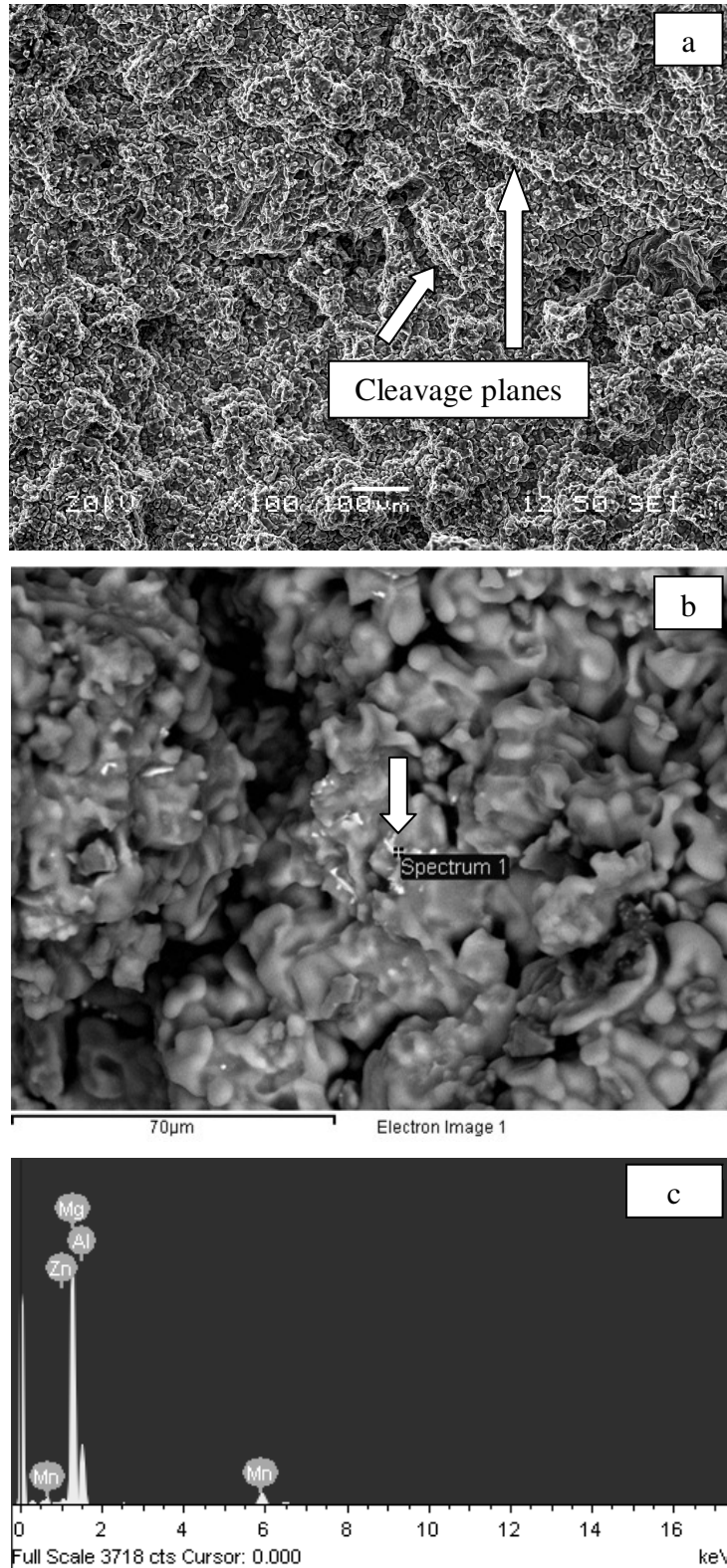
Figure 4.24: Hot tear surface of AZ91E + 2 wt. % ZnO: a) Fracture surface with cleavage planes, b) Location of spectrum analysis (white arrow), c) EDX spectrum.

4.4 – Hardness Measurements

4.4.1 – Al-5TiB$_2$

A graph indicating hardness measurements for all Al-5TiB$_2$ concentrations and holding times is shown in Figure 4.25. Between Al-5TiB$_2$ holding times and levels, the difference in hardness was generally not significant. However, the general trend indicated a slight increase ($P_{\alpha max} > 99.9\%$) in hardness with the addition of Al-5TiB$_2$ to AZ91E. This trend was expected as grain sizes decreased with the addition of this refiner.

4.4.2 – Al-Al$_4$C$_3$

The hardness measurements for all Al-Al$_4$C$_3$ levels and holding times are presented in Figure 4.26. The hardness of the samples increased ($P_{\alpha max} > 99.9\%$) as Al-Al$_4$C$_3$ was added to the base AZ91E. Similarly, between addition levels and holding times, the difference in hardness was not significant. In general, Al-Al$_4$C$_3$ addition resulted in a significant increase in hardness, which was expected as grain size decreased.

4.4.3 – ZnO

The hardness of AZ91E with ZnO additions did not increase ($P_{\alpha max} = 80.3\%$) despite the significant decrease in grain size. Figure 4.27 shows a graph of hardness for all ZnO levels and holding times. Furthermore, there was also no significant change in hardness with holding time, which was consistent with the grain size measurements.

The insignificant change in hardness was attributed to the higher levels of Zn, which segregated to the grain boundaries and lowered the hardness of the intermetallic region. This decrease in grain boundary region hardness was supported by Vickers microhardness testing. The average microhardness of the grain boundary region in unmodified AZ91E was 91.7 ± 2.3 HV. The average microhardness of the grain boundary region with 2 wt. % ZnO was 76.0 ± 0.3 HV.

In general, the hardness of the AZ91E alloy increased slightly with the addition of the grain refiners (Al-5TiB$_2$ and Al-Al$_4$C$_3$).
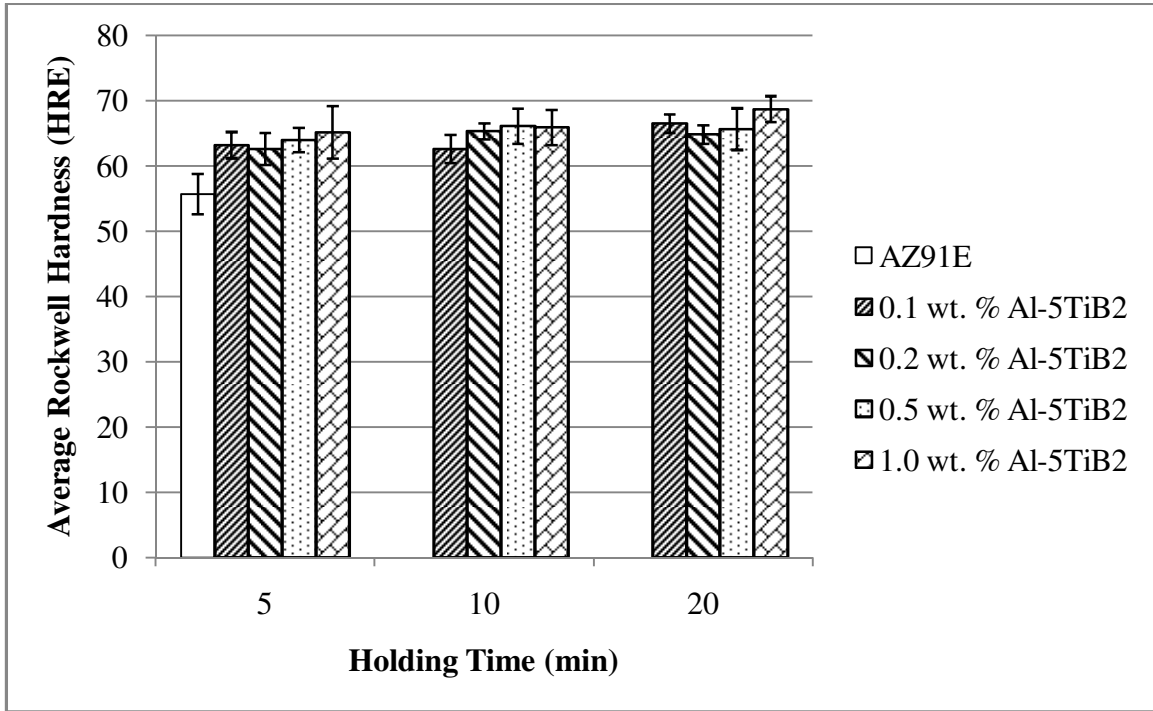
Figure 4.25: Influence of Al-5TiB$_2$ level and holding time on the hardness of AZ91E.
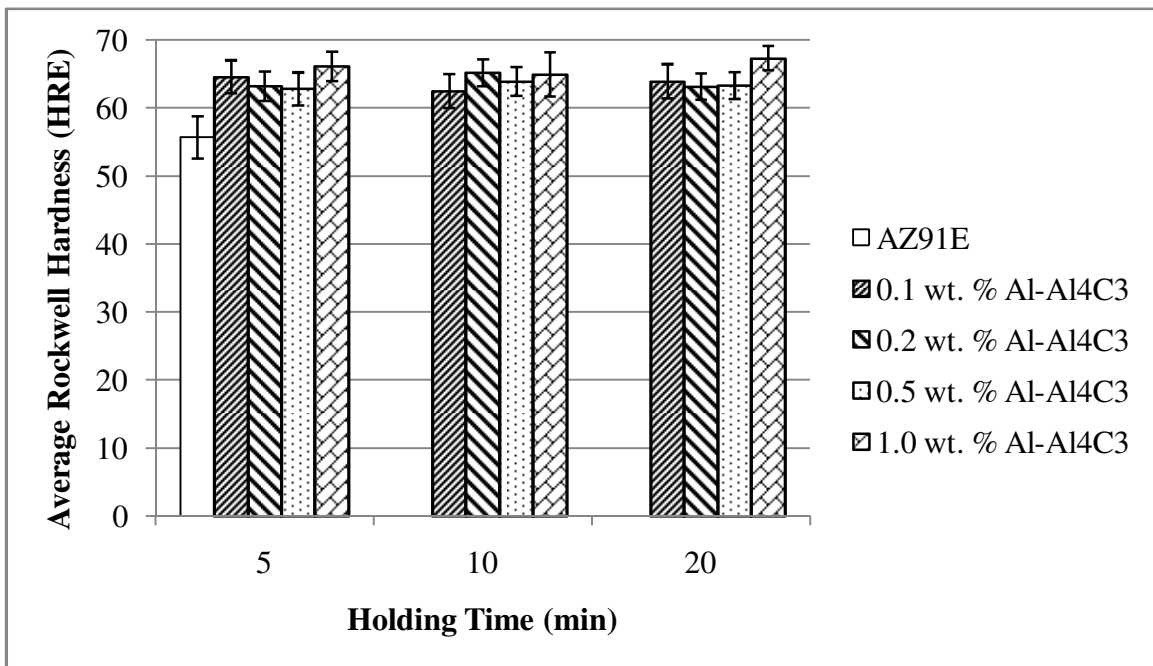
Figure 4.26: Influence of Al-Al$_4$C$_3$ level and holding time on the hardness of AZ91E.
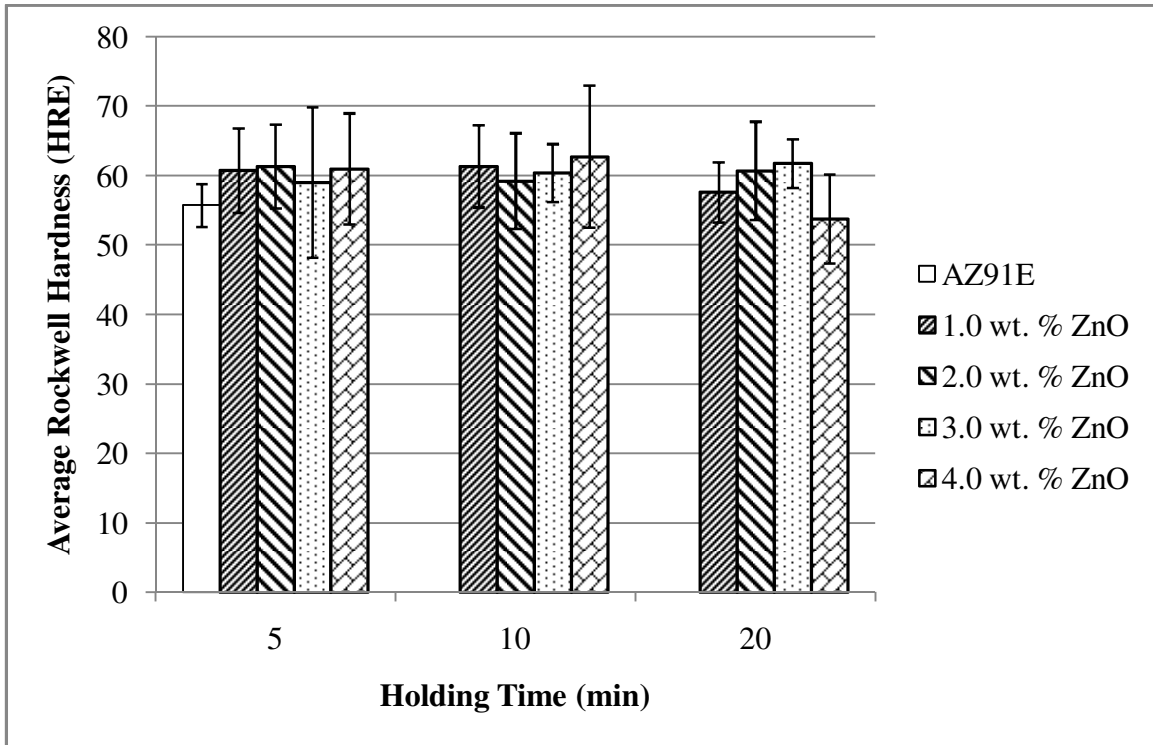
Figure 4.27: Influence of ZnO level and holding time on the hardness of AZ91E.

CHAPTER 5 – CONCLUSIONS

The results of this thesis suggest that the three compounds (Al-5TiB$_2$, Al-Al$_4$C$_3$ and ZnO) were all effective in grain refining the AZ91E alloy. The summary of the results are presented hereunder.

1. The addition of Al-5TiB$_2$ was most effective at 0.2 wt. % (grain size reduction of 59%). No fading was observed for holding times of 5, 10 and 20 minutes. At lower addition levels (0.1 and 0.2 wt. %), undercooling was small (0.2-0.4 °C), which indicated significant heterogeneous nucleation. With grain refinement, the hot tearing severity decreased during permanent mold casting. The hardness increased as the grain size was reduced.

2. The Al-Al$_4$C$_3$ grain refiner was most effective at 0.1 wt. % (grain size reduction of 64%). No fading was observed during holding (20 minutes maximum), while undercooling was small (0-0.6 °C). The nucleation mechanism was considered heterogeneous. The grain refinement effect enabled a decrease in the hot tearing severity. The hardness also increased with a reduction in the grain size.

3. The ZnO grain refiner was most effective at 2 wt. % (grain size reduction of 75%). For holding times of 5, 10 and 20 minutes, no fading was observed. The undercooling was extremely small (0-0.2 °C), which suggested heterogeneous nucleation as the grain refinement mechanism. However, the hot tearing severity was pronounced and is attributed to a significant widening of the freezing range. No hardness increase was observed as the excess Zn softened the AZ91E alloy.

4. For the Al-Al$_4$C$_3$ grain refiner, a combination of grain refinement efficiency (at low addition levels) and the ability to reduce the hot tearing susceptibility of AZ91E makes it the best overall grain refiner among those considered.

CHAPTER 6 – SUGGESTIONS FOR FUTURE WORK

1. Develop cast-in tensile samples with reduced porosity to obtain reliable tensile data.

2. Study the effects of a range of controlled grain refiner particle sizes (e.g. micro, nano) using a ball mill.

3. Study the effect of very fine grain size on hot tearing during casting.

4. Use crystallographic matching models (e.g. lattice disregistry and edge-to-edge models) to predict potential refiners and test them in Mg alloys such as AZ91.

APPENDIX 1 – MELT ADDITION CRYSTAL STRUCTURES AND LATTICE CONSTANTS

- Please refer to the end of Chapter 2.

Table A1: Crystal structures and lattice parameters of melt additions.

(BCC = body-centered cubic, FCC = face-centered cubic,

HCP = hexagonal close-packed, RHL = rhombohedral)

Melt Addition	Crystal Structure	Lattice Constant (Å)	Reference
Mg	*HCP*	*a = 3.209* *c = 5.210*	[53]
Al_4C_3	RHL (stacked)	a = 3.338 c = 24.996	[15]
Ca	FCC	a = 5.588	[53]
Ce	FCC	a = 5.161	[53]
CeSb	FCC	a = 6.40	[55]
$FeCl_3$	HCP	a = 6.064 c = 17.443	[56]
Mn	BCC	a = 8.912	[53]
Sb	RHL	a = 4.506	[53]
SiC	HCP	a = 3.076 c = 15.11	[57]
Sr	FCC	a = 6.084	[53]
TiB_2	HCP	a = 3.028 c = 3.228	[32]
V	BCC	a = 3.024	[53]
ZnO	HCP	a = 3.265 c = 5.219	[45]
Zr	HCP	a = 3.231 c = 5.147	[53]

Table A2: Summary of grain refinement techniques from the literature review (Chapter 2).

Addition/Process	Authors	Mg Alloy	Addition Level	Mold Type	Reference Grain Size (μm)	Smallest Refined Grain Size (μm)	Grain Size Reduction (%)
Carbon Addition	Qian et al. [16]	Mg-3Al	0.6 wt. % C	Steel cone	400	170	58
	Jin et al. [17]	AZ31	0.6 wt. % C_2Cl_6	Steel	400	120	70
	Han et al. [18]	AZ31	2 wt. % Al-1C	Steel	600	150	75
	Pan et al. [20]	AZ63B	1.0 wt. % Al-1.5C	Steel	270	50	81
	Karlsen et al. [13]	AZ91D	0.3 wt. % wax-CaF_2-C	Sand	89	85	4
Al_4C_3 Addition	Xue et al. [14]	Pure Mg	0.5 wt. % Al_4C_3	Sand	5500	700	87
Native Grain Refinement	Cao et al. [23]	High purity Mg-Al	-	Steel cone	300	200	33
SiC Addition	Gunther et al. [24]	AZ31	0.4 wt. % SiC	-	300	110	63
	Easton et al. [25]	Mg-9Al	0.15 wt. % SiC	Steel cup	140	100	29
	Liu et al. [26]	AZ91	0.5 – 1.0 wt. % Al_4C_3-SiC/Al	Steel	-	-	no change
Elfinal Process / Iron Addition	Cao et al. [28]	Mg-9Al	2 wt. % $FeCl_3$	Steel cone	130	60	54

Addition/Process	Authors	Mg Alloy	Addition Level / Processing	Mold Type	Reference Grain Size (μm)	Smallest Refined Grain Size (μm)	Grain Size Reduction (%)
Manganese Addition	Cao et al. [29]	Mg-9Al	0.1 wt. % Mn	Steel cone	130	50	62
	Elsayed et al. [30]	AZ91D	0.5 wt. % Mn	Steel	215	174	19
Titanium Addition	Wang et al. [32]	AZ31B	0.3 wt. % Al-4Ti-5B	Steel	1100	80	93
	Wang et al. [33]	AZ91	7.5 wt. % TiB$_2$	Steel	350	100	71
Calcium Addition	Lee et al. [9]	AZ91D	0.4 wt. % Ca	Steel	1000	250	75
	Li et al. [34]	AZ91D	1.0 wt. % Ca	Steel	275	75	73
	Li et al. [35]	AZ91D	0.95 wt. % Ca	Steel	165	110	33
	Elsayed et al. [30]	AZ91D	1.0 wt. % Ca	Steel	284	846	-198
Vanadium Addition	Buha [44]	Mg-7Zn	0.3 wt. % V	Steel	40	20	50
Strontium Addition	Yang et al. [38]	AZ31	0.1 wt. % Mg-10Sr	Steel	200	63	69
	Pan et al. [39]	AZ91D	0.6 wt. % Sr	Steel	235	53	77
Antimony Addition	Ma et al. [40]	AZ64	0.5 wt. % Sb-C	-	-	50	-
Zinc Oxide Addition	Fu et al. [45]	Mg-3Zn	1 wt. % ZnO	Steel cone	420	310	26
Mechanical Processes	Liu et al. [42]	AZ91D	Melt agitation	Alumina	1800	195	89
	Qi et al. [43]	AZ91D	Melt agitation, 90 seconds	Steel	-	80	-

APPENDIX 3 – MATERIALS

- Please refer to Section 3.1

Al-5TiB$_2$ Master Alloy

1. Pure Al was melted in a furnace heated to 800 °C.
2. Degassing of the Al melt was performed using C_2Cl_6.
3. The K_2TiF_6 and KBF_4 salts were added to the Al melt at 800 °C.
4. The salt and Al were mixed using a zirconia coated stirrer until the mixture was homogeneous.
5. The stirring was then stopped and the melt was held for 60 minutes to ensure salt and Al reaction.
6. The melt was then poured into a graphite crucible 25 mm in diameter and 250 mm in height.

Al-Al$_4$C$_3$ Master Alloy

1. A composite stir casting (composite mixed with liquid metal matrix) of pure Al and 6 vol. % SiC_p was produced at 750 °C.
2. The composite was re-melted and held at 900 °C for four hours.
3. The master alloy was then poured into a cast iron mold.

ZnO Powder

Trace analysis of the ZnO powder from the supplier is shown in Table A3.

Table A3: Trace analysis of ZnO powder (ppm).

Cl	Ca	NO$_3$	Pb	Mg	Mn	K	Na	Fe
< 10	< 50	< 30	< 50	< 50	< 5	< 100	< 500	< 10

The ZnO powder was evaluated using a Horiba CAPA 700 particle size analyzer to determine its size distribution and median particle size. A sample particle size distribution is shown in Figure A3.1. A phase diagram for the Mg-Al system is also presented in Figure A3.2.
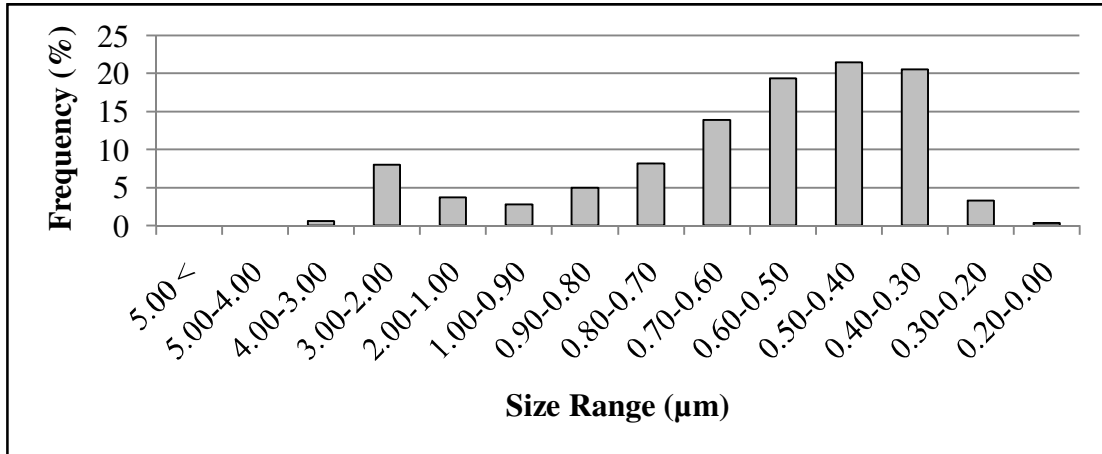
Figure A3.1: A representative ZnO particle size distribution.
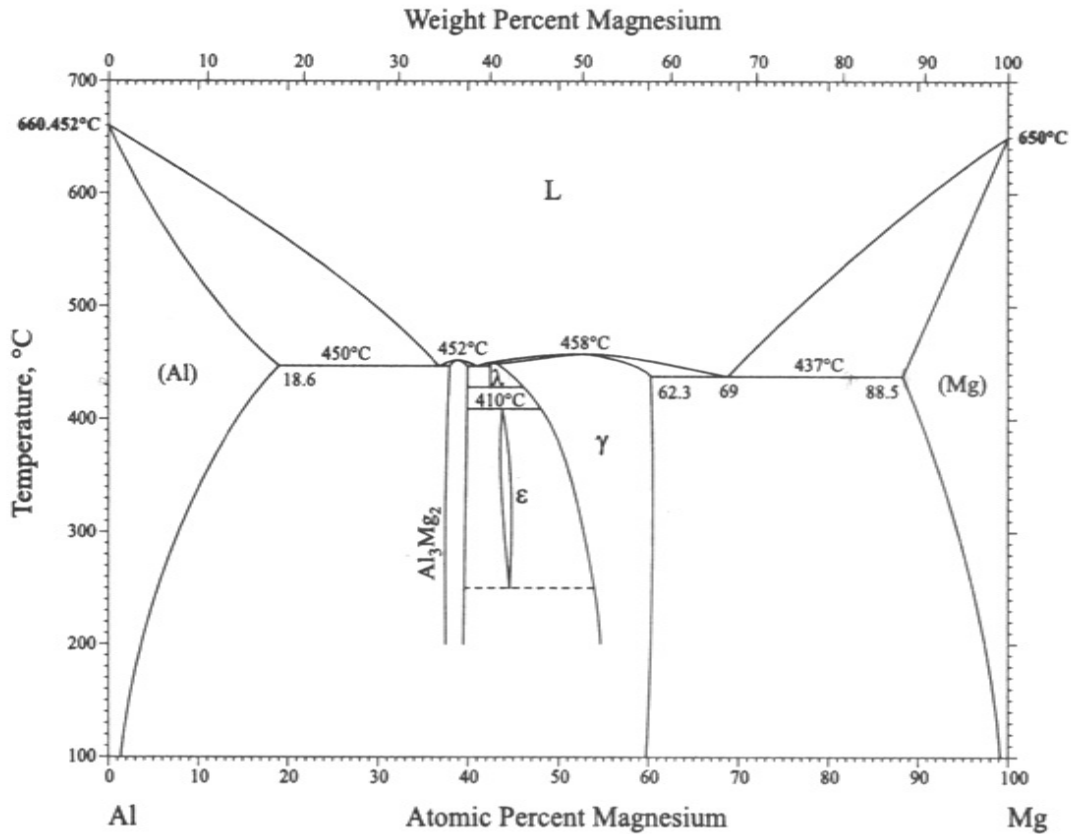
Figure A3.2: Phase diagram for the Mg-Al system [50].

APPENDIX 4 – ANALYSIS OF VARIANCE (ANOVA)

- Please refer to Sections 4.1.1.1-4.1.1.3.

Graphite Mold Grain Size

- Two-factor experiment: addition level and holding time
    - 5 addition levels   (a = 5)
    - 3 holding times   (b = 3)
    - Therefore   (N = ab = 15)
    - No replication used since addition levels and holding times act independently
    - Null hypotheses: Addition level and holding time have no effect

(Variation between treatments): $SS_T = b \sum_{t=1}^{a} (\bar{x}_t - \bar{x})^2$

(Variation between blocks): $SS_B = a \sum_{j=1}^{b} (\bar{x}_j - \bar{x})^2$

(Residual variation): $SS_R = \sum_{t,j} [x_{tj} - (\bar{x}_t + \bar{x}_j - \bar{x})]^2$

(Total variation): $SS = SS_T + SS_B + SS_R$

(Degrees of freedom): $\nu_T = (a-1), \ \nu_B = (b-1),$

$$\nu_R = (a-1)(b-1), \nu = (ab-1)$$

(Mean square value): $S_T^2 = \dfrac{SS_T}{(a-1)}, \ S_B^2 = \dfrac{SS_B}{(b-1)}, S_R^2 = \dfrac{SS_R}{(a-1)(b-1)}$

(F-value): $F_T = \dfrac{S_T^2}{S_R^2}, F_B = \dfrac{S_B^2}{S_R^2}$

- Single-factor experiment: comparing average grain size for two grain refiner levels

(Variation between treatments): $SS_T = \sum_{t,j} (\bar{x}_t - \bar{x})^2$

(Residual variation): $SS_R = \sum_{t,j} (x_{t,j} - \bar{x}_t)^2$

(Total variation): $SS = SS_T + SS_R$

(Degrees of freedom): $\nu_T = (a-1), \nu_R = (N-a), \nu = (N-1)$

(Mean square value): $S_T^2 = \dfrac{SS_T}{(a-1)}, S_R^2 = \dfrac{SS_R}{(N-a)}$

(F-value): $F_T = \dfrac{S_T^2}{S_R^2}$

Al-5TiB$_2$ Addition (Two-factor Experiment)

Table A4.1: Average grain size data for Al-5TiB$_2$ addition.

Holding Times > Addition Levels	5	10	20	Addition Level Mean ($\bar{x}_t$)
0	782.2	782.2	782.2	782.2
0.1	432.9	536.3	386.2	451.8
0.2	332.2	318.3	339.2	329.9
0.5	527.8	570.6	680.7	593.0
1.0	508.3	570.1	565.8	548.1
Holding Time Mean ($\bar{x}_j$)	516.7	555.5	550.8	541.0

Table A4.2: ANOVA table for Al-5TiB$_2$ addition (two-factor).

Source of Variation	Sum of Squares	Degree of Freedom	Mean-Square Value	F
Between Addition Levels	SS$_T$ = 340364.1	$\nu_T = 4$	$S_T^2 = 85091.0$	F$_T$ = 30.4 $\nu_1 = 4$, $\nu_2 = 8$
Between Holding Times	SS$_B$ = 4490.5	$\nu_B = 2$	$S_B^2 = 2245.3$	F$_B$ = 0.8 $\nu_1 = 2$, $\nu_2 = 8$
Residual	SS$_R$ = 22361.8	$\nu_R = 8$	$S_R^2 = 2795.2$	
Total	SS = 367216.4	$\nu = 14$		

- F$_T$ = F$_{4,8,\alpha}$ = 30.4
  - $\alpha < 0.1\%$, P$_{\alpha max}$ = 100 – α
  - P$_{\alpha max}$ is greater than 99.9%
  - Since P$_{\alpha max}$ > 90%, this indicates the effect of addition level on grain size is significant.
- F$_B$ = F$_{2,8,\alpha}$ = 0.8
  - $\alpha > 25\%$, P$_{\alpha max}$ = 100 – α
  - P$_{\alpha max}$ is less than 75%
  - Since P$_{\alpha max}$ < 85%, this indicates the effect of holding time on grain size is not significant.

Al-5TiB$_2$ Addition (One-factor Experiment)

Table A4.3: Grain size measurements from two addition levels of Al-5TiB$_2$.

Addition Levels > Replication	0.1 wt. %	0.2 wt. %
1	558.1	282.6
2	359.5	282.7
3	345.3	327.7
4	411.2	382.4
5	377.4	270.7
6	353.9	248.2
7	365.2	361.8
8	350.8	393.9
9	280.4	299.7
10	324.2	254.1
11	377.1	297.0
12	333.3	400.1
13		336.9
Addition Level Mean > ($\overline{x}_t$)	369.7	318.3

Table A4.4: ANOVA table for Al-5TiB$_2$ addition (one-factor).

Source of Variation	Sum of Squares	Degree of Freedom	Mean-Square Value	F
Between Addition Levels	SS$_T$ = 16495.3	v_T = 1	S_T^2 = 16495.3	F$_T$ = 4.5 v_1 = 1, v_2 = 23
Residual	SS$_R$ = 83512.4	v_R = 23	S_R^2 = 3630.9	
Total	SS = 100007.7	v = 24		

- F$_T$ = F$_{1,23,\alpha}$ = 4.5
    - α = 4.8%, P$_{\alpha max}$ = 100 − α
    - P$_{\alpha max}$ = 95.2%
    - Since P$_{\alpha max}$ > 90%, this indicates the two average grain sizes are significantly different (hence 0.2 wt. % Al-5TiB$_2$ was used).

Al-Al$_4$C$_3$ Addition

Table A4.5: Average grain size data for Al-Al$_4$C$_3$ addition.

Holding Times > Addition Levels	5	10	20	Addition Level Mean ($\bar{x}_t$)
0	782.2	782.2	782.2	782.2
0.1	281.6	301.8	316.9	300.1
0.2	437.6	453.1	442.9	444.5
0.5	372.4	390.4	356.6	373.1
1.0	328.8	382.1	326.8	345.9
Holding Time Mean ($\bar{x}_j$)	440.5	461.9	445.1	449.2

Table A4.6: ANOVA table for Al-Al$_4$C$_3$ addition (two-factor).

Source of Variation	Sum of Squares	Degree of Freedom	Mean-Square Value	F
Between Addition Levels	$SS_T = 448795.8$	$\nu_T = 4$	$S_T^2 = 112198.9$	$F_T = 444.2$ $\nu_1 = 4, \nu_2 = 8$
Between Holding Times	$SS_B = 1270.5$	$\nu_B = 2$	$S_B^2 = 635.3$	$F_B = 2.5$ $\nu_1 = 2, \nu_2 = 8$
Residual	$SS_R = 2020.6$	$\nu_R = 8$	$S_R^2 = 252.6$	
Total	$SS = 452086.9$	$\nu = 14$		

- $F_T = F_{4,8,\alpha} = 444.2$
    - $\alpha < 0.1\%$, $P_{\alpha max} = 100 - \alpha$
    - $P_{\alpha max}$ is greater than 99.9%
    - Since $P_{\alpha max} > 90\%$, this indicates the effect of addition level on grain size is significant.

- $F_B = F_{2,8,\alpha} = 2.5$
    - Interpolate to find $\alpha = 16.3\%$
    - $P_{\alpha max} = 100 - \alpha = 83.7\%$
    - Since $P_{\alpha max} < 85\%$, this indicates the effect of holding time on grain size is not significant.

ZnO Addition

Table A4.7: Average grain size data for ZnO addition.

Holding Times > Addition Levels	5	10	20	Addition Level Mean $(\bar{x}_t)$
0	782.2	782.2	782.2	782.2
0.1	243.7	238.2	254.2	245.4
0.2	283.2	191.7	265.6	246.8
0.5	257.8	275.0	215.2	249.3
1.0	247.8	212.1	249.7	236.5
Holding Time Mean $(\bar{x}_j)$	362.9	339.8	353.4	352.1

Table A4.8: ANOVA table for ZnO addition (two-factor).

Source of Variation	Sum of Squares	Degree of Freedom	Mean-Square Value	F
Between Addition Levels	$SS_T = 694127.1$	$\nu_T = 4$	$S_T^2 = 173531.8$	$F_T = 220.6$ $\nu_1 = 4, \nu_2 = 8$
Between Holding Times	$SS_B = 1347.0$	$\nu_B = 2$	$S_B^2 = 673.5$	$F_B = 0.9$ $\nu_1 = 2, \nu_2 = 8$
Residual	$SS_R = 6292.2$	$\nu_R = 8$	$S_R^2 = 786.5$	
Total	$SS = 701766.3$	$\nu = 14$		

- $F_T = F_{4,8,\alpha} = 220.6$
    - $\alpha < 0.1\%$, $P_{\alpha max} = 100 - \alpha$
    - $P_{\alpha max}$ is much greater than 99.9%
    - Since $P_{\alpha max} > 90\%$, this indicates the effect of addition level on grain size is significant.
- $F_B = F_{2,8,\alpha} = 0.9$
    - $\alpha > 25\%$, $P_{\alpha max} = 100 - \alpha$
    - $P_{\alpha max}$ is less than 75%
    - Since $P_{\alpha max} < 85\%$, this indicates the effect of holding time on grain size is not significant.

ZnO Addition (One-factor Experiment)

Table A4.9: Grain size measurements from two addition levels of ZnO.

Addition Levels > Replication	1 wt. %	2 wt. %
1	210.7	186.0
2	258.5	155.4
3	229.5	253.0
4	231.5	164.1
5	219.2	222.5
6	203.4	169.1
7	275.9	
8	323.9	
9	256.2	
10	272.4	
11	238.5	
12	120.7	
13	327.6	
Addition Level Mean > ($\bar{x}_t$)	243.7	191.7

Table A4.10: ANOVA table for ZnO addition (one-factor).

Source of Variation	Sum of Squares	Degree of Freedom	Mean-Square Value	F
Between Addition Levels	$SS_T = 11094.8$	$\nu_T = 1$	$S_T^2 = 11094.8$	$F_T = 4.5$ $\nu_1 = 1, \nu_2 = 17$
Residual	$SS_R = 41849.5$	$\nu_R = 17$	$S_R^2 = 2461.7$	
Total	$SS = 52944.2$	$\nu = 18$		

- $F_T = F_{1,17,\alpha} = 4.5$
  - $\alpha = 4.9\%$, $P_{\alpha max} = 100 - \alpha$
  - $P_{\alpha max} = 95.1\%$
  - Since $P_{\alpha max} > 90\%$, this indicates the two average grain sizes are significantly different (hence 2 wt. % ZnO was used).

APPENDIX 5 – ADDITIONAL MEASUREMENTS AT LOWER ZnO LEVELS

- Please refer to Section 4.2.2

The grain size measurements for lower ZnO levels (0.1, 0.2 and 0.5 wt. %) in graphite molds are shown in Figure A5. Furthermore, no undercooling was detected at the three lower addition levels of ZnO, which suggested grain refinement via heterogeneous nucleation.
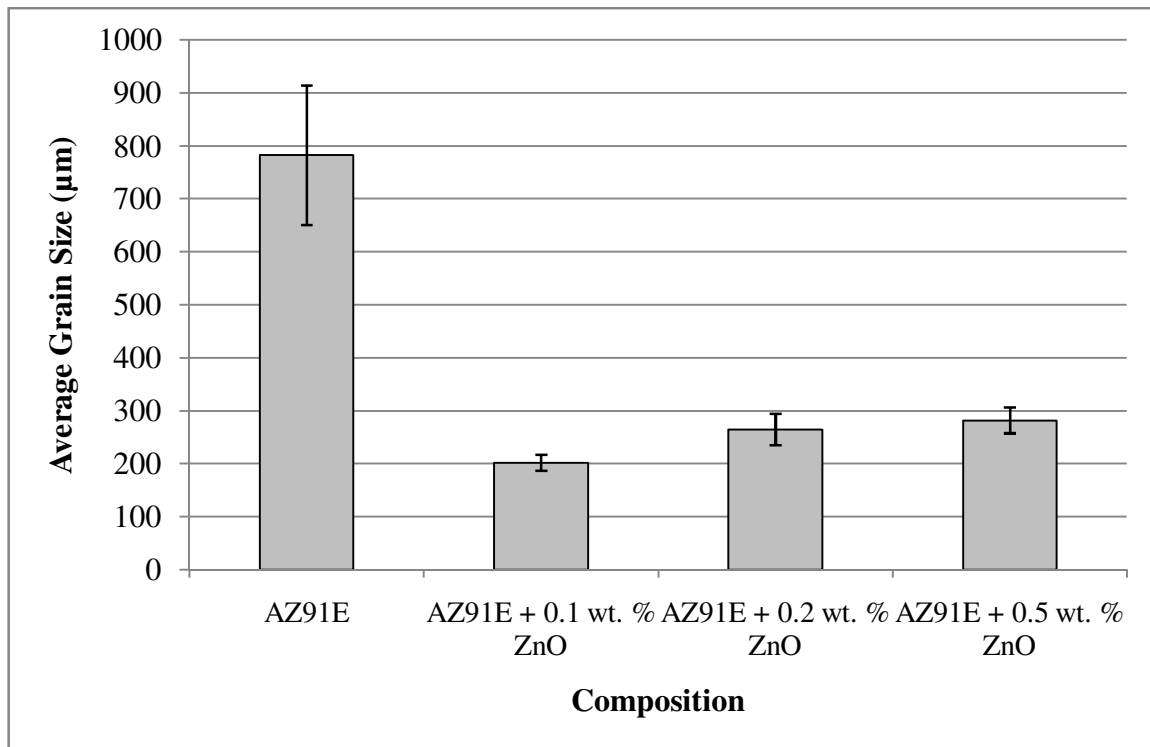
Figure A5: Influence of lower ZnO levels on the grain size of AZ91E in graphite molds.

The amount of Zn within AZ91E samples with ZnO addition was analyzed using XRF (X-ray fluorescence). This spot analysis enabled the determination of the amount of ZnO required to achieve the detected increase in Zn levels, assuming 100 g samples. A sample calculation is presented in addition to the results of the XRF analysis, which are shown in Table A5.

- Example calculation using a sample of 100 g with a detected Zn level of 1.94 wt. %:

$$\text{Mass of ZnO} = \text{Mass of Zn} + \text{Mass of O}$$
$$W_{ZnO} = W_{Zn} + W_O$$
$$= 65.409 \text{ g/mol} + 15.999 \text{ g/mol}$$
$$= 81.408 \text{ g/mol}$$

$$[(\text{Mass of detected Zn} - \text{Mass of Zn in base AZ91E}) / W_{Zn}] \times 1/1 \times W_{ZnO} = \text{Mass of ZnO}$$
$$[(1.94 \text{ g} - 0.53 \text{ g}) / W_{Zn}] \times 1/1 \times W_{ZnO} = \textbf{1.75 g of ZnO}$$

Table A5: Detected increase in Zn levels in AZ91E samples and corresponding ZnO required. These calculations assumed samples of 100 g.

ZnO Addition Level (wt. %)	Increase in Zn from Nominal 0.53 wt. % (Refer to Table 3.1) (wt. %)	Required ZnO Amount to Achieve Increased Zn Level (g)
0.1	0.04	0.05
0.2	0.12	0.15
0.5	0.2	0.3
1	0.25	0.31
2	0.56	0.69
3	0.88	1.1
4	1.41	1.75

These calculations suggest that, generally, at least 50% of the ZnO added to each melt either formed nucleation sites or were part of the losses (e.g. skimming of MgO).

REFERENCES

1. Campbell, J., <u>Castings</u>, Oxford: *Butterworth-Heinemann* (1991).

2. Callister, W.D., <u>Material Science and Engineering: An Introduction - Sixth Edition</u>, New Jersey: *John Wiley & Sons, Inc.* (2003).

3. Dieter, G.E., <u>Mechanical Metallurgy</u>, London: *McGraw-Hill* (1988).

4. Gruzleski, J.E., <u>Microstructure Development During Metalcasting</u>, Des Plaines: *American Foundrymen's Society* (2000).

5. Loper, C.R., Kotschi, R.M., "A Technique for Measuring Grain Refinement", *AFS Transactions*, vol 82, pp 279-284 (1974).

6. Bramfitt, B.L., "The Effect of Carbide and Nitride Additions on the Heterogeneous Nucleation Behavior of Liquid Iron", *Metallurgical Transactions*, vol 1, pp 1987-1995 (1970).

7. Zhang, M., Kelly, P.M., "Edge-to-edge Matching and its Applications: Part I. Application to the Simple HCP/BCC System", *Acta Materialia*, vol 53, pp 1073-1084 (2005).

8. Zhang, M., Kelly, P.M., Qian, M., Taylor, J.A., "Crystallography of Grain Refinement in Mg-Al Based Alloy", *Acta Materialia*, vol 53, pp 3261-3270 (2005).

9. Lee, Y.C., Dahle, A.K., StJohn, D.H., "The Role of Solute in Grain Refinement of Magnesium", *Metallurgical and Materials Transactions*, vol 31A, pp 2895-2906 (2000).

10. Easton, M., StJohn, D.H., "The Key Factors Controlling Grain Refinement", *Light Metals*, pp 391-402 (2001).

11. StJohn, D.H., Qian, M., Easton, M.A., Cao, P., Hildebrand, Z., "Grain Refinement of Magnesium Alloys", *Metallurgical and Materials Transactions*, vol 36A, pp 1669-1679 (2005).

12. Motegi, T., "Grain-refining Mechanisms of Superheat-treatment and Carbon Addition to Mg–Al–Zn Alloys", *Materials Science and Engineering A*, vol 413-414, pp 408-411 (2005).

13. Karlsen, D.O., Øymo, D., Westengen, H., Pinfold, P.M.D., Strømhaug, S., "Development of Grain Refiner for Al-containing Mg-alloys", *Light Metal Processing and Applications*, pp 397-408 (1993).

14. Xue, F., Du, W., Sun, Y., "Microstructure Refinement of Magnesium Based Alloy", *Materials Science Forum*, vol 488-489, pp 143-146 (2005).

15. Lu, L., Dahle, A.K., StJohn, D.H., "Grain Refinement Efficiency and Mechanism of Aluminium Carbide in Mg–Al Alloys", *Scripta Materialia*, vol 53, pp 517-522 (2005).

16. Qian, M., Cao, P., "Discussions on Grain Refinement of Magnesium Alloys by Carbon Inoculation", *Scripta Materialia*, vol 52, pp 415-419 (2005).

17. Jin, Q., Eom, J., Lim, S., Park, W., You, B., "Grain Refining Mechanism of a Carbon Addition Method in a Mg-Al Magnesium Alloy", *Scripta Materialia*, vol 49, pp 1129-1132 (2003).

18. Han, G., Liu, X., Ding, H., "Grain Refinement of Mg–Al Based Alloys by a New Al-C Master Alloy", *Journal of Alloys and Compounds*, vol 467, pp 202-207 (2007).

19. Han, G., Liu, X., "Duplex Nucleation in Mg–Al–Zn–Mn Alloys with Carbon Inoculation", *Journal of Alloys and Compounds*, vol 487, pp 194-197 (2009).

20. Pan, Y., Liu, X., Yang, H., "Role of C and Fe in Grain Refinement of an AZ63B Magnesium Alloy by Al-C Master Alloy", *Journal of Materials Science and Technology*, vol 21, pp 822-826 (2005).

21. Emley, E.F., Principles of Magnesium Technology, Oxford: *Pergamon Press* (1966).

22. Ning, Z., Cao, P., Wang, H., Sun, J., Liu, D., "Effect of Cooling Conditions on Grain Size of AZ91 Alloy", *Journal of Materials Science and Technology*, vol 23, pp 645-649 (2007).

23. Cao, P., Qian, M., StJohn, D.H., "Native Grain Refinement of Magnesium Alloys", *Scripta Materialia*, vol 53, pp 841-844 (2005).

24. Gunther, R., Hartig, Ch., Bormann, R., "Grain Refinement of AZ31 by (SiC)p: Theoretical Calculation and Experiment", *Acta Materialia*, vol 54, pp 5591-5597 (2006).

25. Easton, M., Schiffl, A,. Yao, J., Kaufmann, H., "Grain Refinement of Mg–Al(–Mn) Alloys by SiC Additions", *Scripta Materialia*, vol 55, pp 379-382 (2006).

26. Liu, Y., Liu, X., Xiufang, B., "Grain Refinement of Mg–Al Alloys with Al_4C_3–SiC/Al Master Alloy", *Materials Letters*, vol 58, pp 1282-1287 (2004).

27. Wang, Z., Kang, Y., Dong, W., Zhao, H., Liu, J., Xu, Y., "Study of Grain Refinement and SiC Nanoparticle Reinforced Magnesium Alloys", *Materials Science Forum*, vol 488-489, pp 889-892 (2005).

28. Cao, P., Qian, M., StJohn, D.H., "Effect of Iron on Grain Refinement of High-purity Mg–Al Alloys", *Scripta Materialia*, vol 51, 125-129 (2004).

29. Cao, P., Qian, M., StJohn, D.H., "Effect of Manganese on Grain Refinement of Mg–Al Based Alloys", *Scripta Materialia*, vol 54, pp 1853-1858 (2006).

30. Elsayed, A., Lee, K., Ravindran, C., "Effect of Ca and Mn Additions on the Castability and Mechanical Properties of AZ91D Mg Alloy Permanent Mold Castings", *AFS Transactions*, vol 117, pp 659-672 (2009).

31. Du, J., Yang, J., Kuwabara, M., Li, W., Peng, J., "Effects of Manganese and/or Carbon on the Grain Refinement of Mg-3Al Alloy", *Materials Transactions*, vol 49, pp 139-143 (2007).

32. Wang, Y., Zeng, X., Ding, W., "Effect of Al-4Ti-5B Master Alloy on the Grain Refinement of AZ31 Magnesium Alloy", *Scripta Materialia*, vol 54, pp 269-273 (2006).

33. Wang, Y., Wang, H.Y.., Yang, Y.F., Jiang, Q.C., "Solidification Behavior of Cast TiB_2 Particulate Reinforced Mg Composites", *Materials Science and Engineering*, vol 478, pp 9-15 (2008).

34. Li, P., Tang, B., Kandalova, E.G., "Microstructure and Properties of AZ91D Alloy with Ca Additions", *Materials Letters*, vol 59, pp 671-675 (2005).

35. Li, S., Tang, B., Zeng, D., "Effects and Mechanism of Ca on Refinement of AZ91D Alloy", *Journal of Alloys and Compounds*, vol 437, pp 317-321 (2007).

36. Wang, Q.,Chen, W., Zeng, X., Lu, Y., "Effects of Ca Addition on the Microstructure and Mechanical Properties of AZ91 Magnesium Alloy", *Journal of Materials Science*, vol 36, pp 3035-3040 (2001).

37. Tang, B., Li, S., Wang, X., Wu, D., "An Investigation on Hot-crack Mechanism of Ca Addition Into AZ91D Alloy", *Journal of Materials Science*, vol 40, pp 2931-2936 (2005).

38. Yang, M., Pan, F., Cheng, R., Tang, A., "Comparation About Efficiency of Al–10Sr and Mg–10Sr Master Alloys to Grain Refinement of AZ31 Magnesium Alloy", *Journal of Materials Science*, vol 42, pp 10074-10079 (2007).

39. Pan, Y., Liu, X., Yang, H., "Sr Microalloying for Refining Grain Size of AZ91D Magnesium Alloy", *Journal of Wuhan University of Technology - Materials Science Edition*, vol 22, pp 74-76 (2007).

40. Ma, Y.Q., Chen, R.S., Han, E., "Keys to Improving the Strength and Ductility of the AZ64 Magnesium Alloy", *Materials Letters*, vol 61, pp 2527-2530 (2007).

41. Li, J., Dong, X., Fan, Z., Wang, Y., "Effects of Ce and Sb on the Microstructure and Properties of AZ91D Magnesium Alloy Prepared by the EPC Process", *Rare Metals*, vol 27, pp 41-45 (2008).

42. Liu, X., Osawa Y., Takamori S., Mukai, T., "Microstructure and Mechanical Properties of AZ91 Alloy Produced with Ultrasonic Vibration", *Materials Science and Engineering A*, vol 487, 120-123 (2008).

43. Qi, X., Tang J., Li, S., Zeng D., "Influences of Melt Treatment on Grain Sizes and Morphologies of AZ91D Alloy", *Transactions of Nonferrous Metals Society of China*, vol 17, pp 887-892 (2007).

44. Buha, J., "Grain Refinement and Improved Age Hardening of Mg-Zn Alloy by a Trace Amount of V", *Acta Materialia*, vol 56, pp 3533-3542 (2008).

45. Fu, H.M., Qiu, D., Zhang, M.X., Wang, H., Kelly, P.M., Taylor, J.A., "The Development of a New Grain Refiner for Magnesium Alloys Using the Edge-to-edge Model", *Journal of Alloys and Compounds*, vol 456, pp 390-394 (2008).

46. Villars, P., Calvert, L.D., Pearson's Handbook of Crystallographic Data for Intermetallic Phases, Materials Park: *ASM International* (1991).

47. Bichler L., Elsayed A., Lee, K., Ravindran, C., "Influence of Mold and Pouring Temperatures on Hot Tearing Susceptibility of AZ91D Magnesium Alloy", *International Journal of Metalcasting*, vol 2, pp 43-54 (2008).

48. Metz, S.A., Flemings, M.C., "A Fundamental Study of Hot Tearing", *AFS Transactions*, vol 78, pp 453-460 (1970).

49. Easton, M., Grandfield, J., StJohn, D., Rinderer, B., "The Effect of Grain Refinement and Cooling Rate On The Hot Tearing of Wrought Aluminum Alloys", *Materials Science Forum*, vol 519-521, pp 1675-1680 (2006).

50. Avedesian, M., Baker H., ASM Specialty Handbook: Magnesium and Magnesium Alloys, Materials Park: *ASM International* (1998).

51. Groover, M.P., Fundamentals of Modern Manufacturing: Second Edition, New Jersey: *John Wiley & Sons, Inc.* (2004).

52. Eskin, D.G., Suyitno, Katgerman, L., "Mechanical Properties in the Semi-solid State and Hot Tearing of Aluminum Alloys", *Progress in Materials Science*, vol 49, pp 629-711 (2004).

53. Lide, D.R., <u>CRC Handbook of Chemistry and Physics: 90th Edition</u>, Boca Raton: *CRC Press* (2010).

54. Wang, Y., Wang, Q., Wu, G., Zhu, Y., Ding, W., **"**Hot-tearing Susceptibility of Mg–9Al–xZn Alloy", *Materials Letters*, vol 57, pp 929-934 (2002).

55. Abulkhaev, V.D., "Phase Diagram of the Ce-Sb System", *Russian Journal of Inorganic Chemistry*, vol 42, pp 341-346 (1997).

56. Blairs, S., Shelton, R.A.J., "The Thermal Expansion of Iron (III) Chloride", *Journal of Inorganic and Nuclear Chemistry*, vol 28, pp 1855-1859 (1966).

57. Park, Y.S., <u>SiC Materials and Devices</u>, San Diego: *Academic Press* (1998).